AD NUMBER

AD816960

LIMITATION CHANGES

TO:

Approved for public release; distribution is unlimited.

FROM:

Distribution: Further dissemination only as directed by Air Force Materials Laboratory, Wright-Patterson AFB, OH 45433., JUN 1967, or higher DoD authority. This document contains export-controlled technical data.

AUTHORITY

AFML per DTIC form 55

AFML-TR-67-128

INVESTIGATION OF NONDESTRUCTIVE METHODS FOR THE EVALUATION OF GRAPHITE MATERIALS

G. E. Lockyer
A. W. Shultz
S. Serabian
S. W. Carter

Technical Report AFML-TR-67-128
Contract AF 33(615)-3942

June 1967

AIR FORCE MATERIALS LABORATORY
DIRECTORATE OF LABORATORIES
AIR FORCE SYSTEMS COMMAND
Wright-Patterson Air Force Base, Ohio

NOTICES

When Government drawings, specifications, or other data are used for any purpose other than in connection with a definitely related Government procurement operation, the United States Government thereby incurs no responsibility nor any obligation whatsoever; and the fact that the Government may have formulated, furnished, or in any way supplied the said drawings, specifications, or other data, is not to be regarded by implication or otherwise as in any manner licensing the holder or any other person or corporation, or conveying any rights or permission to manufacture, use, or sell any patented invention that may in any way be related thereto.

Copies of this report should not be returned to the Directorate of Laboratories unless return is required by security considerations, contractual obligations, or notice on a specific document.

This document consists of 170 pages,
80 copies, Series A

AFML-TR-67-128

INVESTIGATION OF NONDESTRUCTIVE METHODS FOR THE EVALUATION OF GRAPHITE MATERIALS

G. E. Lockyer
A. W. Shultz
S. Serabian
S. W. Carter

Technical Report AFML-TR-67-128
Contract AF 33(615)-3942

June 1967

AIR FORCE MATERIALS LABORATORY
DIRECTORATE OF LABORATORIES
AIR FORCE SYSTEMS COMMAND
Wright-Patterson Air Force Base, Ohio

FOREWORD

This report was prepared by Avco Corporation, Research and Development Division, Lowell, Massachusetts, under USAF Contract No. AF33(615)-1601. The contract was initiated under Project No. 7360, "The Chemistry and Physics of Materials," Task No. 736002, "Nondestructive Methods." The work was administered under the direction of the Air Force Materials Laboratory, Directorate of Laboratories, with Mr. W. L. Shelton, MAMD, acting as Project Engineer, and Mr. R. R. Rowand, Technical Manager for Nondestructive Methods.

This report covers work conducted from 15 April 1966 to 15 April 1967, at Avco SSD, Mr. G. E. Lockyer, Project Engineer, and Mr. C. H. Hastings, Project Manager. The authors appreciate the contribution of several members of the Nondestructive Test Development Group - Messrs. A. M. Chetson, S. A. LoPilato, T. M. Ludwig, M. A. Pennissi, and E. A. Proudfoot, Group Leader.

Manuscript released by authors June 1967 for publication as an AFML Technical Report. It is also assigned Avco document No. AVSSD-0228-67-CR.

This technical report has been reviewed and is approved.

W. J. TRAPP
Chief, Strength and Dynamics Branch
Metals and Ceramic Division
Air Force Materials Laboratory

ABSTRACT

A program of investigation was begun in April 1964, to determine nondestructive methods and techniques for evaluating and characterizing graphite materials under contract Nos. AF33(615)-1601 and AF33(615)-3942. The properties and behavior characteristics of graphite which are important to ablative applications were identified and correlated with the applicable NDT methods and techniques during the first year, April 1964 to April 1965. During the second year, April 1965 to April 1966, development of a novel infrared technique to measure thermal properties was initiated. Additionally, studies were performed to evaluate complex thermal and mechanical loading characteristics for graphite. In this regard, combined use of the various NDT techniques in relation to thermo-mechanical stresses and related thermal shock phenomena was also studied.

During the past year, April 1966 to April 1967, emphasis has been directed in several areas as reported herein. Verification of the applicability of the various NDT techniques and correlation to characterize graphite in relation to service performance has been an item of major concern. Statistical analysis of these correlations has been performed which establishes the significance of the correlations for predicting the related material properties. An extensive analysis of the application of NDT flaw testing and properties evaluation in regard to quality and reliability is presented. A detailed discussion of infrared technique development activities for measuring thermal properties is also presented. The influence of attenuation and the related effects of frequency distortion on velocity measurements is evaluated and described.

Page iv is intentionally blank.

CONTENTS

Page vi is intentionally blank.

ILLUSTRATIONS

ILLUSTRATIONS (Cont'd)

ILLUSTRATIONS (Cont'd)

ILLUSTRATIONS (Cont'd)

ILLUSTRATIONS (Concl'd)

Page xii is intentionally blank

PART I.

GENERAL DISCUSSION - G. E. LOCKYER *

I. Introduction

Despite improvements in the processing of graphite on the part of the producers, the use of graphite in aerospace applications continues to frustrate designers because of its unpredictable service performance. Much has been written which attributes a large part of this erratic behavior to variations in properties in given grades of bulk graphite material. Where the range of properties variability is high within and between parts, such as it is in graphite, identification of this variability for design purposes by random destructive testing requires extensive statistical sampling on each part prior to fabrication. Otherwise, there is no assurance that the extremes of the variability in each part are represented in the destructive test data. Moreover, without such extensive destructive testing, which is often prohibitive from the standpoint of cost and material availability, there is no way to predict the thermomechanical stress gradients associated with these properties variations, and thereby assess their influence on performance in severe environments. As a step toward improving design and performance reliability for graphite components, Avco/SSD has been involved in a continued three-year program aimed at the development of nondestructive testing techniques for determining properties of graphite which have been identified to be of significance to service in ablative applications.

Ultrasonic longitudinal-wave velocity measurements, combined with radiometric density gauging, have been used to establish correlations with, and thereby determine, mechanical properties, and infrared techniques have been developed for measuring thermal properties.[1, 2] Associated with determining the level and range of properties in graphite billets and hardware components has been the task of determining the significance of this level and range upon service behavior. To this end, nondestructive properties measurements have been studied singly and in combination in relation to thermomechanical environmental effects in an effort to establish correlations between this nondestructive characterization of graphite and environmental test performance.

II. Communication with Industry

A. Seminar Plan

One of the important phases of this past year's effort has been the communication of the technique developments and associated materials evaluation capabilities to the industry. In this regard, emphasis has been

*Faculty member, Lowell Technological Institute, Lowell, Massachusetts

placed on the benefits of judicious use of these techniques in material process control, and for nondestructive characterization for sample selection to embrace magnitude and range of properties variability, as well as for improving graphite component performance reliability.

Among the more effective means for disseminating this information to the industry is through the organization and conduct of seminars. To this end, a detailed program of lectures and demonstrations covering theory, application and implementation is appended to this paper (Appendix I). The design of this format has been guided to a large extent by what has been observed to be the more effective aspects of presentations and discussions during the past year.

B. Technical Papers and Other Presentations

In addition to the seminar activity described above, Avco/SSD has disseminated information related to this program to the industry through the presentation and publication of technical papers. The title, author, time and place of presentation and publication, together with an abstract for each of these papers follows:

1. "Nondestructive Determination of Mechanical Properties of Refractory Materials" by G. E. Lockyer and E. A. Proudfoot. Presented at 68th Annual Meeting, The American Ceramic Society, Washington, D. C., April 1966. To be published in the American Ceramic Society Bulletin.

Abstract

Basic principles of ultrasonic and radiometric measurements are combined with knowledge of physical and chemical make up of several materials to provide measurement of density, elastic modulus, and ultimate tensile strength. Application to bulk graphite, ceramic reinforced plastic and porous tungsten is stressed, with limited reference to alumina, magnesia and cast iron. These methods may be used in materials development as well as for evaluation of finished hardware.

2. "Mechanical Properties Predictions for Graphite", by G. E. Lockyer and E. A. Proudfoot. Presented at Seventh Annual Symposium on Physics and Nondestructive Testing, Chicago, Illinois, September 1966. To be published in the Proceedings for this symposium.

Abstract

Use of graphite materials in critical, high reliability, applications requiring low safety factors has resulted in a need for a more

sophisticated nondestructive test (NDT) technology for these materials. Judicious use of known material-energy interactions, through application of the well known "scientific method", supplies the means to develop this technology. In this paper, elementary basic principles of ultrasonic and radiometric measurements are combined with knowledge of the physical and chemical make-up of graphite materials to provide measurement of density, elastic modulus, and ultimate tensile strength. These methods may be used in materials development efforts as well as for nondestructive evaluation of finished hardware.

3. "A Unique Infrared Comparative Method for Determining the Thermal Conductivity and Diffusivity of Solids" by A. W. Schultz. Presented at the Seventh Annual Symposium on Physics and Nondestructive Testing, Chicago, Illinois, September 1966. To be published in the Proceedings for this symposium.

Abstract

A unique method has been developed for rapidly determining, nondestructively, the localized thermal conductivity and thermal diffusivity of graphites near room temperature. The method employs transient heating and requires access to only one surface of a solid. It involves simultaneously heating a small area on the surface of an apparent "semi-infinite" solid with radiant energy and observing the parabolic-shaped temperature history of this area's center using an infrared radiometer as the radiance sensor. To determine thermal conductivity and/or diffusivity, this history is first analyzed in terms of its geometrical characteristics, then corrected for the effect of surface emissivity, then compared with a history for a "standard" material, and finally combined with the unknown's density and specific heat values. Preliminary results indicate that typical heat pulse duration is 3 seconds, surface temperature rise is less than 10° C., present precision is approximately 8 percent, and accuracy is limited to that of the standard. Four particularly useful features of this method are that: (1) point-to-point conductivity/diffusivity determinations are possible due to the localized nature of the measurement, thereby affording an additional tool for nondestructively evaluating material variability; (2) restraints on specimen geometry are minimal to the extent that accuracy is improved as specimen size increases; (3) the method can be extended to include measurements of both good and poor thermal conductors; and (4) application to materials at elevated temperatures should be possible.

4. "An Analytical Approach to Infrared Nondestructive Testing" by A. W. Schultz. To be presented at the Fifth Internation Conference on Nondestructive Testing, Montreal, Canada, May 1967.

Abstract

A theoretical analysis of the infrared radiometric scan method is presented in a generalized parametric form that can be applied to a wide range of problems concerned with void detection. Principles of the method and the several facets involved in surface image formation of voids and their radiometric detection are detailed in a manner that provides a practical foundation for designing test techniques and establishing inspection procedures. Working graphs for determining test parameters for a range of void characteristics are given, and their use is illustrated. Limited preliminary experimental evidence is presented to substantiate, in part, the validity of the analysis.

The thermal diffusivity and thermal conductivity of a material must be known if the theory is to yield specific quantitative results. Two convenient and rapid transient radiation methods are discussed. One is an extension of a well-known through-transmission method for measuring diffusivity absolutely. The other is presently undergoing development at the Avco Corporation, Space Systems Division, and is a novel comparative method for determining diffusivity and conductivity when only one surface of a material is accessible. A desirable characteristic of both methods is that knowledge of heat flux input is unnecessary.

In addition to presentation of formal papers at technical meetings, somewhat more informal presentations were made to civilian and military staff of the Air Force Materials Laboratory and other Air Force installations, to users of aerospace grades of graphite, such as Rocketdyne, UTC and Douglas Aircraft, and to producers, such as Union Carbide, Carborundum, Speer Carbon and Great Lakes Carbon. Technical coordination meetings were also held with Carborundum, General Electric MSD, and Aerospace Corporation for the purpose of establishing the requirements, including NDT testing and evaluation, for a procurement specification for aerospace graphite grades. At this writing, a draft of this specification is under revision.

III. NDT Characterization Versus Service Behavior

Two major aerospace applications for bulk graphite are for heat shield and rocket nozzle components. One of the more predominant types of failure in these applications is thermal cracking ; and while the mechanism of failure is not well understood, some of the contributing thermomechanical parameters involved have been analyzed by comparing varying thermal and mechanical properties of different materials in relation to their relative resistance to thermal cracking. In order to appreciate the significance of the level and range of properties measurable by NDT techniques in relation to these

applications and failure modes, efforts to obtain correlations between NDT characterization and service behavior have occupied an area of primary interest throughout the past year. Early attempts to establish a program of correlation between NDT characterization and service behavior centered around the prospects of nondestructively evaluating rocket nozzle components prior to firing, and then to test fire those nozzles shown to contain a range of materials variability. Not only was this approach frustrated by scheduling difficulties with other Air Force and civilian contractors, but prospects of any success faced obvious limitations. One limitation was that the test firing programs which were available were designed to evaluate firing parameters other than material behavior and were, therefore, likely to be insufficient in firing degree and/or duration to produce material failures. A case in point was Project Bates, wherein firings were designed to evaluate rocket propellant formulations rather than nozzle material behavior. Although the Project Bates test facility might have been of use to us in a program designed especially to evaluate nozzle material behavior, the potential benefits to be derived from the existing program were questionable.

Another limitation was the possibility that the materials variability present in a given nozzle component, together with the corresponding thermomechanical stresses in a firing environment, might not be sufficient to cause failure because of overdesign of the nozzle. Still another factor is that it is difficult to convince contractors and other Air Force agencies of the merits of testing "questionable" material in programs seeking successful firings without specific funding to cover the cost of such work. In relation to cost, consideration must also be given to what constitutes a statistically adequate number of rocket motor firing tests to establish the required performance correlations since such firings involve considerable expense.

Obstacles such as those cited above were typical of those encountered in joint programs with UTC in the Scout Nozzle Program. For reasons such as these, attempts in this program to correlate relative quality of ATJ nozzle blanks characterized by NDT/properties measurements and macroscopic NDT flaw inspection with static firings have yet to bear fruit. Similar results have been experienced in a cooperative program with Douglas Aircraft, although prospects of future benefits here still look promising.

Among the efforts to generate correlations between NDT characterization and actual environmental firing performance was that initiated with Rocketdyne, McGregor, Texas. Post-fired graphite nozzle sections, some of which failed by cracking, were supplied by Rocketdyne for NDT evaluation. Specimens from 13 such nozzle sections were characterized by ultrasonic velocity and gravimetric density measurements. In all cases, the specimens were too small to observe significant point-to-point differences within a given specimen. However, the NDT measurements did show significant variations from one specimen to another. Density, for example, ranged from 1.75 grams/cc to 1.91 grams/cc between the specimens. Estimates of modulus variations based upon velocity

and density measurements ranged from approximately 1.01 x 10^6 psi to 1.71 x 10^6 psi in a given grain direction. The techniques used and the results obtained from this preliminary investigation were impressive to Rocketdyne's staff even though no firm correlation between post-fired NDT evaluation and firing was established. Avco has been funded by Rocketdyne to pursue related NDT/properties studies which are now in progress. The significant point here is that a user of aerospace graphite has become aware of the benefits to be derived from the use of the NDT techniques developed under this contract and, hopefully, will continue to cooperate in future NDT/environmental test studies.

As a result of the difficulties experienced in obtaining NDT correlation with actual environmental test data, a more direct and economical approach has been pursued in recent months; namely, attempting to establish a meaningful simulated environmental test program to be used in conjunction with actual service testing. The essence of one such proposed program was to determine the threshold of the level and range of the material properties variations within a marginally designed specimen, beyond which failure would occur in an arc environment. Ultimately, this simulated environmental test program would provide for the intelligent selection of material to be tested in a real service environment such as in a rocket motor firing. The design of the specimen would be handled by a computer program, wherein the thermomechanical stresses for a given environment would be analyzed in relation to the specimen design based upon thermal and mechanical properties input for various configuration. In theory, specimens containing variability greater than the threshold for a given design would then result in predictable failure.

While there are existing computer programs which suggest the feasibility of determining such a marginal specimen for use in an arc facility, they are not directly adaptable in their present form. Moreover, although the arc testing phase of such an approach is a state-of-the-art capability at Avco, the extent to which a given computer program would have to be reworked to accommodate the specimen design problem has not been determined. In consideration of time and funding, coupled with the desire to pursue infrared technique development and related studies, this program was dropped from the past year's effort per agreement with the AFML Project Engineer. However, interest is still high in this area and prospects of pursuing this work at a later date are still open.

Since no single simulated environmental test simulates all the thermomechanical stresses encountered in an actual service test, several prospective simulated environmental tests were considered as potentially useful. Another such test, although it has not yet been available for use in our program, is the TRW Thermal Shock Test. This apparatus uses an electron beam heater to produce rapid heating and associated thermomechanical shock in small specimens (hollow cylinders approximately 3/4 inch O.D. by 1/2 inch I.D. by 1 inch long). It is unlikely that significant properties gradients would occur in such size volumes of graphite. Moreover, even if they did exist,

the specimen size and design limits the use of this equipment for evaluating the effects of properties gradients within specimens measurable by NDT since any differences in properties present in such size specimens could not be resolved with the existing NDT techniques. For example, present point-to-point NDT/mechanical properties resolution is on the order of that which is associated with adjacent volumes of 3/4 inch diameter by the material thickness. However, point-to-point differences within bulk material of this proximity could perhaps be evaluated with some significance by separate shock tests. Perhaps the greatest limitation of this equipment, however, is that it in no way simulates the pressure or chemical environments of a real service test. Still, as was the case for the arc test, it offers some potential in conjunction with real service environmental testing once properties thresholds are established. Ultimately, perhaps with cooperative funding, a simulated environmental test program can be used in conjunction with real service tests, such as those discussed above in connection with Project Bates and Rocketdyne.

IV. Analysis of NDT/Mechanical Properties Data

The nondestructive test parameter, ρV_L^2, where ρ is the radiometrically determined density and V_L is the longitudinal-wave velocity, has been correlated to the dynamic modulus, E_D, and to the secant modulus, E_s, (defined as the ratio of ultimate tensile stress to total strain to failure), for various graphite grades. These correlations have been described in detail in the various reports and papers mentioned above. Appended to this paper (Appendix II by C. A. Lermond) is a summary of the analysis which was performed on the data from these correlations. Briefly, punch cards were made up containing the complete destructive and nondestructive data and from these cards individual plots of ρV_L^2 vs E_D and ρV_L^2 vs. E_s for each grade and grain direction were obtained using a Benson-Lehner Plotter. Regression lines and coefficients were obtained for the related equations, together with the root mean squares (RMS) of the difference between the experimental data and that calculated from the best linear fit. The correlation coefficients which were obtained are indicative of good fits. Using the graphs given in Appendix II, it is possible to predict E_D and E_s from the corresponding NDT values of ρV_L^2 to within less than 10% and 15%, respectively, at the 98% confidence level.

REFERENCES

1. Lockyer, G. E., "Investigation of Nondestructive Methods for the Evaluation of Graphite Materials," AFML-TR-65-113, June 1965.

2. Lockyer, G. E., E. M. Lenoe, and A. W. Schultz, "Investigation of Nondestructive Methods for the Evaluation of Graphite Materials," AFML-TR-66-101, June 1966.

PART II.

A NONDESTRUCTIVE INFRARED METHOD FOR MEASURING THE THERMAL PARAMETER $(k\rho C_p)$ FOR GRAPHITE -- A. W. SCHULTZ

I. Introduction

The high degree of reliability that must be achieved in designs for today's critical applications in thermal environments has given rise to a need for the nearly total determination of property variability within materials. Nondestructive methods for measuring thermal properties and their variabilities are essential for providing the necessary degree of confidence to be placed in the integrity of finished hardware. A material exhibiting a high degree of variability, and which is widely used in thermal applications, is graphite. Because of the current interest in graphite, a nondestructive method for measuring certain of its thermal properties has been a development goal undertaken by this author. To this end, a novel technique has been developed which can measure, nondestructively and rapidly, the thermal parameter, $(k\rho C_p)$, in a localized region, and from which graphite's thermal conductivity and diffusivity can be derived; the determination of variability in these properties being limited principally by the measurement precision of the technique. A desirable consequence of this study is that the technique can be extended to include essentially all solids in bulk form and in a variety of geometrical configurations, and, with modification, may also be useful for elevated temperature measurements.

The technique consists of simultaneously heating a small area on the surface of a "semi-infinite" solid with radiant energy for a few seconds and observing the characteristically-shaped temperature history at this surface using an infrared radiometer as the sensor; the temperature rise being limited to the order of 10 degrees C above room temperature. Analysis of the resulting history record and comparison with a record for a standard material yields the $(k\rho C_p)$-value for the material of interest. Conductivity and diffusivity are derived from $(k\rho C_p)$ by determining density, employing other nondestructive tests, and using a characteristic specific heat for the material. For graphite, only density need be known. Because of the comparative nature of the method, measurement accuracy is essentially limited to that of the reference standard.

It is believed that prior to this study direct nondestructive measurements of the so-called thermal inertia, $(k\rho C_p)$, and determinations of the conductivity, k, and diffusivity, $k/\rho C_p$, have not been performed. It is also believed that the proposed technique for performing these measurements is unique in character. For these reasons, this report attempts to support each step in the design of the technique in order to provide a foundation for its critical evaluation. The underlying method has been developed from first principles; these having served

as a guide in the procedure and a basis against which all results are ultimately compared. Because of this detail, some repetition in the report has been considered desirable to emphasize certain aspects and to reduce the need for retracing the text.

II. Theory

The thermal parameter, $(k\rho C_p)$, of a solid, which is often referred to as its thermal inertia, can be rapidly determined by observing the temperature history of its surface while this surface is subjected to a constant radiant heat flux. These observations are transient in nature and usually require knowledge of the flux. However, when a comparison of histories can be made between a solid having known thermal properties (the reference standard) and one having unknown properties then knowledge of the flux is unnecessary. To provide a theoretical basis for this comparison, adherence to certain heat transport boundary conditions within a solid is necessary. These boundary conditions require that heat flow be unidirectional from the surface into the solid, that it appear semi-infinite in extent during the period of observation, and that it be initially at a uniform temperature.

The thermal conductivity and thermal diffusivity of solids can also be determined from these comparative measurements if the density and specific heat of the test material are known. Moreover, the inertia, conductivity and diffusivity determinations each represent a localized value within a material to the extent of the observation period, so that measurements are influenced by and tend to reflect a material's variability. Consequently, not only are localized absolute values determinable, but also the relative values of $(k\rho C_p)$, k, and α for a test material are determinable without requiring standardization.

The development that follows provides a theoretical foundation upon which this method has evolved. Its criteria and fundamentals have served as a guide for designing an experimental technique. The theory is applicable to solids initially at any environmental temperature, as long as those properties which affect measurements remain constant within the temperature rise caused by heating. In this study, temperature detection was accomplished using an infrared radiometer, since initial ambient conditions corresponded to room temperature and typical surface temperature increases were of the order of 10 degrees Centigrade; IR radiometry being superior to other detection devices for this application. This development, then, incorporates the general characteristics and features of such a radiometer.

A. Fundamentals

The temperature behavior of a solid's surface while it absorbs a constant radiant heat flux is described by Equation (1):

$$T(Q, t) - T_o = \frac{2Q}{k}\left(\frac{\alpha t}{\pi}\right)^{1/2}, \quad \text{(Ref. 1)} \qquad (1)$$

The quantity, T, is the temperature of this surface above an initial ambient temperature, T_o, for the solid. The constant amount of heat absorbed by the solid is represented by Q, while k represents the thermal conductivity and α the thermal diffusivity of the solid, and t represents the time after heating begins. By definition, α is related to k and to the density, ρ, and specific heat, C_p, of the solid in accord with the expression:

$$\alpha \equiv \frac{k}{\rho C_p} \quad . \tag{2}$$

The unusual simplicity of the formulation in (1) for the temperature history of a surface arises in heat transport theory as a result of essentially two assumptions. These are: (1) that heat flows unidirectionally from the surface into the solid's interior; and (2) that the solid is dimensionally large enough so that it appears semi-infinite to heat flow during the heating period. The first criterion necessarily presumes that the heat flow front is spatially uniform in intensity, so that negligible lateral heat flow loss occurs within the solid. The second criterion can best be expressed in mathematical terms as:

$$L_\infty \geq (3\alpha t)^{1/2}, \quad \text{(Ref.2)}, \tag{3}$$

where L_∞ is the distance into the solid at which semi-infiniteness can still be presumed after a heating time, t. Equations (1) and (3) form the theoretical basis of the method. Additional theory to follow essentially adapts and extends these basics into a form that is useful for guiding the development of a practical method for determining the $(k\rho C_p)$, k, and α of a solid. Before proceeding, however, particular notice should be given to the form of Equation (1). It states that surface temperature is proportional to the square root of the heating period, for constant values of Q, k, and α, so that generation of a solid's surface history will result in a function that characteristically has a parabolic shape. This convenient prescription for the history is a most useful facet of the theory and its character will be preserved in the following development.

Since this study is concerned with heating solids to only a few degrees above room temperature, temperature detection is best performed using an infrared radiometer that is particularly sensitive to radiant heat flux in the 7 to 10 micron wavelength region. The first extension of the basics is by way of a modification to Equation (1) that will incorporate typical characteristics of such a radiometer into it. To this end, the expression

in Equation (4)

$$W = \frac{1}{\pi} \epsilon_T \sigma (T^4 - T_o^4) \simeq \frac{4}{\pi} \epsilon_T \sigma T_o^3 (T - T_o) \qquad (4)$$

is a form of the well-known Stephan-Boltzmann law, and describes the rate of heat loss, or radiance, W, (assuming a cosine law flux distribution) emitted from a warm surface at temperature, T, to a cooler surface, or environment, at T_o. The quantity, ϵ_T, is the radiant emissivity, or emittance, of the surface, and the quantity, σ, is the Stephan-Boltzmann constant. Values for ϵ_T range between 0 and 1, where, in a practical sense for an opaque solid, it can be said that the former value indicates a surface that reflects all incident radiation while the latter absorbs all radiation. Also included in Equation (4) is the approximate form of the radiation law; a form that is most convenient to use when the temperature rise, $T - T_o$, is small, as is the case here. The difference between the exact, 4th-power form and the approximate, linear form of the law is 4 percent for a temperature rise of 10 degrees centigrade above room temperature (300 deg. Kelvin). Within this error, the radiance emitted from a surface heated a few degrees above ambient will be proportional to its temperature rise, and thus will also be proportional to the square root of the time during heating ($W \propto t^{1/2}$).

B. Practical Formulation

The radiance, W, is the quantity that a radiometer actually senses. Usually, a radiometer system produces a signal voltage that is proportional to the radiance, and which in turn is correlatable with temperature. This conversion can be expressed by the relationship:

$$V = KW' \qquad (5)$$

where V is the radiometer output signal voltage and K is a constant that accounts for the transformation of the W′ entering the optics of the radiometer into a signal. W′ is analagous to W in (4), except that it includes the actual process occurring within most radiometers for producing a voltage; the usual mechanism consisting of a sensing element that alternately observes the external radiance of interest and a radiance emitted by an internal radiation reference source. The signal voltage corresponds to the difference between these two radiances. Importantly, ambient temperature is to be regarded as that of this reference source rather than room temperature; the difference usually being a few degrees. W′ is then expressed

as in Equation (4), but with T_o being replaced by the radiometer's reference temperature, T_o'. The significance of this shift in ambient, or reference, temperature is that a voltage history for a solid's surface will still correspond to its temperature history within the aforementioned error, so that characteristics of its parabolic shape will be preserved in the readout. Nevertheless, it must be recognized that a difference between T_o' and T_o will usually exist in practice, so that the location of the true vertex of any parabolic history that is generated will be suppressed by an amount equivalent to the sum of this difference and the minimum voltage necessary to distinguish a signal above inherent system noise, that is, radiometer response. A comparative approach, that is used in this development, normally makes it unnecessary to have knowledge of the location of the vertex; this being one of the most desirable facets of the method. However, if the period of interest of a history lies partially within this suppressed region, then a correction to the signal voltage must be made; the procedure for making this correction being only slightly cumbersome. These ideas may be seen more clearly in the mathematical development to follow.

The quantity, Q, in Equation (1) is the flux of heat absorbed at the solid's surface. The most practical means for delivering the Q to the surface in this method is by radiant heating. Letting a radiant source emit a flux F incident to the surface, Q and F can be related by the following expression:

$$Q = a_T F \simeq \epsilon_\lambda F \quad , \tag{6}$$

where a_T is the total radiant absorptance of the surface, and $\epsilon_T = a_T$ for opaque gray surfaces. An important assumption is now made to facilitate accounting for emissivity differences between surfaces; these differences oftentimes being large. Surface heating is presumed to be caused principally by the infrared wavelength region of the incident radiation spectrum. Both this IR region and the IR spectrum emitted by a surface, as its temperature increases from ambient, correspond to the sensible spectrum of the radiometer. Consequently, the approximation $\epsilon_T \simeq \epsilon_\lambda$ is made, where ϵ_λ is the emissivity within the detectible IR region.

One undesirable problem arising from radiant heating, and obvious from Equation (6), is that a certain fraction of the incident flux to the surface will be reflected into the optics of the radiometer. For opaque materials, the reflected component of F is expressible in terms of ϵ_λ using the following relationship:

$$r_\lambda = 1 - \epsilon_\lambda \quad , \tag{7}$$

where r_λ represents the radiant reflectance in the IR region. The self-emitted radiation from the solid's surface due to heating, W', is superposed on the reflected component, $r_\lambda F$, so that the radiometer signal voltage is the sum of these two components. The use of radiation filters can reduce the magnitude of the reflected component without affecting the self-emitted component appreciably. A less complicated and more satisfactory solution is to subtract from the total signal an amount equal to the reflected component, thereby leaving only the information-bearing, self-emitted component. Many radiometer systems feature a means for performing just such a subtraction.

By combining Equations (1), (2), and the W'-form of (4), (5), and (6), and solving for signal voltage the following expression obtains:

$$V = \frac{4 K \epsilon_\lambda \sigma T_o'^3}{\pi} \left[\frac{2 \epsilon_\lambda F}{\pi^{1/2} (k\rho C_p)^{1/2}} t^{1/2} - \delta \right] \qquad (8)$$

where $\delta = T_o' - T_o$. This equation incorporates the several practical aspects of the method into the theory. The δ-term accounts for the difference between the environmental, or room, temperature and the radiometer's reference source temperature. Its importance lies in the relation it has to the $t^{1/2}$-term. For observability of a history, V must be positive, so that the magnitude of the $t^{1/2}$-term must be greater than that for the δ-term. The effect of δ on the shape of the history is then to suppress the vertex of the parabola below an observable signal level. It will have no effect on the characteristic shape of a parabolic history after a period of time, t, equal to $\pi (k\rho C_p) \delta^2 / 4 \epsilon_\lambda^2 F^2$. Vertex suppression will usually be a most important consideration when the thermal inertia, $(k\rho C_p)$, for a material is large, and/or the incident radiant flux and surface emissivity are small when compared with t; the net effect being to produce a "weak" signal voltage.

Only two situations of interest will arise from Equation (8), both of which result in a comparative method for measuring $(k\rho C_p)$; one case being where δ can be neglected, and the other where it must be considered. The former case will be discussed first and the latter case is described in detail in Appendix III and will be outlined only briefly here. Equation (8) can be written equivalently as:

$$V_{t_a} = C_a t^{1/2} - V_A \qquad (9a)$$

and

$$C_a = \frac{8KF\sigma T_o'^3}{\pi^{3/2}} \cdot \frac{\epsilon_{\lambda_a}^2}{(k\rho C_p)_a^{1/2}} \qquad (9b)$$

where V_{t_a} represents the signal level at a time, t, after initial incidence of the flux to solid "a's" surface, and C_a is a proportionality constant for a particular set of experimental conditions (K, F, and T_o) for solid a. V_A represents the signal that corresponds to the temperature difference between ambient and the radiometer's reference source. It is presumed that the reflected component has been subtracted from the total signal received by the radiometer, so that only the self-emitted component remains. V_A is noted to be the value of V_{t_a} at t = 0 and is the magnitude of the vertex suppression. Equation (9) states, in part, that the self-emitted signal level is inversely proportional to the square root of the thermal inertia. A material, such as copper, which has a high inertia value, will then cause a smaller signal to be generated than that from a material such as lead, which has a lower inertia value, if all parameters including their emissivities are identical. A higher flux and/or a higher emissivity will also increase the magnitude of a signal, i.e., the width of the parabola.

C. The Comparative Relationships

At any two points in time along a history curve, the signal voltage difference will be:

$$V_{t_{a_2}} - V_{t_{a_1}} = C_a \left(t_2^{1/2} - t_1^{1/2}\right) , \qquad (10)$$

where $t_{a_2} > t_{a_1}$. A second solid, labelled "b", will give rise to an analagous relationship, so that their voltages can be compared, in the same time interval and for identical experimental conditions, in the form of the following ratio:

$$\frac{V_{t_{a_2}} - V_{t_{a_1}}}{V_{t_{b_2}} - V_{t_{b_1}}} = \left(\frac{\epsilon_{\lambda_a}}{\epsilon_{\lambda_b}}\right)^2 \cdot \frac{(k \rho C_p)_b^{1/2}}{(k \rho C_p)_a^{1/2}} . \qquad (11)$$

Equation (11) constitutes the basis of the comparison method. The emissivity ratio accounts for differences existing between materials; this quantity being readily measurable, as will be described. Thus, a measurement of the voltage difference between a selected time interval for a material of interest will yield its inertia value when it is compared with a corresponding difference for a standard material. Moreover, Equation (11) can be restated in terms of voltage differences to yield the following comparative expressions for thermal conductivity and thermal diffusivity:

$$\frac{k_a}{k_b} = \left(\frac{\epsilon_{\lambda_a}}{\epsilon_{\lambda_b}}\right)^4 \frac{(\rho C_p)_b}{(\rho C_p)_a} \left[\frac{V_{t_{b_2}} - V_{t_{b_1}}}{V_{t_{a_2}} - V_{t_{a_1}}}\right]^2 , \qquad (12a)$$

$$\frac{a_a}{a_b} = \left(\frac{\epsilon\lambda_a}{\epsilon\lambda_b}\right)^4 \frac{(\rho C_p)_b^2}{(\rho C_p)_a^2} \left[\frac{V_{t_{b_2}} - V_{t_{b_1}}}{V_{t_{a_2}} - V_{t_{a_1}}}\right]^2 \quad (12b)$$

To completely determine these two quantities, however, it is evident that the volumetric heat capacity, (ρC_p), of the material of interest must be known. Other nondestructive test methods can be used to determine localized density values, and C_p is an atomic or molecular quantity and can be predetermined for the particular chemistry involved in the material. For manufactured graphites, C_p can be considered constant when comparing either two sections of the same grade or of different grades, (Reference 3).

D. Correction for Suppressed Vertex

It is particularly emphasized that the expressions in Equations (11) and (12) necessarily require the voltage differences measured to be in an interval entirely unaffected by suppression of a parabola's vertex. For a situation that results in a voltage difference being only partially observable within the time interval of interest, a correction must be made to this voltage. Graphic illustrations of the nature of vertex suppression and those geometries that require signal correction are shown in Figures 1 and III-1. Using geometrical characteristics of a parabola, a relationship has been developed, in Appendix III, which accounts for that portion of the voltage difference that would lie below a zero signal level, and which cannot be observed. This relationship is:

$$V_C + V_D = (V_A + V_D) \left[1 - \left(\frac{t_1}{t_2}\right)^{1/2}\right], \quad (13)$$

where V_D is the measured voltage deflection, and V_C is the voltage correction to be added to V_D to give the corrected quantity $(V_C + V_D)$ that can be compared with either a suppressed or an unsuppressed voltage difference for the standard. The measurable quantity, V_A, is the voltage-deflection equivalent of the temperature difference between ambient and the radiometer reference source, and it locates the vertex of the parabola below zero signal at t = 0. Consequently, for comparing a suppressed history with a normal history, $(V_C + V_D)$ will replace the $(V_{t_2} - V_{t_1})$ -term in Equation (11) for the material of interest; this also being the case for the conductivity and diffusivity relationships in Equation (12).

Equations (1) through (13) constitute the mathematical foundation of the comparative method. The two principal underlying premises in this

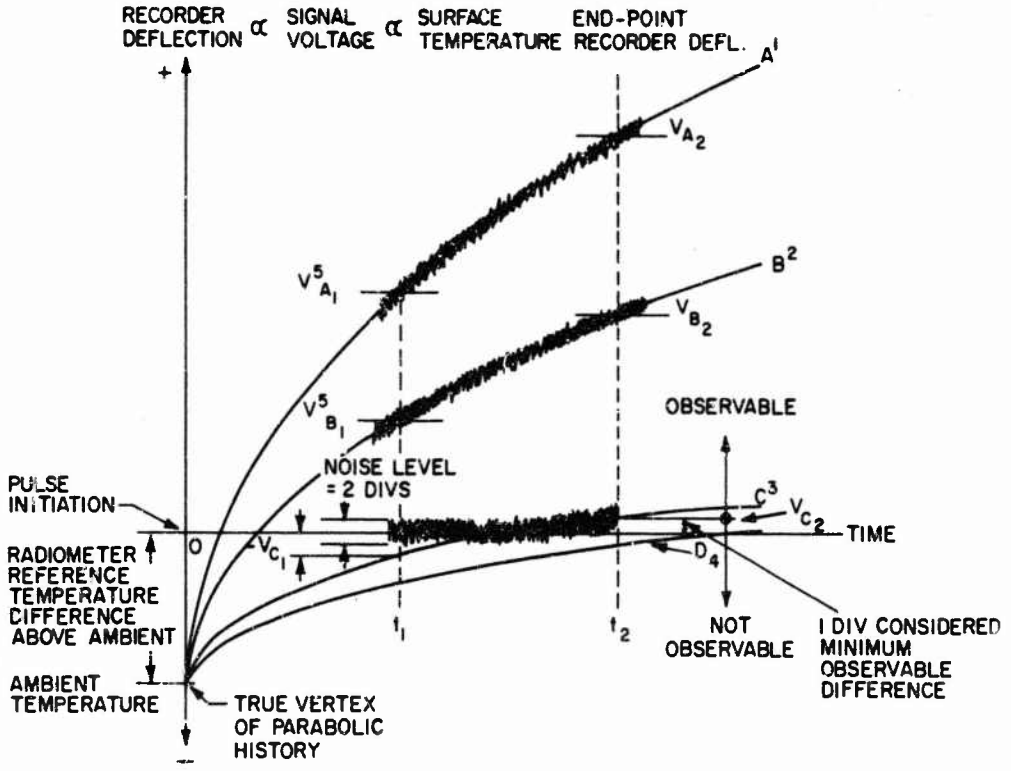

NOTES:

1. THE DEFLECTION DIFFERENCE, $V_{A_2}-V_{A_1}$, IS COMPLETELY OBSERVABLE. NO CORRECTION FOR VERTEX SUPPRESSION IS NECESSARY.

2. SAME AS ABOVE NOTE FOR THE DIFFERENCE, $V_{B_2}-V_{B_1}$

3. THE DEFLECTION DIFFERENCE, $V_{C_2} - 0 = V_{C_2}$, IS OBSERVABLE IF EQUAL TO 1 DIVISION OR GREATER. THE TRUE DEFLECTION DIFFERENCE MUST INCLUDE THE CORRECTION TERM, $-V_{C_2}$, WHICH ACCOUNTS FOR THE SUPPRESSION CAUSED BY THE DIFFERENCE BETWEEN THE RADIOMETER REFERENCE AND AMBIENT TEMPERATURES. THE TRUE DEFLECTION THEN EQUALS $V_{C_2} - (-V_{C_1}) = V_{C_2} + V_{C_1}$, RATHER THAN THE OBSERVED 1 DIVISION

4. CURVE D IS TOTALLY UNOBSERVABLE SINCE IT FALLS BELOW THE SIGNAL NOISE LEVEL AT LEAST UNTIL THE TIME t_2.

5. THE DEFLECTIONS V_{A_1}, V_{B_1} ARE USED AS ORIGINS IN DETERMINING THE CORRESPONDING V_{A_2}, V_{B_2} DEFLECTIONS, THAT IS, V_{A_2}, V_{B_2} WILL EACH BE A DEFLECTION ABOVE THEIR V_{A_1}, V_{B_1} VALUES.

7713410

Figure 1. GRAPHIC ILLUSTRATION OF SEVERAL HISTORIES TO DEMONSTRATE THE DEGREE OF OBSERVABILITY AND THE ORIGIN OF THE RADIOMETER REFERENCE TEMPERATURE VOLTAGE CORRECTION

foundation are that the solid must appear semi-infinite in extent during heating and that the radiometer signal voltage must nearly be proportional to surface temperature rise when the effect of reflected radiation is excluded. If the dimensions of a solid cause it to appear finite, then a temperature history will be generated that exhibits a shape different from that of a parabola. This shape will be functionally related to time by a power greater than one half. As a result, a comparison of finite and infinite histories will result in an inertia value that is apparently less than expected. This apparent smaller value of inertia can also arise when the approximate linear relation between voltage and temperature is violated, such as would occur when excessive radiant flux causes too great a surface temperature rise. It must be appreciated, however, that resultant history distortions, due to temperature-signal nonlinearity, can be corrected back to a common temperature base and then compared in a manner analagous to that described.

E. History Analysis

Before a generated history curve is segmented to yield a voltage difference in a selected time interval, the curve must be shown to be parabolically shaped. Otherwise, as just described, an incorrect and smaller value for $(k\rho C_p)$ will result. Since the vertex of a history will be suppressed for all radiometric systems that contain a reference source at a temperature greater than ambient, a question arises as to a convenient means for determining curve shape. One scheme for accomplishing this could consist of constructing a set of identifiable parabolic curves that span a range of latus recta for a particular recording speed, and which can be overlayed on an experimental curve. This approach, however, tends to be both cumbersome and inherently inaccurate; the inaccuracy arising from the several situations of vertex location and latus recta that will exhibit very similar over-all curvatures.

A simple and accurate technique has been developed for verifying curve shape and determining the latus rectum. This technique takes advantage of both the one property common to all parabolas and the unique characteristics of logarithmic display. This is to say, a graphical presentation of any complete parabolic history on logarithmic scales will always result in a straight line having a slope equal to one half, but only if the true value of amplitude is known; this, unfortunately, requiring knowledge of the location of the vertex. However, knowledge of the true value of amplitude is unnecessary for determining curve shape using this manner of presentation. Since the time from initiation of the radiant flux to a solid's surface is one parameter that is accurately known, a segment of a history within any time interval will always result in a characteristic shape, as displayed logarithmically, which is dependent only on the time that has elapsed to this segment. It is then necessary to plot a few relative values of amplitude

on logarithmic scales and then overlay the curve shape that corresponds to the time that has elapsed to this segment.

In illustration of this analytical approach, a family of curves, which are common to any parabolic function, is displayed on log-log scales in Figure 2. A straight line of slope equal to one half has been arbitrarily located on the recorder deflection-time axes (recorder deflection being directly related to radiometer signal voltage). The family of curves lying below this line are all derived from it and represent curve shapes for parabolic history segments beginning at the times noted after heat pulse initiation. For example, if a time interval between 1 and 4.5 seconds after pulse initiation is of interest, the relative deflection from the straight line, beginning at 1 second, is plotted; this corresponding to the curve labelled as the 1 second time base. Thus, a few relative deflection values taken from any experimentally-generated parabolic history between this time interval, and then plotted on similar logarithmic scales, will result in a curve shape identical to that from theory for a 1 second time base. By aligning the theoretical time base curve with experimental points plotted on a second graph, the actual straight line function for the experimental parabola can be located on the recorder deflection axis; thereby, making possible a direct comparison of latus recta, or inertia values.

Shown in Figure 3 are curves for time bases of 0.9, 1.0, and 1.1 seconds for a parabolic function. This illustrates the range of curvature that will result if an error of 0.1 second from pulse initiation is made in selecting the beginning of the history segment in the 1 to 4.5 second interval. This error, of course, will be translated into a corresponding error for an inertia value.

As a consequence of vertex suppression, low signal-to-noise ratio, finite geometry, and/or excessive radiant flux level, an experimental history segment may exhibit little curvature. A logarithmic plot of this segment will result in a curve that has a much steeper slope than normal for the same time base. To obtain a measure of the degree of the function from which this segment arises, a family of theoretical time base curves for a linear function (slope = 1) is shown in Figure 3. Very likely, logarithmic plots of history segments for anomalies, such as mentioned, will lie between the time-base curves derived from the parabola and the straight line. Ideally, then, history segments will appear as those shown in Figure 2 for the parabola. The more closely a segment aligns with the curves shown in Figure 4, the more likely an irregularity exists and the smaller will be the inertia value obtained by comparison with an ideal standard material.

III. Experimentation

The experimentation was designed with two distinct purposes in mind. Since

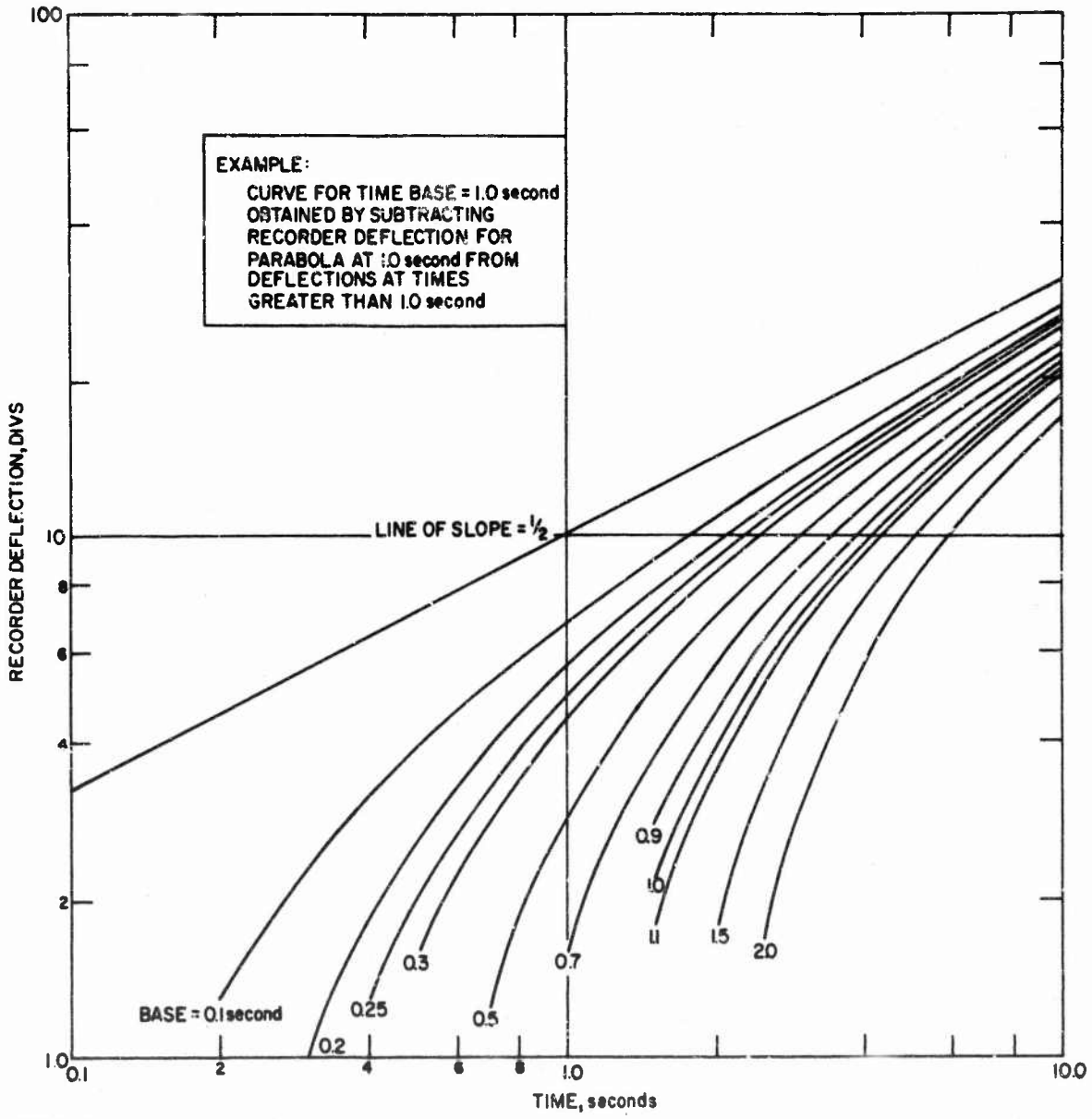

Figure 2. THEORETICAL CURVES FOR SEVERAL TIME BASES FOR A PARABOLIC FUNCTION

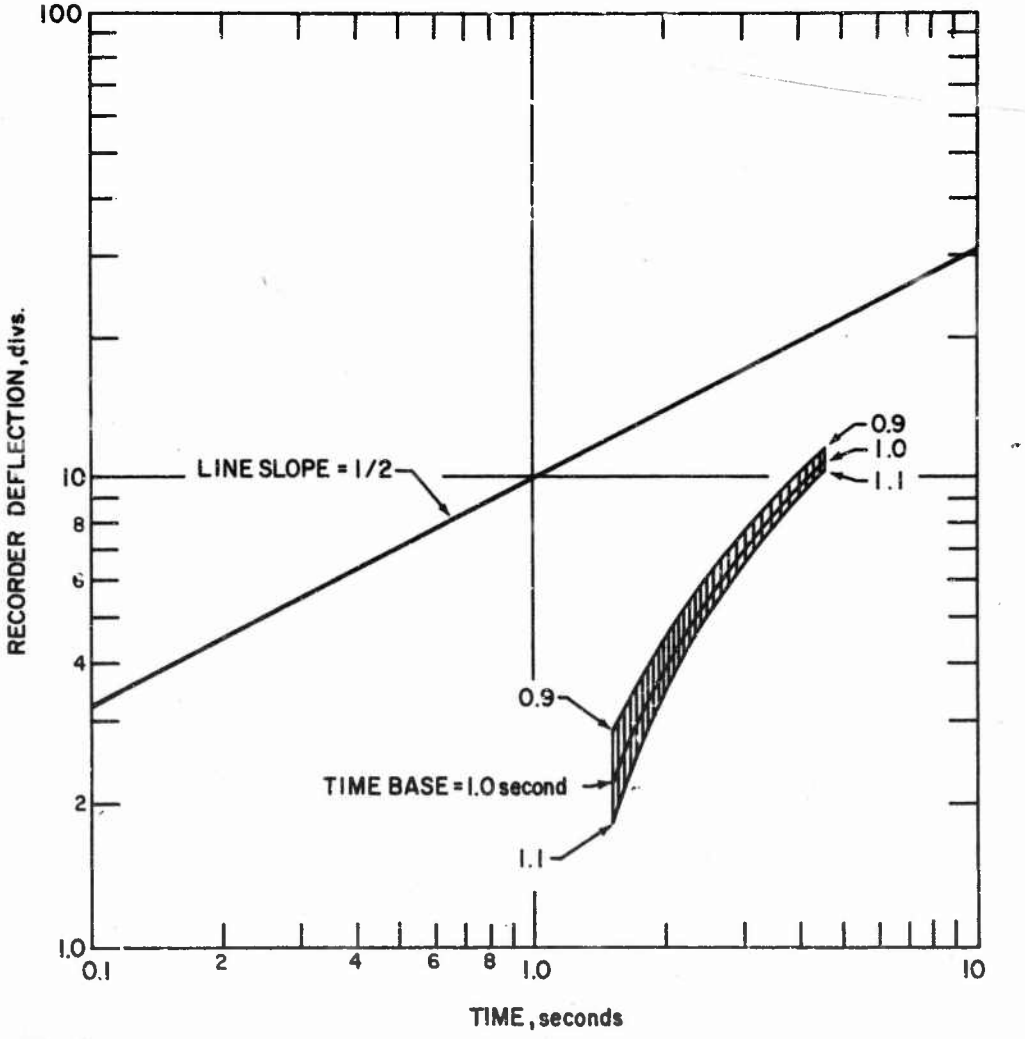

Figure 3. RECORDER DEFLECTION RANGE FOR A TIME DIFFERENCE OF 0.1 SECOND AT A TIME BASE EQUAL TO 1.0 SECOND FOR A PARABOLIC FUNCTION

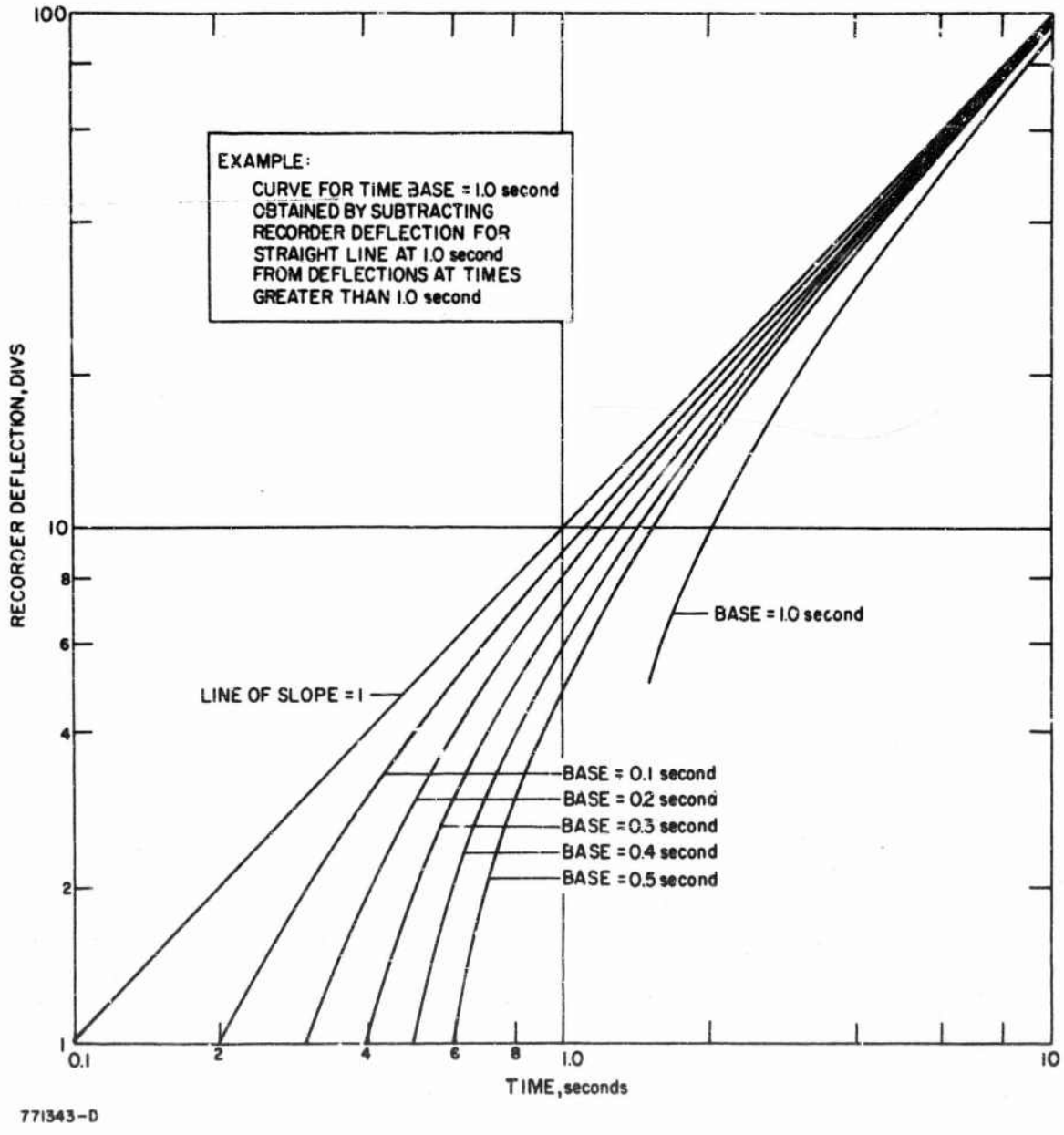

Figure 4. THEORETICAL CURVES FOR SEVERAL TIME BASES FOR A STRAIGHT LINE FUNCTION

the method is believed to be novel, the first and most important intentions were to provide sufficient evidence of its validity and determine its limitations. Emphasis was then placed on graphite, because of current interest in this material, to indicate the feasibility of determining its $(k\rho C_p)$, and k, as well as their variabilities, using present techniques. Improved apparatus has been constructed with an aim toward increasing over-all sensitivity, measurement precision, and accuracy; this being a continuing effort in the course of these studies. The apparatus will be described.

A. Basis for Method Evaluation

To lend credence to the method, the approach taken has been to demonstrate that parabolically-shaped histories are indeed generated in accord with theory, and that results of comparison measurements for $(k\rho C_p)$ agree, within reason, with values reported by other investigators. Since constraints are placed on the method by the theory, such as that of semi-infiniteness, these have been tested to a degree in order that limitations can be assessed and additional facets of the theory can be tested.

A family of test specimens were fabricated to provide a basis for method evaluation. Materials selected for study included copper, 2024-aluminum, grain-oriented ATJ-graphite, 1010-steel, and 96-4-hard lead, because of the broad range of pertinent property values that they span in the high-k region near that of graphite. Densities range from about 1.7 to 11 gm. per cu. cm., specific heats from 0.03 to 0.2 cal. per gm.-deg. C, thermal conductivities from 0.07 to 0.9 cal. per cm.-sec.-deg. C, and $(k\rho C_p)$ values from about 0.02 to 0.7 cal.^{2} per cm.^{4}-sec.-deg. C^2. Armco iron was selected as the standard material because its $(k\rho C_p)$-value lies within the range tested and because of its generally wide acceptance as a standard material in thermal measurement studies. Near room temperature property values for these materials are listed in Table I and represent the most consistent set of values found in the literature; it being recognized that reported k-values, in particular, for materials such as these differ in their extremes by as much as 50 percent and more. The geometries of the family of test specimens were all cylindrically-shaped and ranged in size from 1 to 2 inches in diameter and from 1/4 to 1 1/2 inches in thickness. These sizes were estimated to provide finite and semi-infinite conditions within a particular time interval that was dictated by experimental limitations, which will be discussed.

Additional specimens of ATJ graphite were fabricated to provide a means for demonstrating the ability of the method to distinguish variability in thermal conductivity. The geometry for these specimens was a 1-inch cube; the cubes being grain-oriented and selectivity extracted from a billet to give a representative range of density values. This geometry constitutes "finite" dimensions with respect to the history time interval selected. Because of

TABLE I

MATERIAL PROPERTIES (Near Room Temperature)

Material	Density (gm/cm^3)	Specific Heat C_p (cal/gm-°C)	Thermal Conductivity k (cal/cm-sec-°C)	Calculated[6] (k C_p) (cal^2/cm^4-sec-$°C^2$)	Calculated[6] $(k\ C_p)^{1/2}$ (cal/cm^2-$sec^{1/2}$-°C)
Copper	8.93[1]	0.092[2]	0.91[2]	0.746	0.86
Aluminum (2024)	2.78[1]	0.203[2]	0.44[2]	0.299	0.55
Graphite (ATJ, AG. GR)	1.73[1]	0.172[3]	0.21[3] 0.4[4]	0.063 0.12	0.25 0.35
Steel (1010)	7.88[1]	0.105[2]	0.153[2]	0.127	0.36
Armco Iron	7.87[1]	0.107[2]	0.175[2]	0.147	0.38
Lead (96 Pb-4Sb)	11.03[1]	0.031[2]	0.073[5]	0.025	0.16

1. Measured at Avco SSD
2. "Thermo-Physical properties of pure metals, alloys, non-metals and plastics," Avco Corp. Tech. report, RAD-TR-2-58-20, December 1958
3. Industrial Graphite Engineering Handbook, National Carbon Co. (Continuously updated).
4. Conductivities of this magnitude have been reported in several places.
5. Metals Handbook, Eighth Ed., 1, P. 1065
6. Calculated by taking the product of k, ρ, and C_p.

this finiteness, the density effect on thermal conductivity, and consequently on inertia and signal voltage, can be eliminated if it is assumed that density variability is negligible within each cube.

B. Apparatus

A schematic diagram of the most recent experimental arrangement that has been used to measure $(k\rho C_p)^{1/2}$ is shown in Figure 5. The radiant source consists of 2 Type CYS, 1200 watt, projection lamps; each lamp being focussed by means of an ellipsoidal, front surface, aluminum mirror having a 6-inch aperture and a 2-inch principal focus. The lamps are focussed into a radiation collector-homogenizer-intensifier unit, located 7 1/2 inches from each lamp, in a manner that produces maximum flux intensity at its exit port. This unit consists of a large aluminum block into and through which has been machined a funnel shape having dimensions comparable to that of a 125 ml erlenmyer type flask. The surface of this funnel shape is highly polished. By focussing the lamps into the entrance port of the collector (corresponding to the base of a flask), the radiation is reflected many times from the walls, thereby becoming homogenized to a great extent, and then becoming concentrated into a circular area of diameter equal to 7/8-inch at the exit port (corresponding to the neck of the flask). Since surface reflection is not total, the block must be large to serve as a heat sink, thereby contributing little additional transient infrared radiation to the exit flux. The lamps are operated in parallel through a variable transformer, and at 120 volts, they combine to deliver, for optimum focus and steady state conditions, approximately 6 calories per sq. cm. per. sec. (equivalent to about 120 watts per sq. in.). Cooling of the lamps is not required since their duration of operation does not exceed 15 seconds. Homogeniety of the output flux is estimated to be within a few percent as evidenced by burn density patterns on sensitized paper. The area of a specimen's surface to undergo heating is placed a few mils from the exit port.

Dual, simultaneously actuated, sliding scissors shutters are placed in front of the entrance port to the collector-intensifier unit and in front of the infrared radiometer. The principal purposes for using such a shutter are to obtain as nearly a constant flux as possible incident to a specimen and to protect the detection element within the radiometer against excessive irradiation. This is accomplished by delaying the opening of the shutters until the lamps have reached a steady radiant output (including the infrared radiation emanating from the lamps' glass envelopes). Because of this initial delay, the collector-intensifier shutter is provided with cooling fins to prevent possible self-emitted infrared radiation from entering the collector and adding heat to the specimen prior to actuating the shutters. The shutters are simultaneously actuated by means of two, intermittent-duty, 1-inch stroke, 145 lift ounce solenoids, and are closed using a mechanical spring return. The shutter

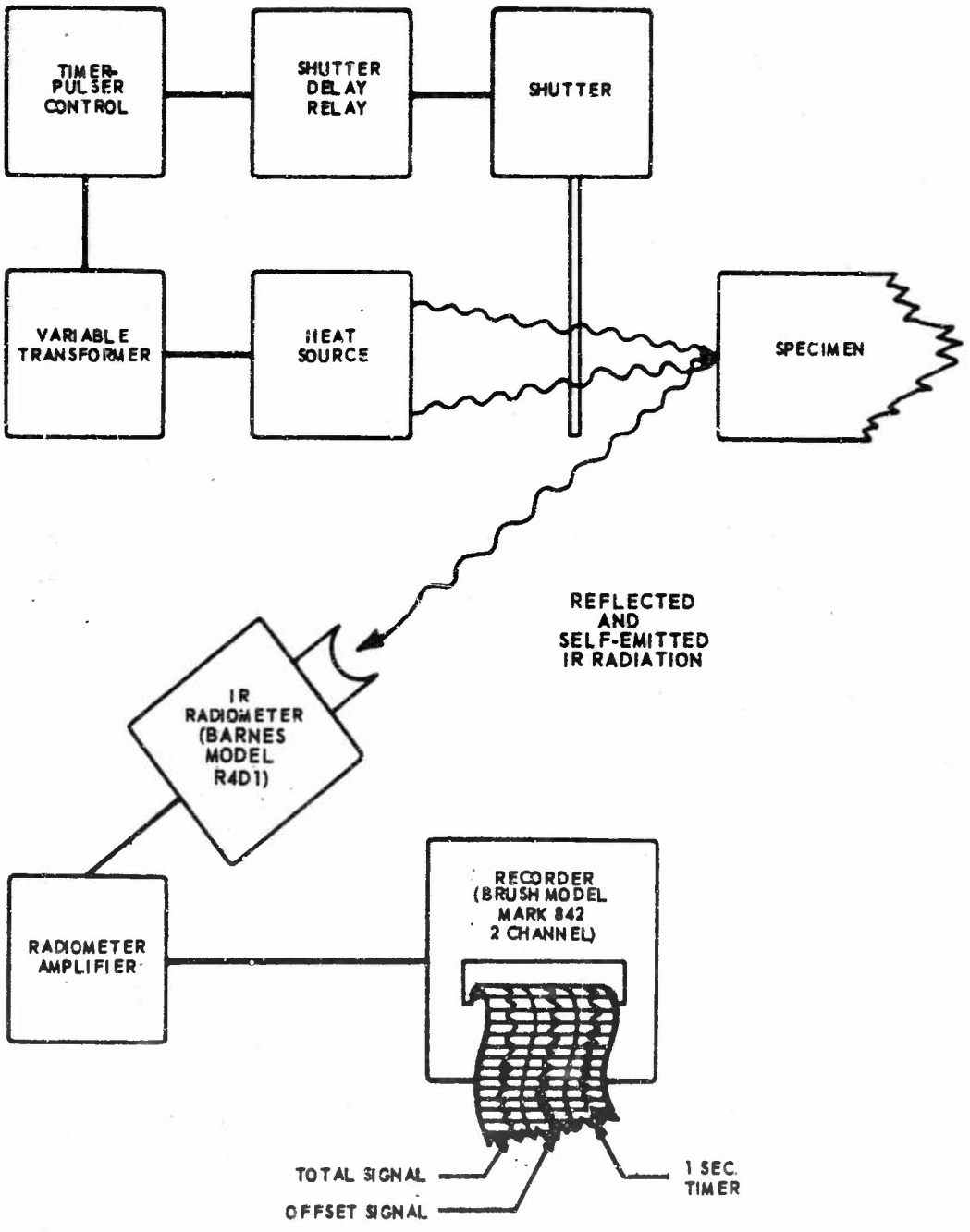

770363 D

Figure 5. SCHEMATIC DIAGRAM OF THE EXPERIMENTAL ARRANGEMENT USED TO MEASURE THE THERMAL PARAMETER ($k\rho\ c_p$)

aperture geometry is diamond-shaped to provide heating from the center of the area outward and fully opens in approximately 80 milliseconds.

The solenoids are energized through a precision, 0.2 to 15.0 second, pneumatic-type, time delay relay, which in turn is activated by a precision, electronic interval timer. The delay time set on the solenoids' relay will be the pulse length desired to heat the specimen. The time set on the interval timer corresponds to the sum of this heat pulse length and the length of time necessary for the lamps to reach a steady state output. Typically, the lamps reach a constant output after 4.5 seconds, and the heat pulse duration to the specimen is 5 seconds, so that the total elapsed time for a test is 9.5 seconds; this period being set into the interval time.

The infrared detection instrument used was a Barnes Engineering Co., Industrial Infrared Radiometer, Model R4D1. The infrared wavelength band passed by its filter is nearly linear from 1.8 to 25 microns (a peak wavelength of 10 microns for a Planck's black body radiation distribution corresponds nearly to room temperature). The radiometer exhibits two features that are desirable for this application: (1) its response time is as fast as 10 milliseconds; and (2) it can be easily focussed to a circular field of view having a diameter as small as 1/16-inch at a target-detector distance of 30 inches. The importance of having a small field of view is that the area undergoing heating can then be relatively small. This is to say that the area being heated should be several times larger than the central area being observed, so that plane parallel heat flow into the solid can be nearly realized.

The radiometer also exhibits two undesirable limitations in that: (1) its initial temperature response near ambient is approximately 5 deg. C; this being a consequence of the normal running temperature of its internal reference source; and (2) its peak-to-peak noise equivalent temperature is approximately 1 deg. C, which results in a useful sensitivity of 0.5 deg. C (assuming that a signal-to-noise level equal to 0.5 is observable over a reasonable span length). The 5 deg. C initial response implies that only surface temperatures exceeding this amount are observable (neglecting noise); this giving rise to the cause of vertex suppression of the parabolic histories.

All voltage histories were recorded using a Brush Instrument Co., Model 13-6624-00, dual channel, plug-in amplifier, recorder. The maximum sensitivity for the d.c. amplifier is 100 microvolts per division over dual, 50 division channel charts. Two desirable features of this recorder are: (1) it provides variable chart speeds up to 200 mm. per sec, affording flexibility in readout analysis; and (2) one plug-in amplifier contains a calibrated zero suppression, or voltage offset control, making possible elimination of the reflected radiation component entering the optics of the

radiometer by simple voltage subtraction. This offset channel permits the self-emitted, information-bearing component to be observed with optimum sensitivity; the second channel being used to observe the superposed, two-component signal. As will be described, a surface's emissivity is measured using this superposed signal. Timing accuracy of a history is made possible by a 1 second time-mark trace included in the chart readout.

C. Specimen Preparation

All flat surfaces of the cylindrical- and cube-shaped specimens were machined to have smooth finishes. Their reflectances to lamp radiation were high, so that little absorption, and thus heating, was possible. As a result, all surfaces measured were first cleaned and then coated with a high emissivity material to increase heating. The coating material selected was 3M Brand, Black Velvet Coating, No. 101-C10, which is purchased in a spray container. Its emissivity was determined to be 0.96. It is to be recognized that inherently low-k coatings, such as this, when applied to high-k materials tend to inhibit heat flow; the observed effect of this thermal resistance being to initially distort the shape of the temperature history. However, this distortion can be neglected after a suitable time delay, so that its principal advantage of increasing heating outweighs several of its disadvantages; one obvious disadvantage of using any coating being the control problem for applying it to a surface. In this method, coatings should be applied both uniformly and sparingly. For this study, only reasonable care in applying coatings was taken, so that variability in thickness will constitute a significant portion of measurement precision. The average coating thickness applied was estimated to be approximately 10^{-4} cm. for "1 coat". This descriptive unit of measure for thickness was used in reporting results and will be understood to mean two "light" spray passes; one being perpendicular to the other.

D. Procedure

Before the method itself can be evaluated, an experimental technique must be established which reasonably satisfies certain critical aspects required and implied by the theory. These aspects must be assessed in terms of their being affected by test conditions such as the degree of linearity that exists between temperature and signal voltage rise, the correction required for differences in emissivity, the optimum time delay between lamp energization and shutter activation to achieve a constant radiant flux, the degreeof history distortion caused by coatings, the optimum time interval for analyzing a family of histories, and so forth. Once these effects have been resolved, a particular technique can be characterized for a set of experimental conditions and then can be discussed in terms of its limitations for measuring material properties.

Method evaluation first consists of comparing experimental results with theory to show essentially that the results are within the concept of the theory, and hence are predictable to a degree. To accomplish this requires that specimen geometries be ideal, or appear semi-infinite in extent for a selected history analysis interval, so that specimen dimensions are parameters requiring study to determine those minimum dimensions that can be regarded as equivalent to semi-infiniteness. Next, the precisions of the measurements must be determined for ideal specimens to afford a means for establishing test significance (the accuracy of measurement is essentially directly related to that of the standard material, since the method is comparative; this being discussed later).

To evaluate the method in its ability to measure the inertia and conductivity of graphite, as well as to discuss differences in its conductivity, finite-size specimens must be used in order to eliminate the k -dependency on density. These results must then be interpreted in terms of their application to ideal specimens.

E. Analysis

To illustrate typical histories generated by the system, simulated recordings of the superposed reflected and self-emitted radiation components, and of just the self-emitted component, for a semi-infinite, coated graphite specimen, are shown in Figure 6. Pertinent characteristics are noted in the figure. The radiometer's 1/16 inch diameter field-of-view is focussed at the center of the 7/8 inch diameter area undergoing heating to produce these histories. The superposed history, in Figure 6a, is used to determine the emissivity correction for the coated specimen; the correction being a relative one, which serves to normalize the flux absorbed at the surface to a constant value. This correction is determined by simply measuring the amplitude of the signal at the characteristic minimum, which occurs after an initial system transient and at approximately 1/4 second after pulse initiation, that is, after shutter actuation. This minimum point corresponds very nearly to the value of the constant reflected signal. From other reflection measurements made on opaque surfaces having known values of reflectivity, a graph of a correction factor as a function of reflected amplitude has been prepared for this technique, and is shown in Figure 7; the derivation being given in Appendix IV. This correction factor, K_{Ry}, multiplies the measured recorder deflection (the magnitudes of which will be described in units of chart divisions rather than volts) in a selected interval on the self-emitted radiation history to give a corrected and normalized value of heating deflection. An illustrative calculation is included in the figure. It is to be noted, for instance, that a 10 division difference in the reflected signal necessitates a correction of only 4 percent; a 10 division difference being unusually large for the coatings used.

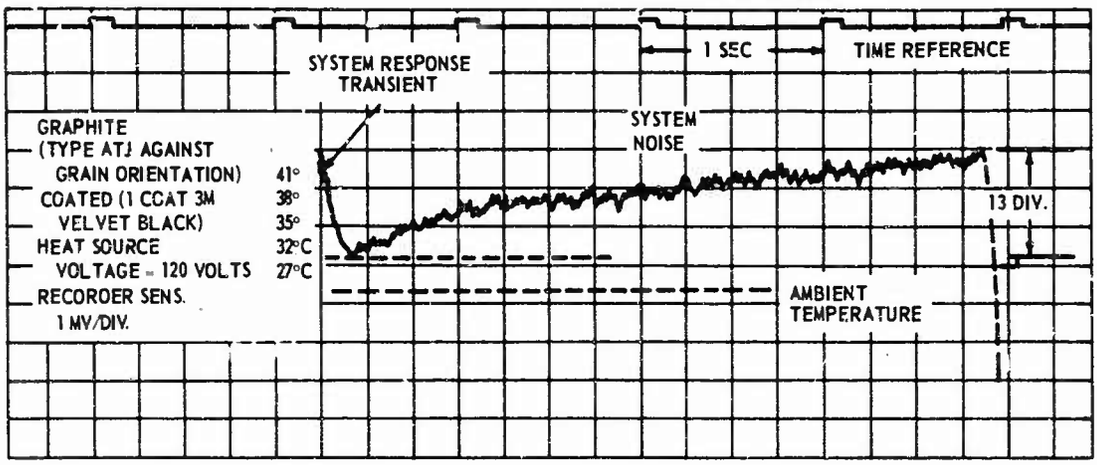

Figure 6b. SELF-EMITTED RADIATION HISTORY (VOLTAGE AMPLIFICATION OF IR RISE IN FIGURE 6a)

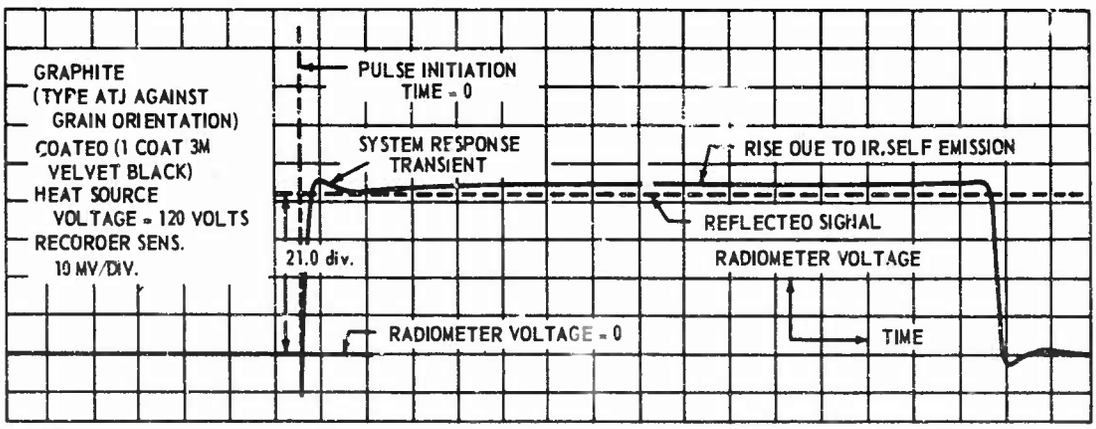

77036ID-1

Figure 6a. TOTAL INFRARED RADIANT SIGNAL RECEIVED BY RADIOMETER (REFLECTED PLUS SELF-EMITTED COMPONENTS)

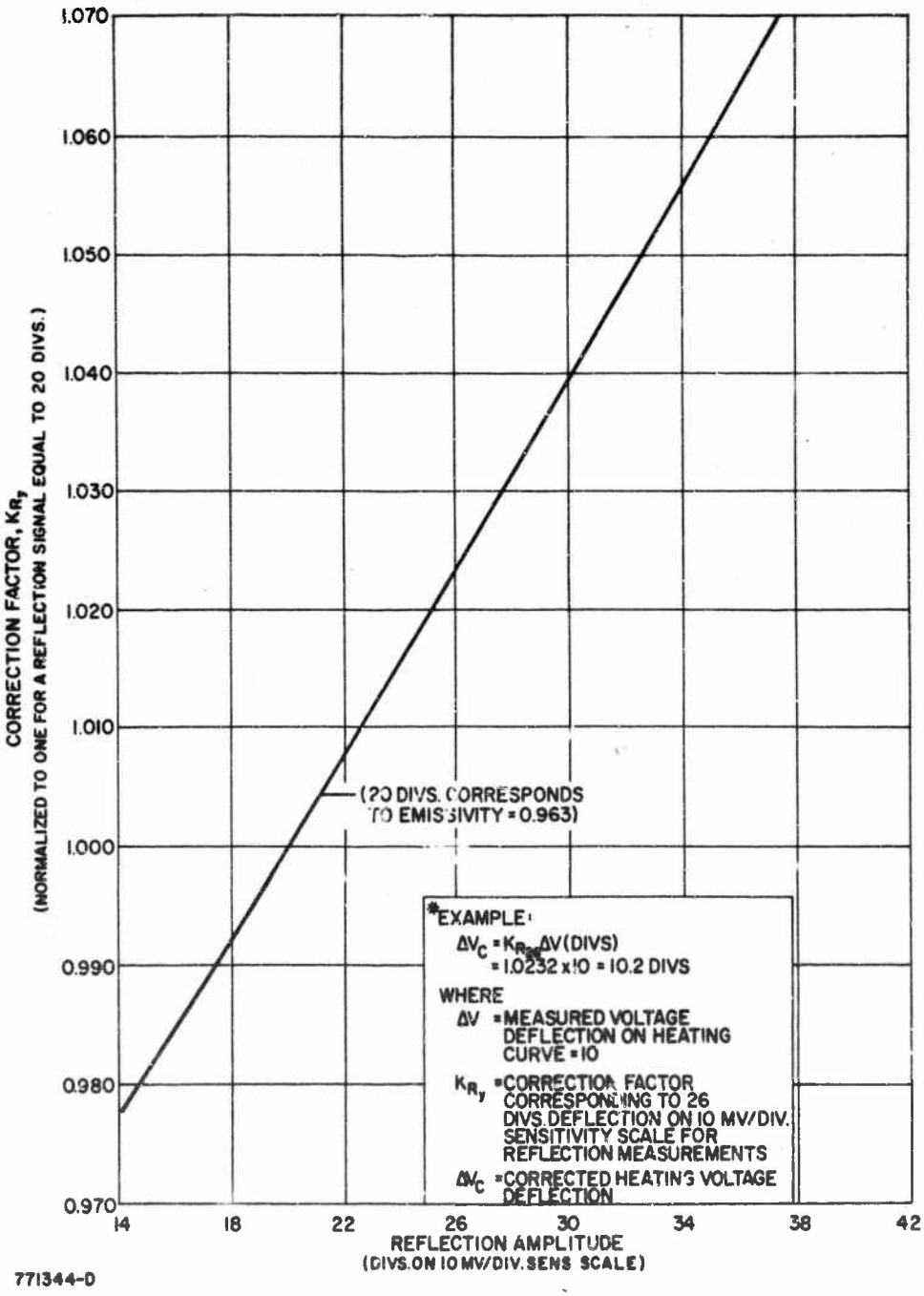

Figure 7. EMISSIVITY CORRECTION FACTOR, K_{R_y}, AS A FUNCTION OF REFLECTION AMPLITUDE

One practical requirement of the theory is that radiometer signal voltage be linearly related to surface temperature rise, so that parabolic shapes will obtain. An assessment of the degree of this linearity is shown in Figure 8. The constant reflected radiation component corresponds to a certain temperature above ambient. For a 20 division reflected recorder deflection (equal to a 400 mv. radiometer signal), this temperature equals 249 deg. C, as determined from calibration characteristics of the radiometer and indicated in the graph. Riding on top of the reflected signal is the self-emitted component, and recorder deflections for this component is plotted as a function of temperature, again using characteristics of the radiometer. In the chart's channel range of 50 deflection divisions (on a scale that is 10 times as sensitive as that used for recording the superposed signal), which corresponds to a temperature rise of about 25 deg. C, the linearity is noted to be ±0.5 deg. C, or ±1 division. This is to say, a self-emitted temperature history will be faithfully reproduced by the recorder to ±0.5 degree C for full scale deflection, or to a measurement accuracy of ±0.5 x 100/25 = ± 2 percent. Inherent linearity of the radiometer's detector output within a 25 degree C range improves this measurement accuracy for recorder deflections less than full scale. Similar linearity is evidenced in the figure for two other values of reflected signal.

It is to be realized that temperature-signal linearity is a very desirable requirement, but is not necessarily mandatory for achieving successful results. If linearity obtains then one parabolically-shaped history can be easily compared to another on the basis of recorder deflection alone. If nonlinearity obtains then histories must first be translated into some common basis before they can be compared; the original basis being that of temperature.

F. Technique

Theory requires that the radiant flux to the solid's surface be constant during the period of simultaneous heating and observation. Since the heat source consists of filament lamps, a period of time is required, after voltage is applied, before the lamps can produce a steady radiant output. The total radiation emanating from a lamp consists of that from the filament and that from the glass envelope. The filament attains a steady output within 2 seconds after being energized at 120 volts. The glass envelope attains a state output within 1 to 2 seconds after the filaments. These periods were determined using the radiometer and observing the filament through the envelope and then observing just the envelope itself. A delay of 4.5 seconds, before opening the shutters, was thus selected to insure that the source output was constant.

Self-emitted histories for several coated solids of interest have been superposed on an enlarged scale, in Figure 9, as an illustration of the

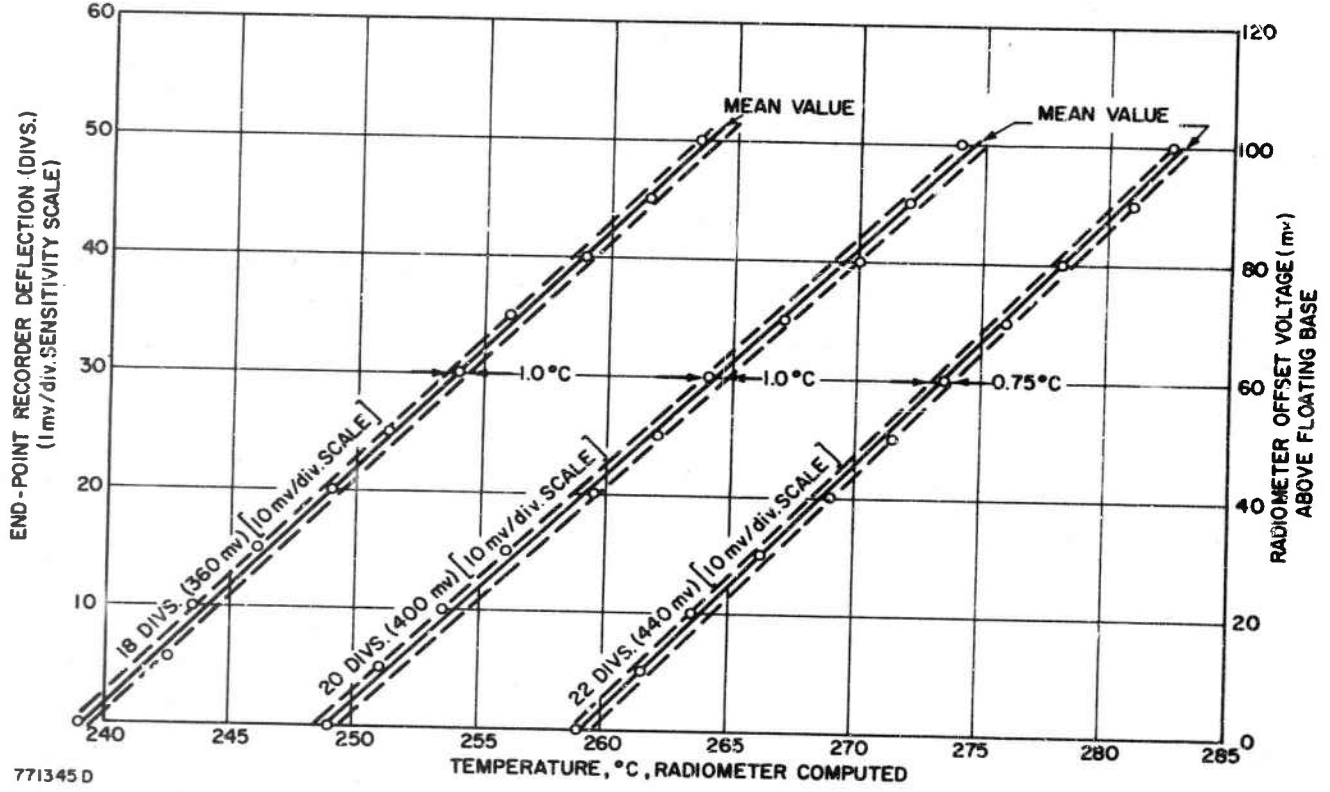

Figure 8. RECORDER OFFSET DEFLECTION VERSUS SURFACE TEMPERATURE FOR THREE VALUES OF REFLECTED RADIATION

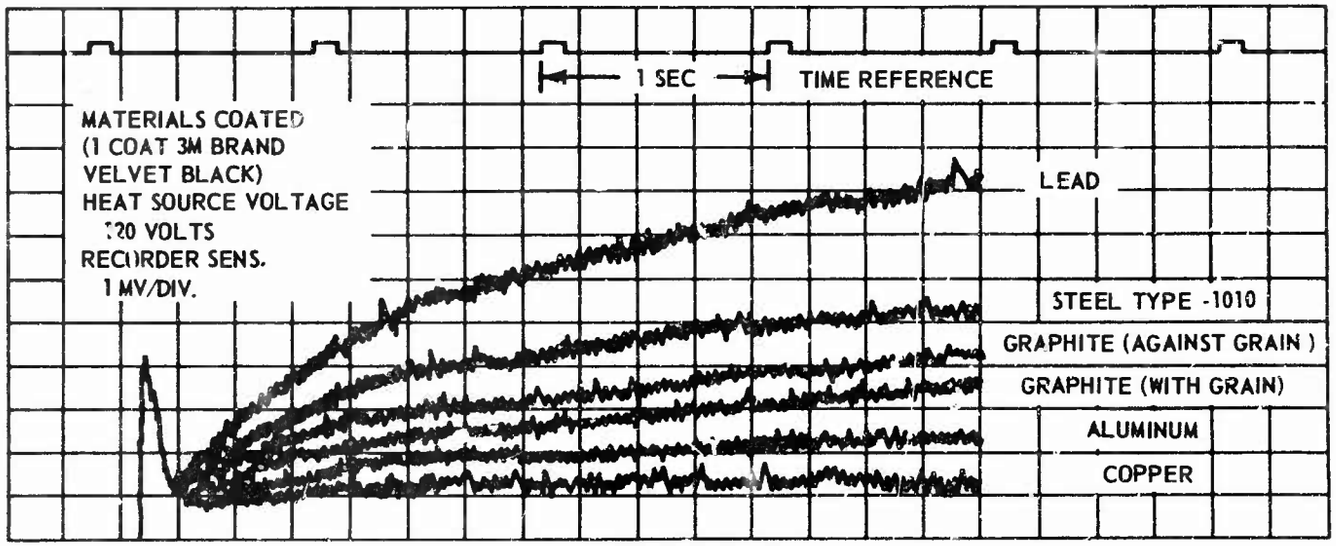

770362D-1

Figure 9. SUPERPOSITION OF SELF-EMITTED RADIATION HISTORIES OF COPPER, ALUMINUM, GRAPHITE, STEEL, AND LEAD

history shapes and relative displacements that are typically generated by the technique. Close inspection of the histories reveals that they are only approximately parabolic in shape. Aside from the small (2 percent) temperature-signal nonlinearity, two principal causes contribute to distorting the shapes. As described in Appendix III, suppression of a history's vertex results in a partially observable trace that will appear to originate within the noise level of the system. The higher the inertia of the material, the smaller will be the self-emitted radiation signal amplitude, so that materials such as graphite, aluminum, and copper will generate histories that lie within the noise level for longer periods of time, respectively, than will those for lead and steel. Thus, histories for high inertia materials will tend to appear more linear than for low inertia materials. Coating the surfaces of high conductivity solids with low conductivity materials also distorts a curve's shape by initially retarding heat flow into the solid, thereby causing the surface temperature to increase faster than it normally would for the solid itself. This effect diminishes as the conductivity of the material approaches that of the coating; it being evident that coatings having high- k values relative to those for the solid substrates will cause essentially no distortion of the solids' history shapes. However, the coating material used in this study has a lower conductivity than any of the solids tested (as a trade off for its high emissivity property), so that coatings will create greater distortion, within a short period after pulse initiation, for the copper, aluminum, and graphite histories, than for the steel and lead histories.

A measure of history distortion must be obtained in order that an optimum time interval for history analysis can be selected; one which exhibits negligible distortion and which is common to all the materials. It is to be recognized that it is not absolutely necessary to compare materials' histories within the same time interval, since general characteristics of a parabola can be used to develop relationships between curve segments (as in Appendix III), but it is very convenient to do so. The procedure used to measure distortion consisted of first translating the recorder-generated histories to logarithmic graph paper, then comparing the resulting experimental curve plots for different time bases with those derived mathematically for a parabola (presented in Figure 2), and finally selecting the earliest common time base that exhibited the best curve match. Examples of matched curves for graphite, steel, and lead, for a constant set of experimental parameters, are shown in Figures 10, 11, and 12. The dashed lines and points represent the actual experimental curves, and the solid lines the theoretical curves for a parabola. Overlaying one set on the other for each of the materials resulted in selecting an earliest, common, and convenient time-base value equal to 1 second. It is to be noted that the experimental curve for graphite after the 1 second time base is essentially linear; this being the result of measuring a curve that is largely contained within the zero noise signal. It is to be particularly noted that excellent

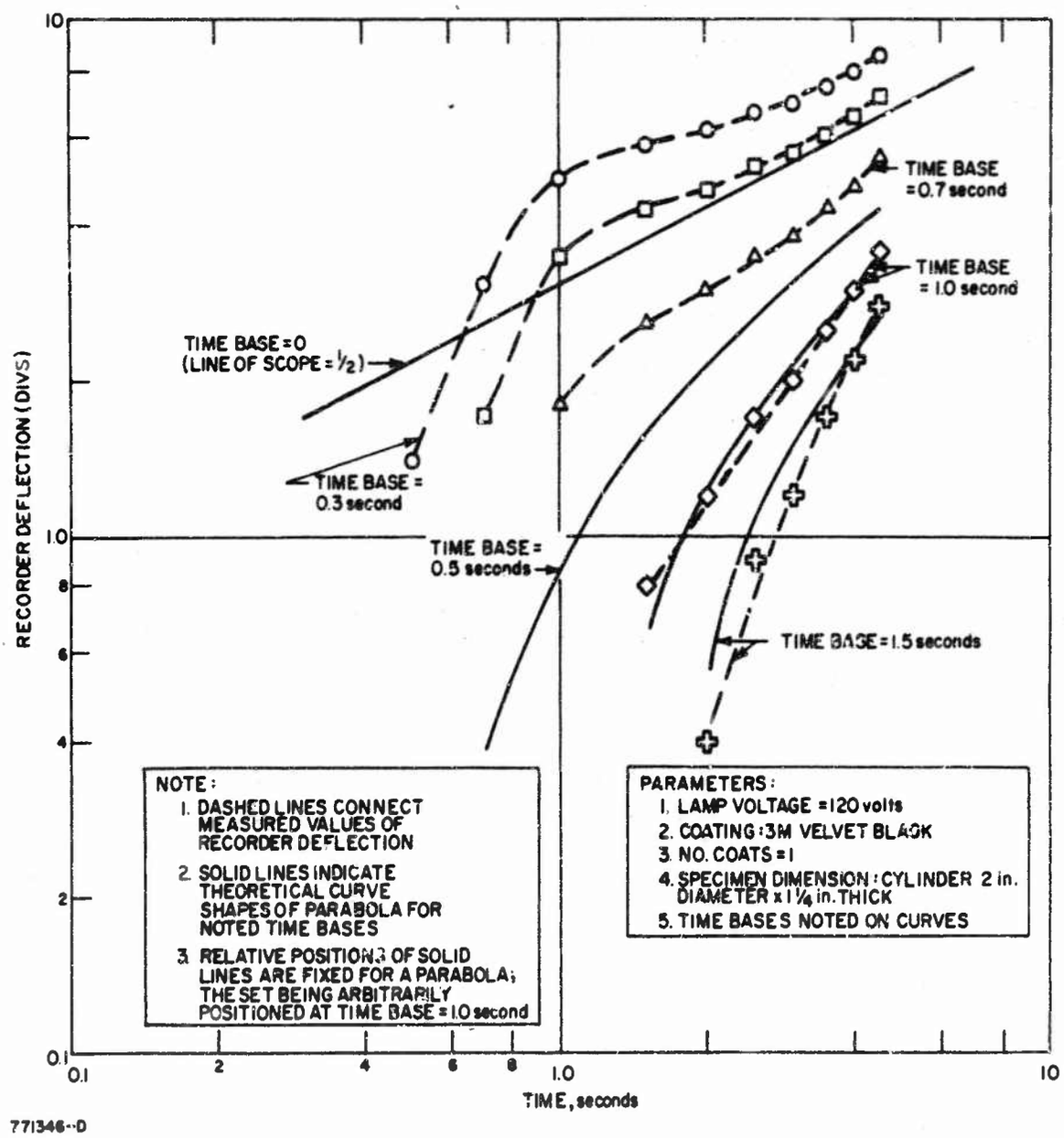

Figure 10. SURFACE TEMPERATURE HISTORIES FOR AYJ GRAPHITE (FOR SEVERAL TIME BASES)

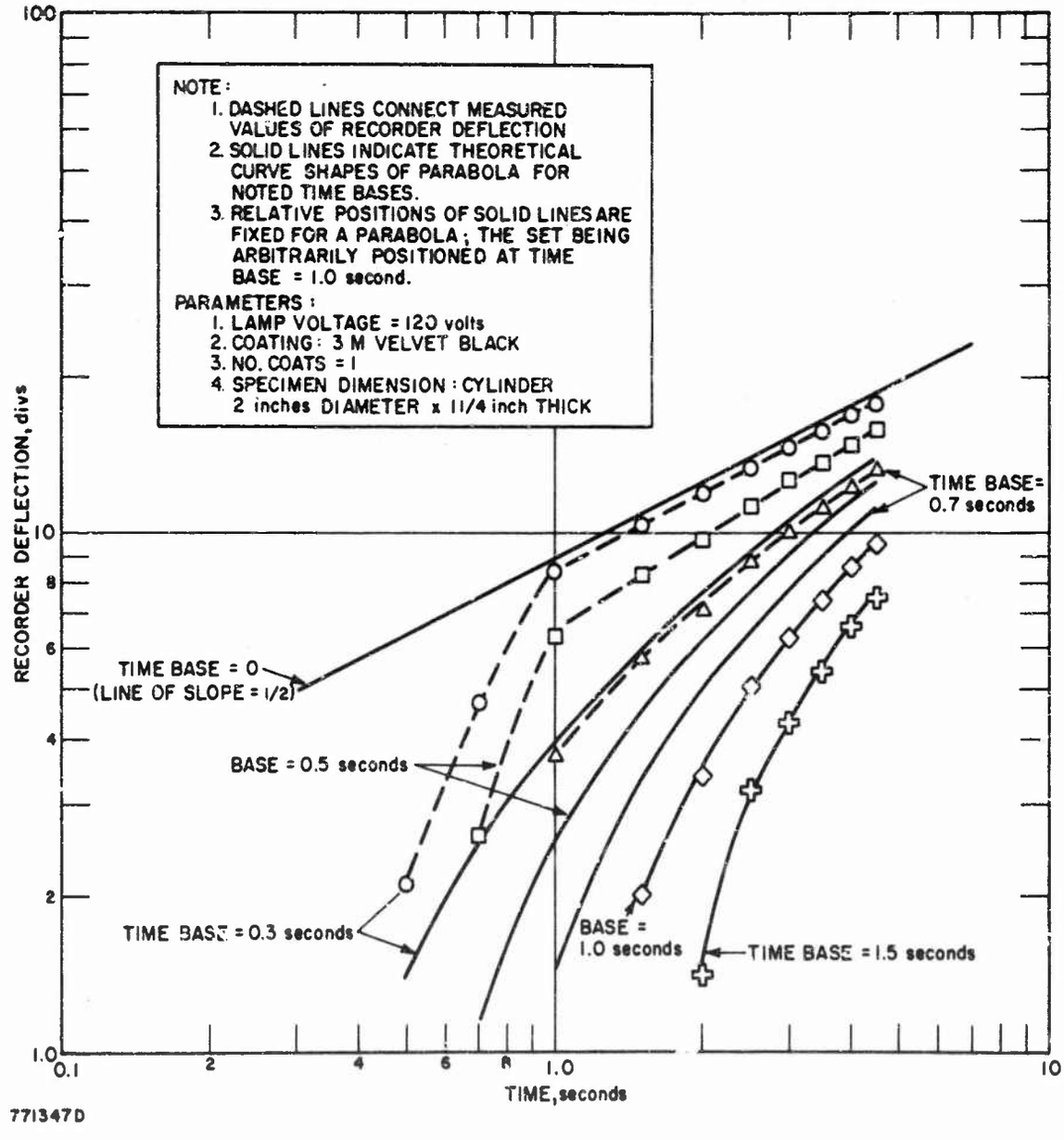

Figure 11. SURFACE TEMPERATURE HISTORIES FOR 1010-STEEL (FOR SEVERAL TIME BASES)

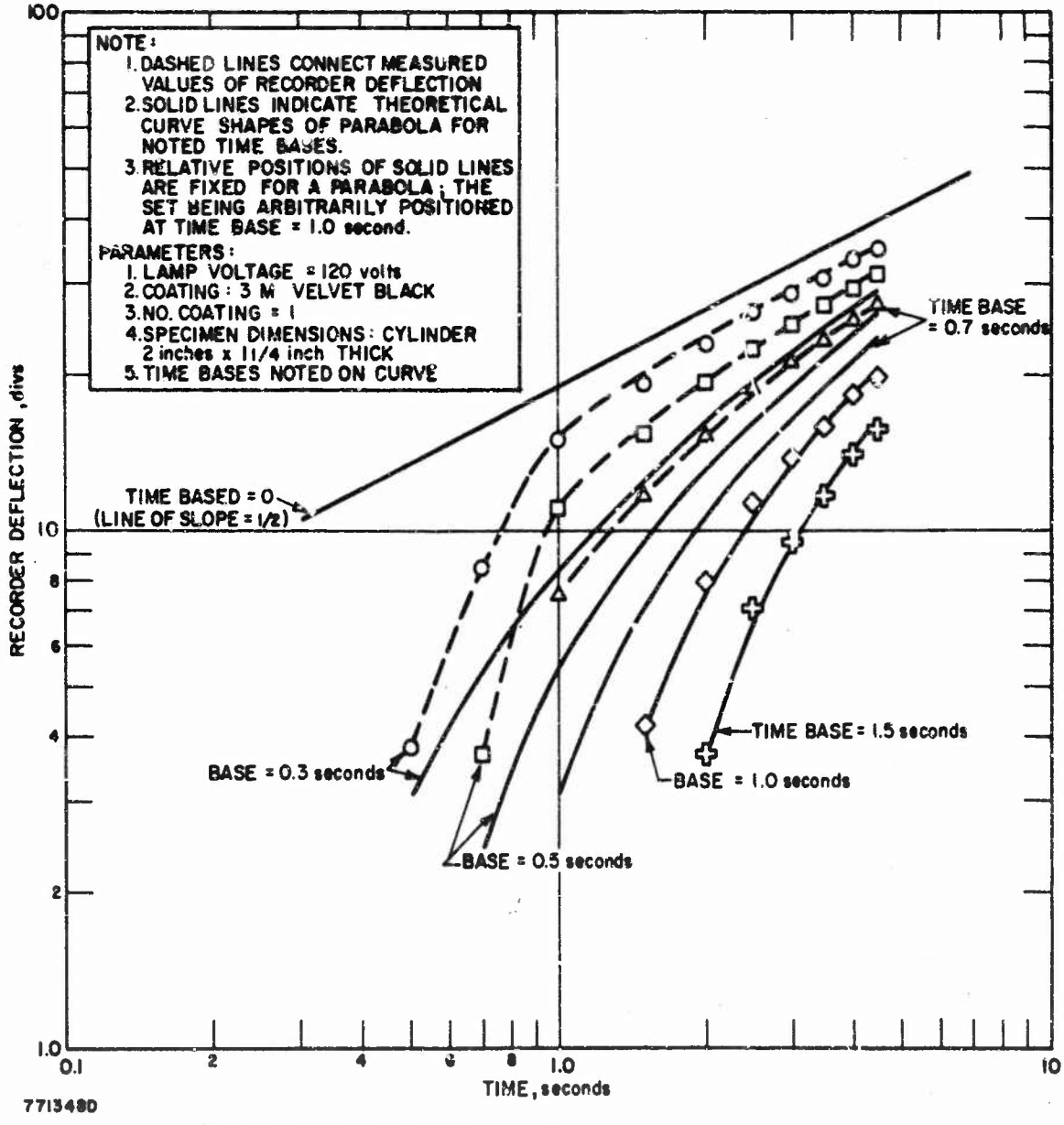

Figure 12 SURFACE TEMPERATURE HISTORIES FOR LEAD (FOR SEVERAL TIME BASES)

curve matches simultaneously occur for the steel and lead histories at 1 and 1.5 second time bases, indicating that their histories are indeed parabolically-shaped 1 second after pulse initiation. The effect of coatings is made vivid by observing the greater degree of over-all time-base curve matching that develops as the thermal inertia decreases, or recorder deflection increases. Had vertex suppression been negligible, then the zero time base curves could also have been plotted and probably would have nearly matched for steel and lead beyond 1 second. The reason for selecting a pulse cut-off time of 4.5 seconds was principally due to the use of copper as one of the test materials. Since a 1 division recorder deflection above a 2 division zero level noise signal was regarded as being consistently observable, ideal copper specimens had to be heated for 4.5 seconds to produce this 1 division deflection; a longer period producing excessive temperature increases for the other materials. As a consequence of these tests, a time interval between 1 and 4.5 seconds after pulse initiation was selected as the history segment to be consistently used as a basis for comparing recorder deflections. Somewhat coincidentally, general characteristics of a parabola are such that an amplitude rise between 0 and 1 seconds is very nearly equal to the rise between 1 and 4.5 seconds (see Appendix III), so that a rapid means for noting if a history is nearly of parabolic shape is to compare its absolute amplitudes at 1 and 4.5 seconds (presuming that vertex suppression can be regarded as negligible).

As the final consideration in designing a test technique for evaluating the method, the effect of coating thickness on recorder deflection must be assessed. Although a measure of this effect was just described, only 1 coat was used in those tests. Consequently, the question arises as to the degree of care that must be used in applying a coating, in order to minimize the deflection variability that will result from differences in coating thickness. Recalling that 1 coat consists of 1 pass of spray applied in each of two perpendicular directions over a surface, 1, 2, and 3 coats were carefully applied to each of the materials. Histories for the three coating thicknesses on graphite and steel, in the 1 to 4.5 second interval, are shown in Figures 13 and 14. For graphite, it is seen that 2 and 3 coats increase deflection by 92 percent and 155 percent, respectively, compared to 1 coat. For lead, 2 and 3 coats increase deflection by 32 percent and 89 percent, respectively, compared to 1 coat. It is immediately evident that coating thickness will have a pronounced effect on comparative results. A relationship between coating thickness and recorder deflection has been developed from graphical results for all the materials, and is presented in Figure 15. As expected, coating thickness has less effect on the lower inertia materials. If it is presumed that 1 coat can be consistently applied to surfaces in a thickness that varies by about 15 percent, then for aluminum, for example, a 15 percent increase in thickness between 1 and 2 coats is equivalent to approximately 0.15 x 120% (from Figure 15) = 18% difference in recorder deflection, which is in reasonable agreement with results of

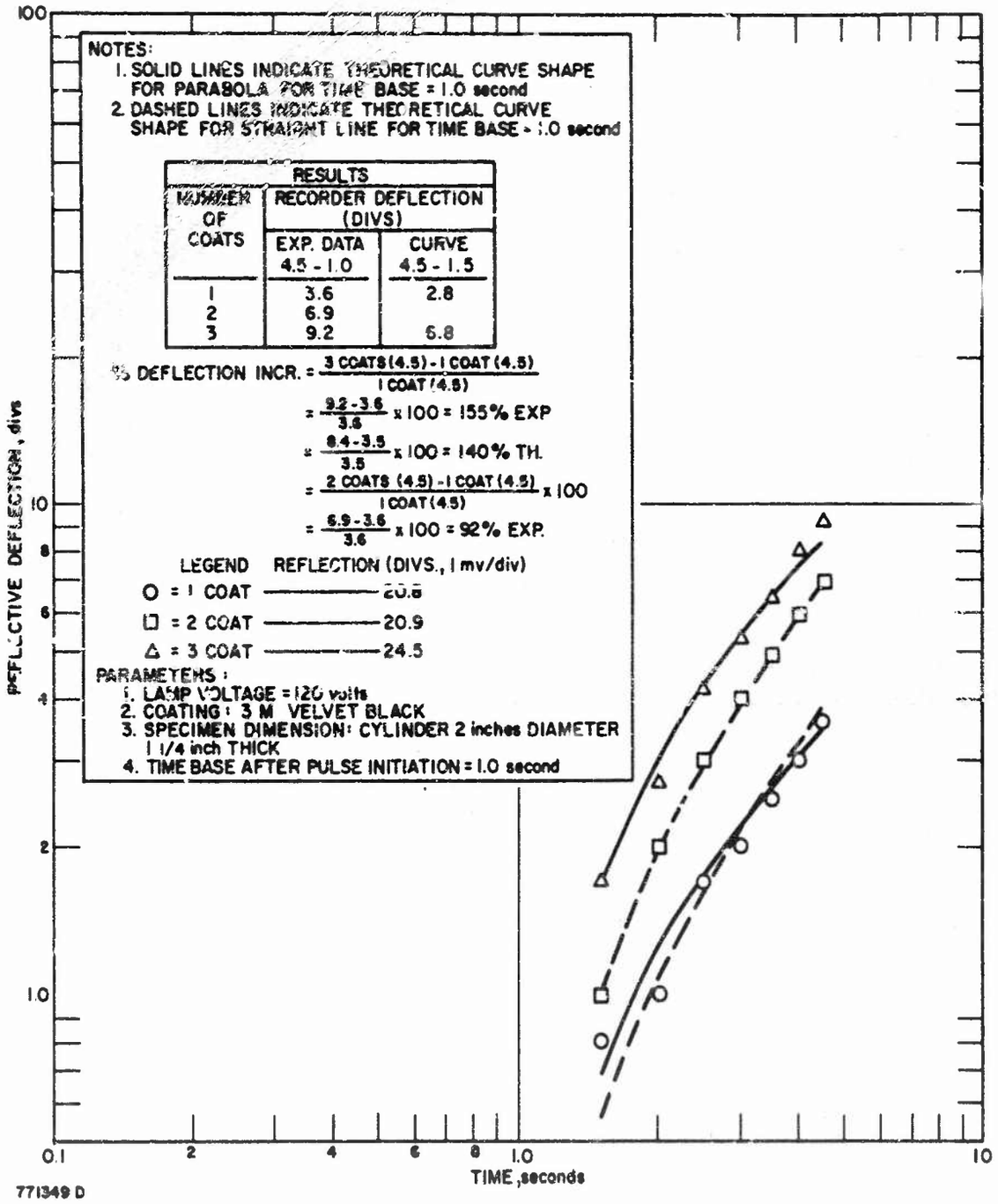

Figure 13. EFFECT OF COATING THICKNESS ON RECORDER DEFLECTION FOR ATJ GRAPHITE

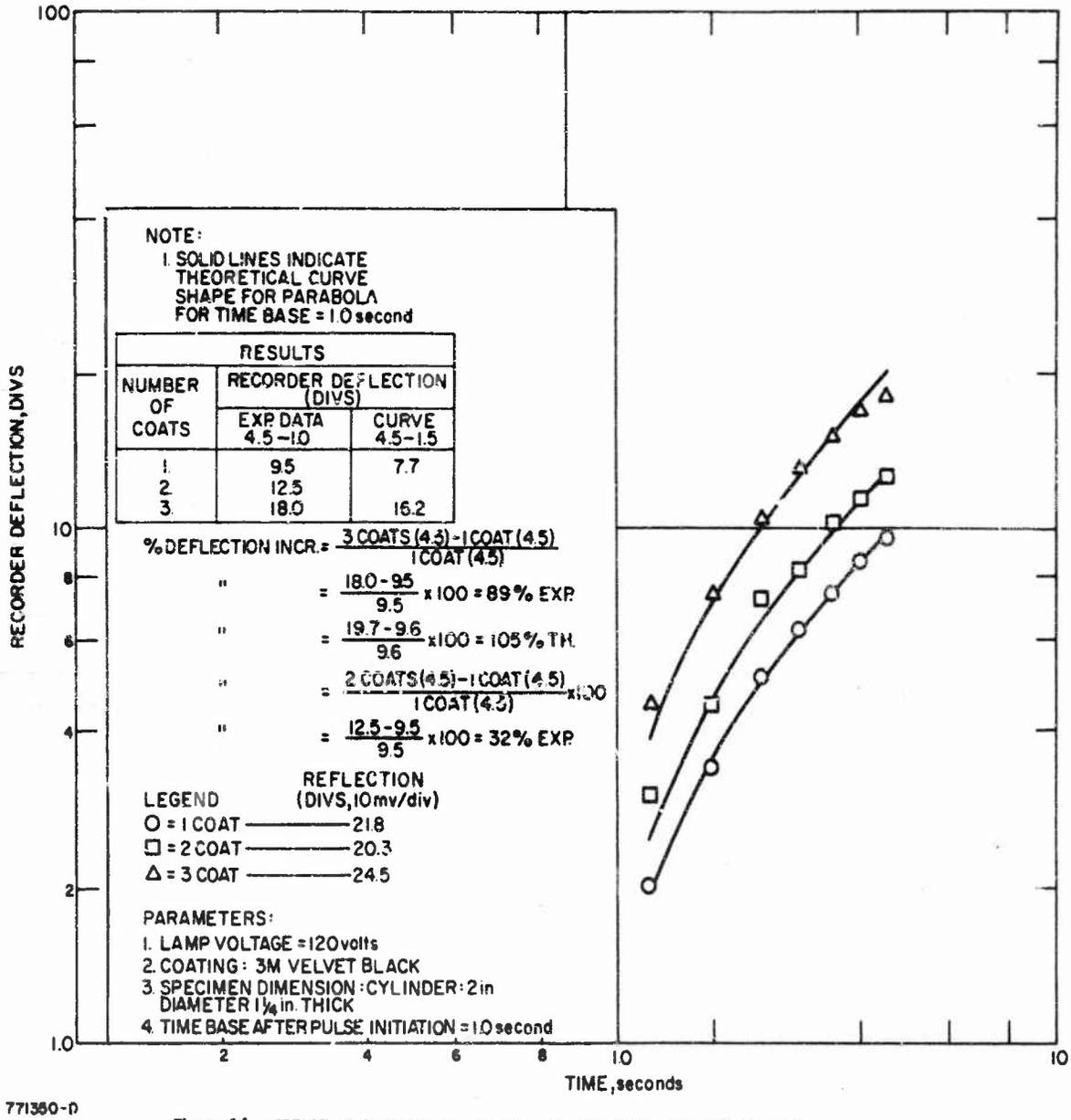

Figure 14. EFFECT OF COATING THICKNESS ON RECORDER DEFLECTION FOR 1010-STEEL

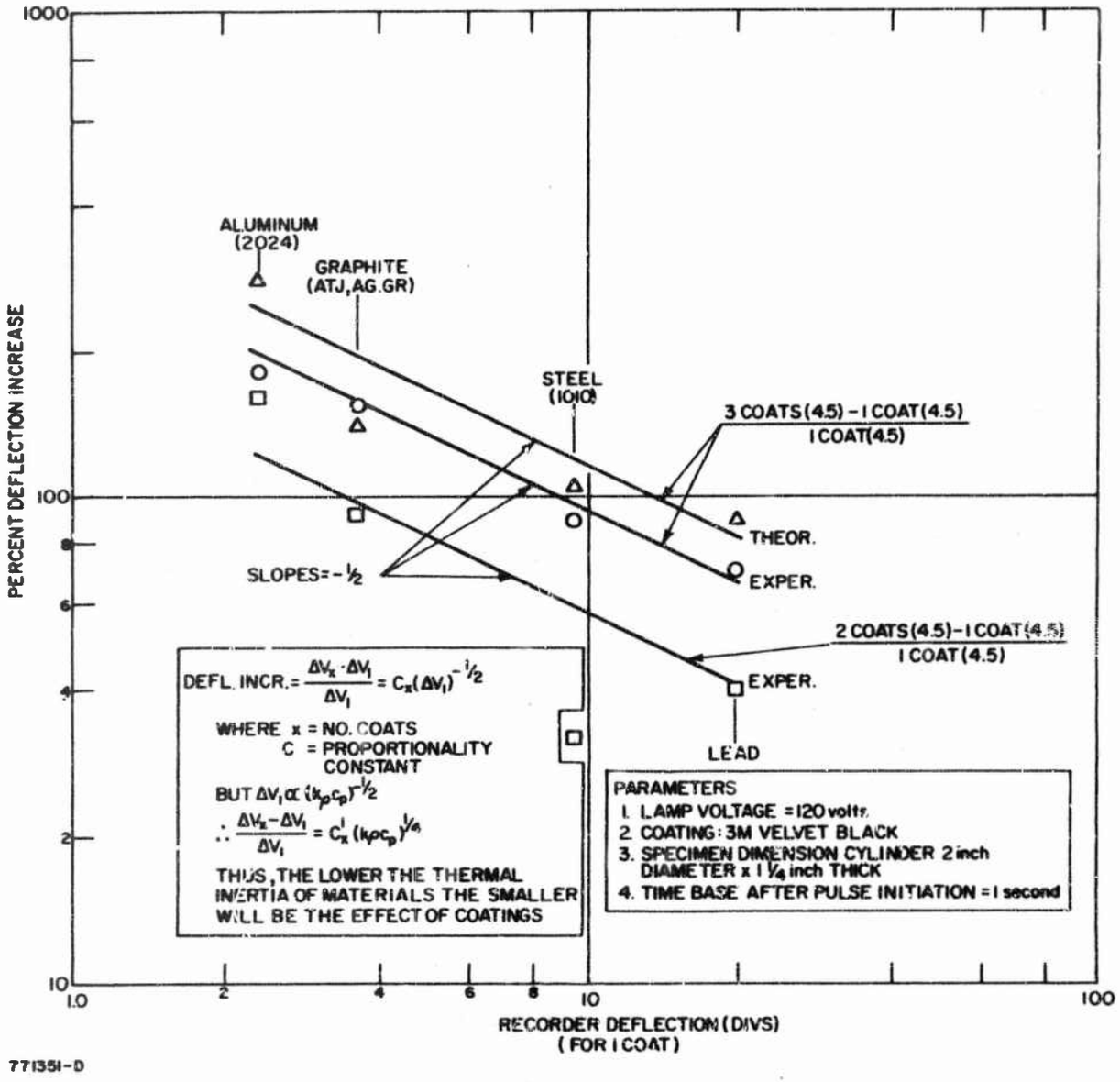

Figure 15. EFFECT OF COATINGS ON THERMAL INERTIA MEASUREMENTS

measurement precision for aluminum to be discussed later (Figure 22). Similarly for lead, a 15 percent variability in applying 1 coat results in a recorder deflection difference of 0.15 x 40% = 6 percent, which is again in reasonable agreement with precision measurements. Four principal conclusions can be drawn from these estimates. These are: (1) coating thickness must be controlled to better than 15 percent for especially high inertia materials like graphite, aluminum and copper; (2) coatings can be applied in the present manner to low inertia materials like lead without seriously affecting results; (3) a coating material having an emissivity similar to that of 3M Velvet Black, but a much higher thermal conductivity, would increase measurement precision greatly; and (4) the current measurement precision of recorder deflection for the solids studied (to be discussed) can be related in large part to coating thickness variability. Ideally, of course, future technique development should aim at eliminating entirely the need for coatings.

IV. Results

Employing the experimental technique described, tests were performed on sets of solids, which varied in thickness and diameter, for the purpose of determining the critical, semi-infinite dimensions that make it possible to evaluate the method using ideal geometries. The effects of different specimen thicknesses on recorder deflection for graphite and steel are shown in Figures 16 and 17. It is seen for graphite that recorder deflection increases markedly as thickness decreases from 1 1/2 inches to 1/4 inch. Semi-infiniteness in the thickness dimension can then be said to exceed 1 1/2 inches, for this technique and time interval, for ATJ graphite oriented in a direction against the grain with respect to the predominant direction of heat flow. It is also to be noted, in Figure 16, that the experimental data approaches a more linear than parabolic curve shape as thickness decreases. As remarked earlier, a nearly linear curve shape can be expected when the signal voltage, or recorder deflection, is low and the history lies mainly within the system's zero noise level. However, these nearly linear curves occur for comparatively high deflections (large surface temperature increases). Consequently, a means for detecting a finite condition in the thickness dimension is made possible by carefully noting the departure of the history from the parabolic form. For steel, semi-infiniteness in the thickness dimension occurs at approximately 1/2 inch, as readily seen from the tabulated data included in Figure 17.

These results and similar results for copper are plotted in Figure 18, in a manner that more vividly illustrates the approach of each material to semi-infiniteness. Included in the figure, at the 10 inch position, are measurements made on massive graphite and copper blocks, which are regarded as truly semi-infinite. The measurement precisions indicated were determined from test results still to be described.

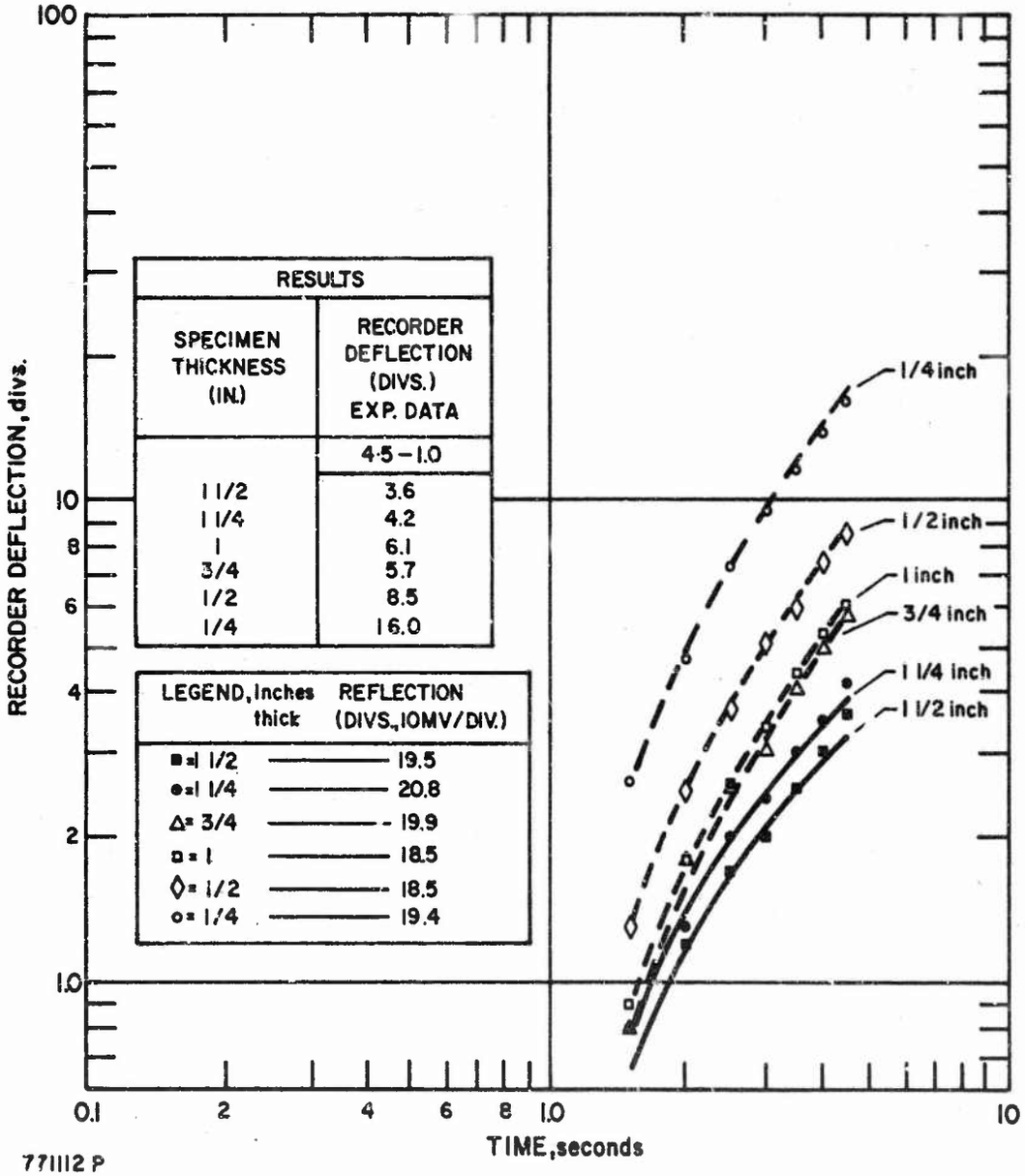

PARAMETERS:

1. LAMP VOLTAGE = 120V
2. COATING: 3M VELVET BLACK
3. NO. COATS = 1
4. SPEC. DIAM. = 2 INCHES
5. TIME BASE AFTER PULSE INITIATION = 1.0 SECOND

NOTE:

1. SOLID LINES INDICATE THEORETICAL CURVE SHAPES FOR PARABOLA FOR TIME BASE = 1.0 SEC.
2. DASHED LINES INDICATE THEORETICAL CURVE SHAPES FOR STRAIGHT LINE FOR TIME BASE = 1.0 SEC.

Figure 16. EFFECT OF SPECIMEN THICKNESS ON RECORDER DEFLECTION FOR ATJ GRAPHITE

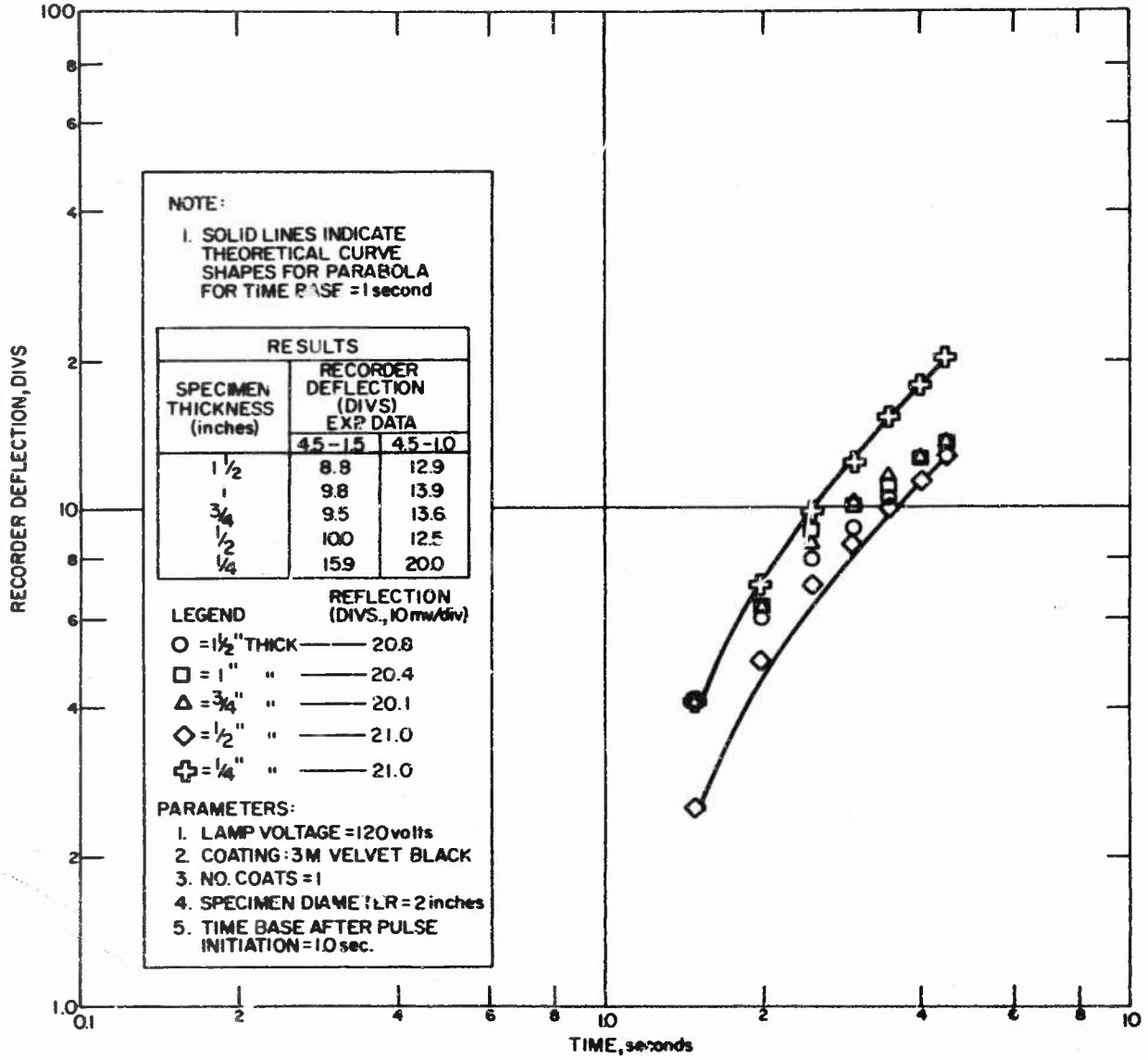

Figure 17. EFFECT OF SPECIMEN THICKNESS ON RECORDER DEFLECTION FOR 1010-STEEL

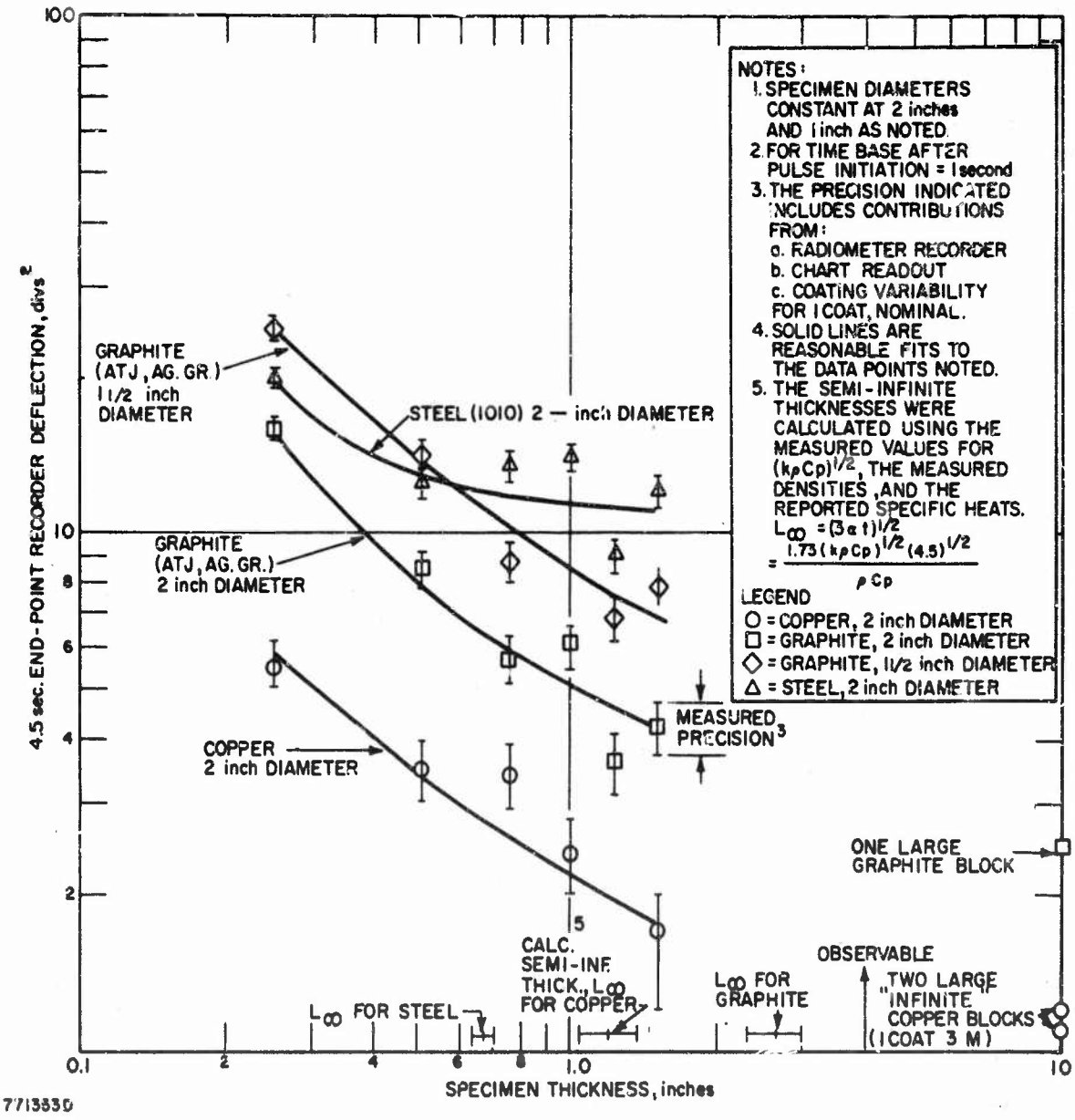

Figure 18. EFFECT OF SPECIMEN THICKNESS ON THE CRITERION OF SEMI-INFINITENESS (STEEL, GRAPHITE, AND COPPER)

The effects of different specimen diameters on recorder deflection for copper and steel are shown in Figures 19 and 20. For copper, it is seen that recorder deflection increases greatly as diameters decrease from 2 inches to 1 inch. Since the deflection difference in this diameter range is much greater than the difference arising from coating thickness variability, these results are significant. Consequently, semi-infiniteness in the lateral direction for copper can be said to exceed 2 inches in diameter for this technique. Measurements for diameters greater than 2 inches produce nearly unobservable recorder deflections. For steel, much less of a deflection decrease is noted as diameters are varied from 1 to 2 inches. This is to be expected since steel's thermal inertia is less than that for copper. From the table in Figure 20, semi-infiniteness in the lateral direction for steel can be said to exist probably at about a diameter of 2 inches. Also included in Figure 20 are the results for a 1-inch diameter rod of Armco iron, the standard material. It is seen that its deflection is identical to that for a 1-inch diameter (1010) steel specimen. This test was performed to show that (1010) steel and Armco iron have equivalent values of thermal inertia within the precision of measurement; thus, an ideal steel specimen can be and was substituted for an ideal Armco iron specimen in all tests, because a satisfactory geometry for the standard material was unavailable. These results are replotted in Figure 21 to vividly illustrate the approach of the lateral dimensions toward semi-infiniteness.

The inference to be made from these finite measurements is that one geometry can be used to facilitate all ideal measurements on all materials having thermal inertia values equal to and less than that for copper. One geometry was selected, and this consisted of a cylinder having a 2-inch diameter and a thickness equal to 1 1/2 inches.

The results for a series of measurements performed on the ideal materials of interest are shown in Figure 22. These measurements are representative of numerous tests and are regarded collectively as valid measures of overall technique precision. This is to say, specimens were coated and recoated a number of times, critical test parameters were reset, histories were analyzed by different personnel, and tests were performed over an extended period, in order that the broadest range for assessing reproducibility would obtain. From the table included in this "working" graph, mean, reflection-corrected values of recorder deflection are tabulated together with their precisions of measurement. These particular values have been used for evaluating the method. Measurement precision has been plotted as a function of mean recorder deflection in Figure 23. It is seen that this function exhibits regular characteristics, so that it serves as a valuable aid for rapidly estimating the precision error of a measurement using this technique.

Since the mean deflection values that are tabulated in Figure 22 cannot be compared without additionally correcting them for the effect of vertex suppression, this corrective procedure must be discussed next. It is

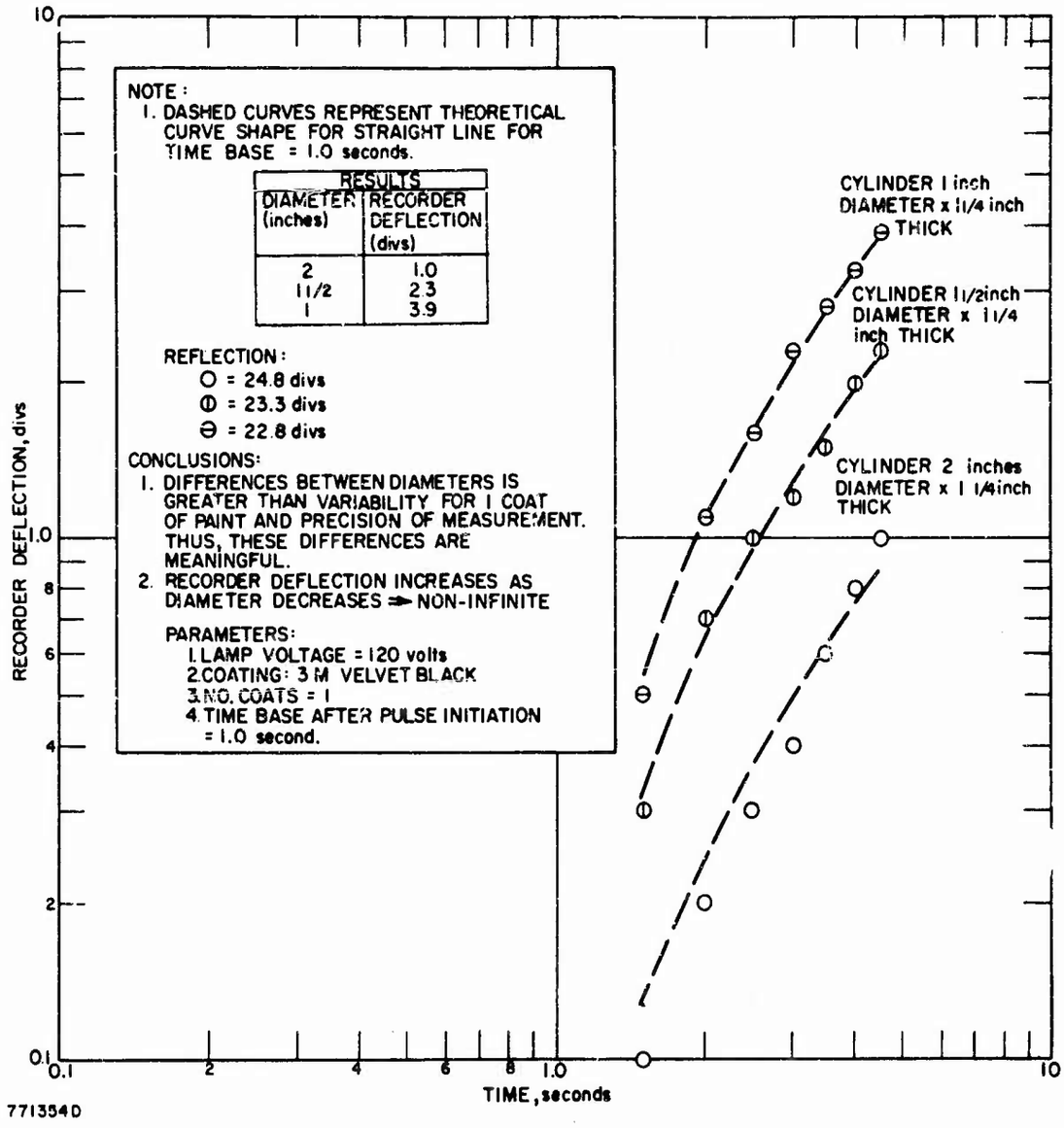

Figure 19. EFFECT OF SPECIMEN DIAMETER ON RECORDER DEFLECTION FOR COPPER

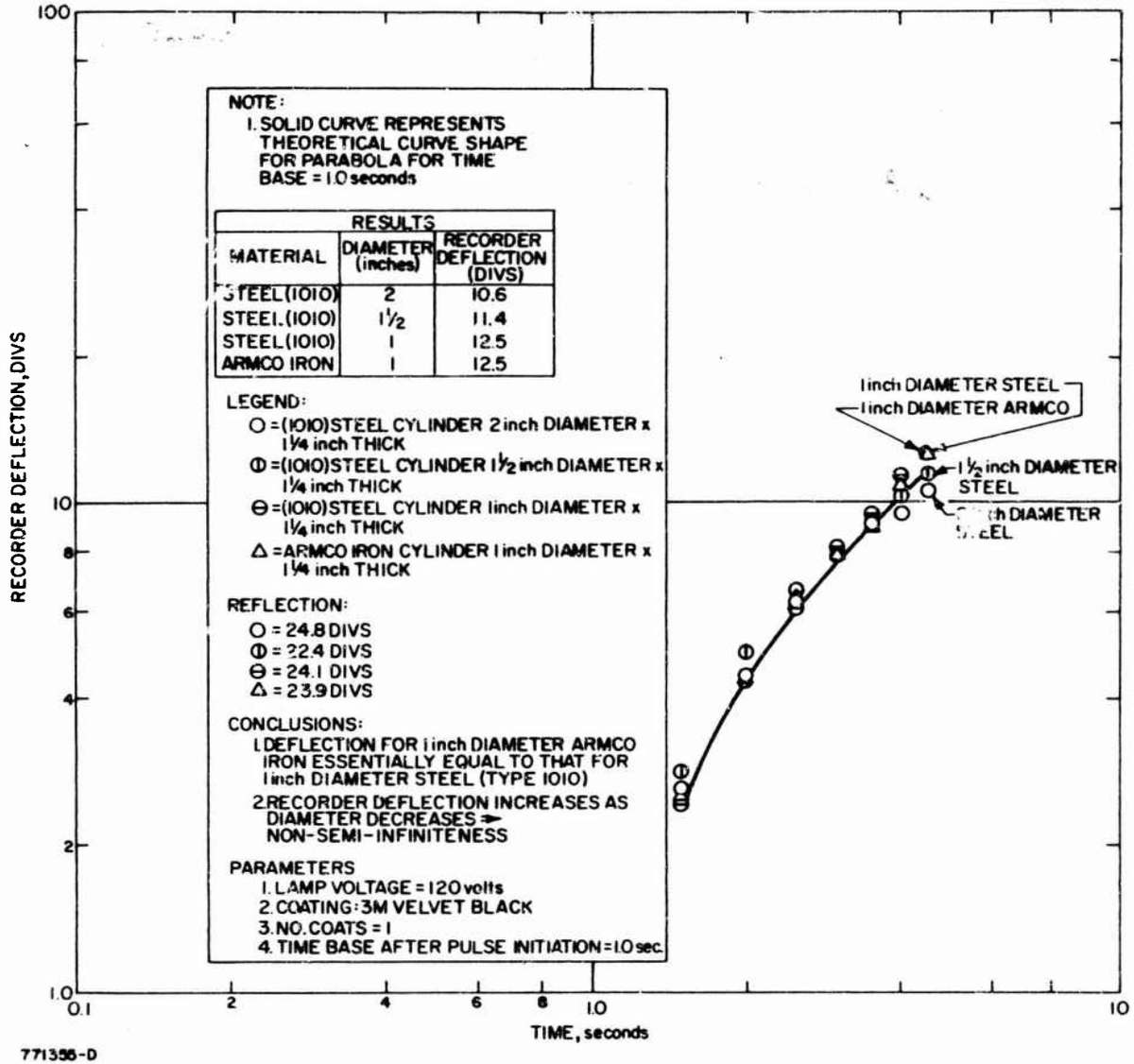

Figure 20. EFFECT OF SPECIMEN DIAMETER ON RECORDER DEFLECTION FOR 1010-STEEL AND ARMCO IRON

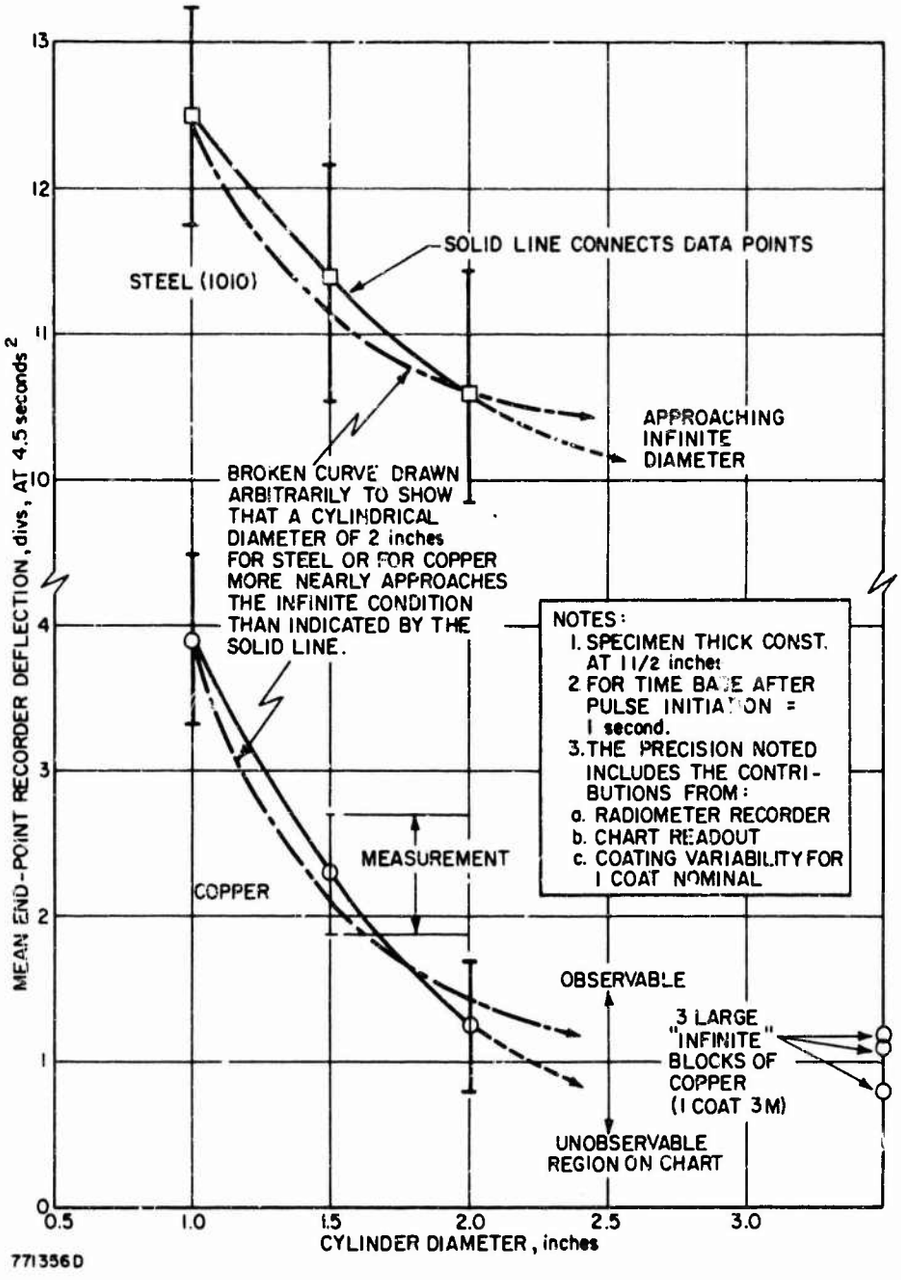

Figure 21. EFFECT OF SPECIMEN DIAMETER ON THE CRITERION OF SEMI-INFINITENESS (STEEL AND COPPER)

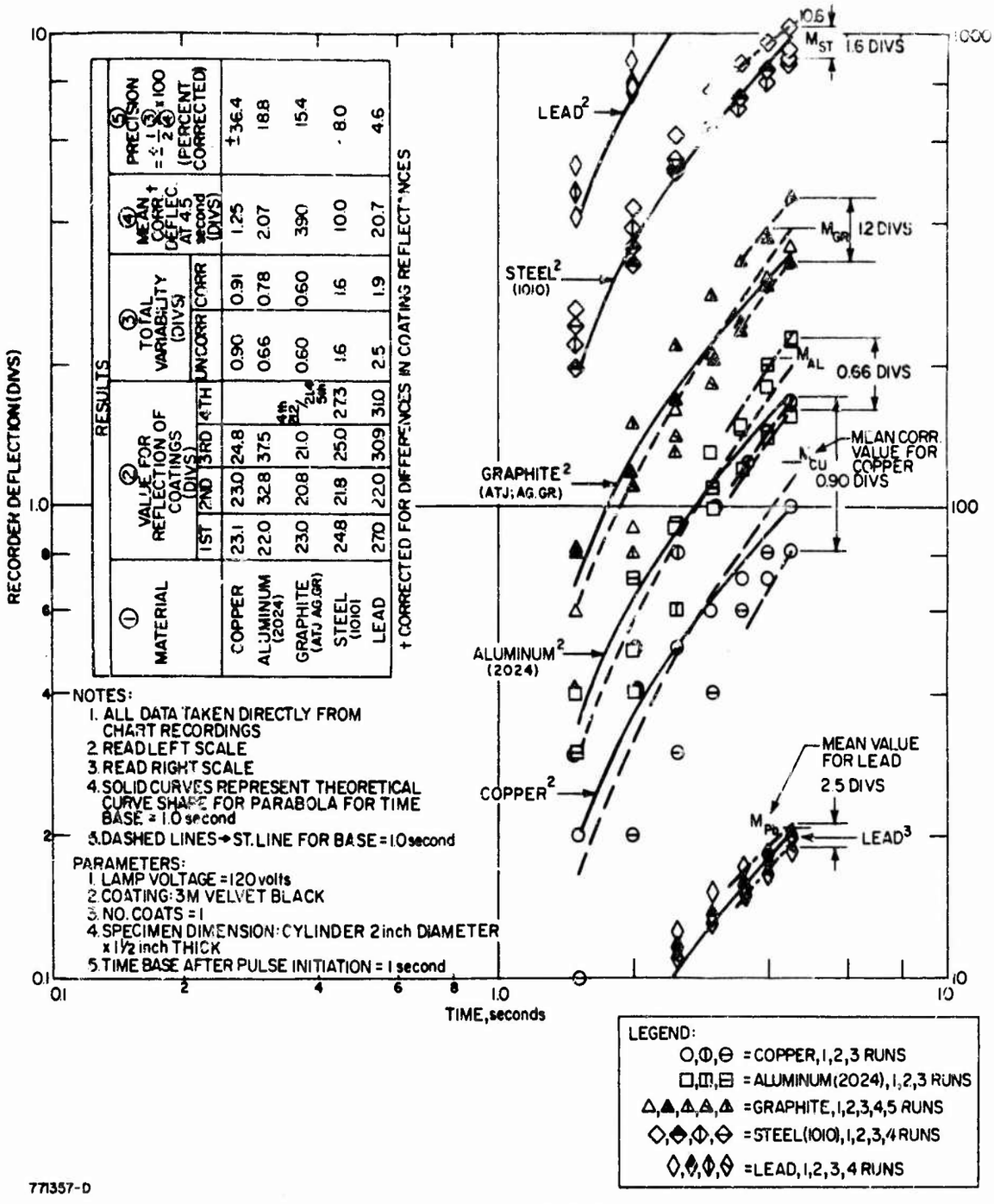

Figure 22. DETERMINATION OF MEASUREMENT PRECISION

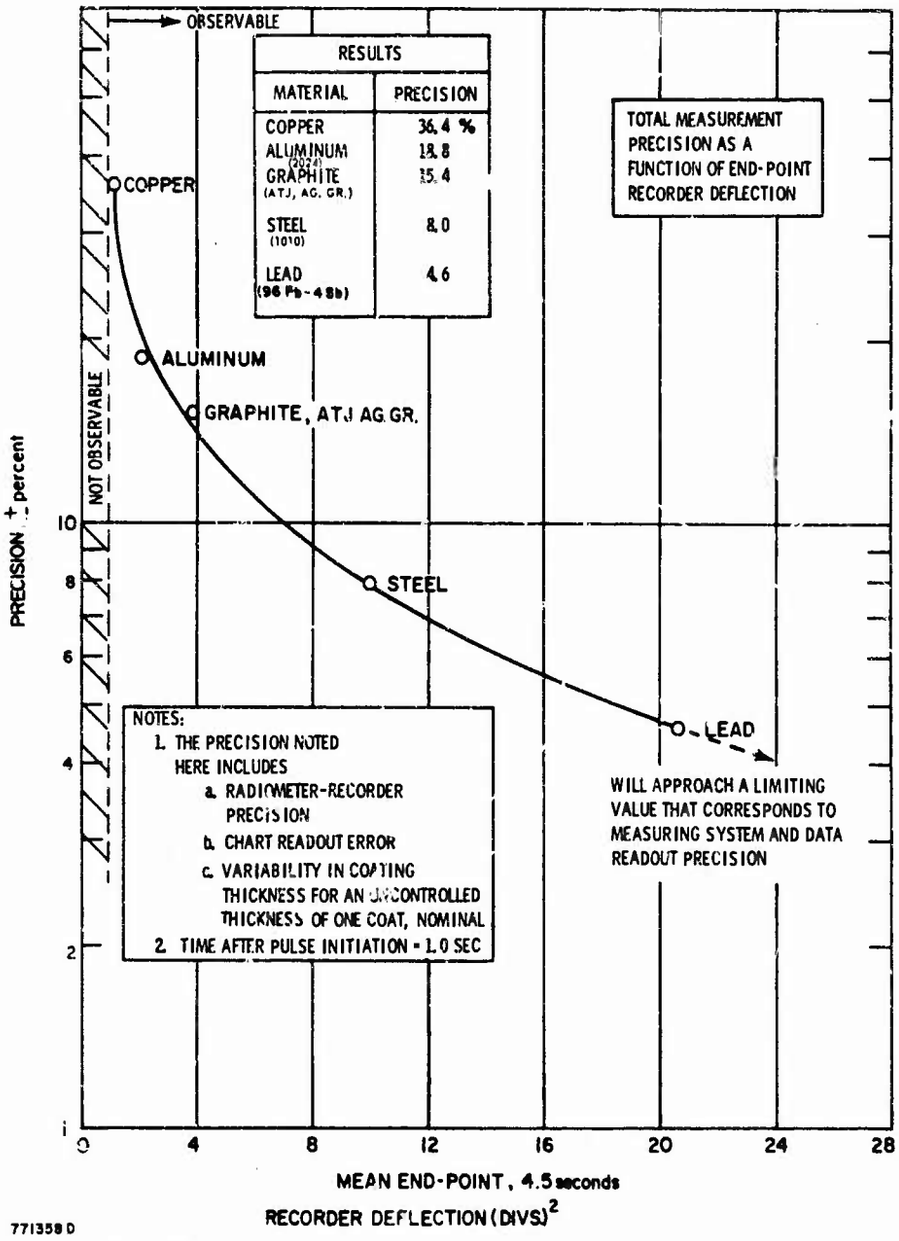

Figure 23. TOTAL MEASUREMENT PRECISION AS A FUNCTION OF RECORDER DEFLECTION

to be recalled that vertex suppression arises from the difference that exists between the radiometer reference source temperature and ambient temperature. Essentially, all that is required for correcting recorder deflection for this effect is to add to the measured deflection a value of deflection that is equivalent to this temperature difference. A graphical aid for determining the suppression-corrective term, Γ_C , to be added to the reflection-corrected, measured deflection, Γ_D , for several values of temperature difference equivalence, Γ_A , is presented in Figure 24. The deflections that were obtained and their measurement errors are indicated on the Γ_A -line equal to 5 degrees C. The corresponding Γ_C -values and their resultant errors are tabulated in the graph. The resultant error includes the error associated with estimating Γ_C and that associated with determining the temperature difference responsible for suppression; the error in this latter difference being estimated as 0.2 degrees C.

Tabulated in Table II are the fully-corrected, measured recorder deflections, the corresponding $(k\rho C_p)^{1/2}$ -values using Armco iron as the calibration standard, the reported $(k\rho C_p)^{1/2}$ -values, and the difference between the extremes of the measured and reported values. Footnotes are provided to indicate the origins and details of the data. In part, evaluation of the method is viewed in terms of comparing the difference between extremes. The only extreme difference seen is for graphite, whereas the magnitudes of the differences for the other materials are regarded as being within reasonable expectations. Arguments supporting "reasonableness" are discussed in the following section.

By combining results of several of the graphs into one, a very useful graph that displays $(k\rho C_p)^{1/2}$ as a function of recorder deflection is presented in Figure 25. Also included in this figure for comparison are reported values of $(k\rho C_p)^{1/2}$ for the materials of interest. It is apparent from the trend of the graph that this method not only can be extended to include a broad range of inertia values, but also becomes more precise as the thermal inertias of materials decrease. In the region beyond 50 divisions recorder deflection, temperature-deflection nonlinearity will begin to have significance. This distortion of the history curve would only complicate, but not limit the usefulness of the method, since correction back to a common base of temperature can be employed.

An illustration of measurements performed on two finite graphite specimens are shown in Figure 26. These specimens are grain oriented and differ markedly in density. It is seen that the specimens are easily distinguishable both in orientation and in density. The curves drawn are derived from a straight-line function, which is to be expected for finite size specimens.

Tabulated in Table III are recorder deflection results for six, oriented, finite graphite specimens selected to provide a range of density values that are representative of a manufactured billet. Orientations were determined

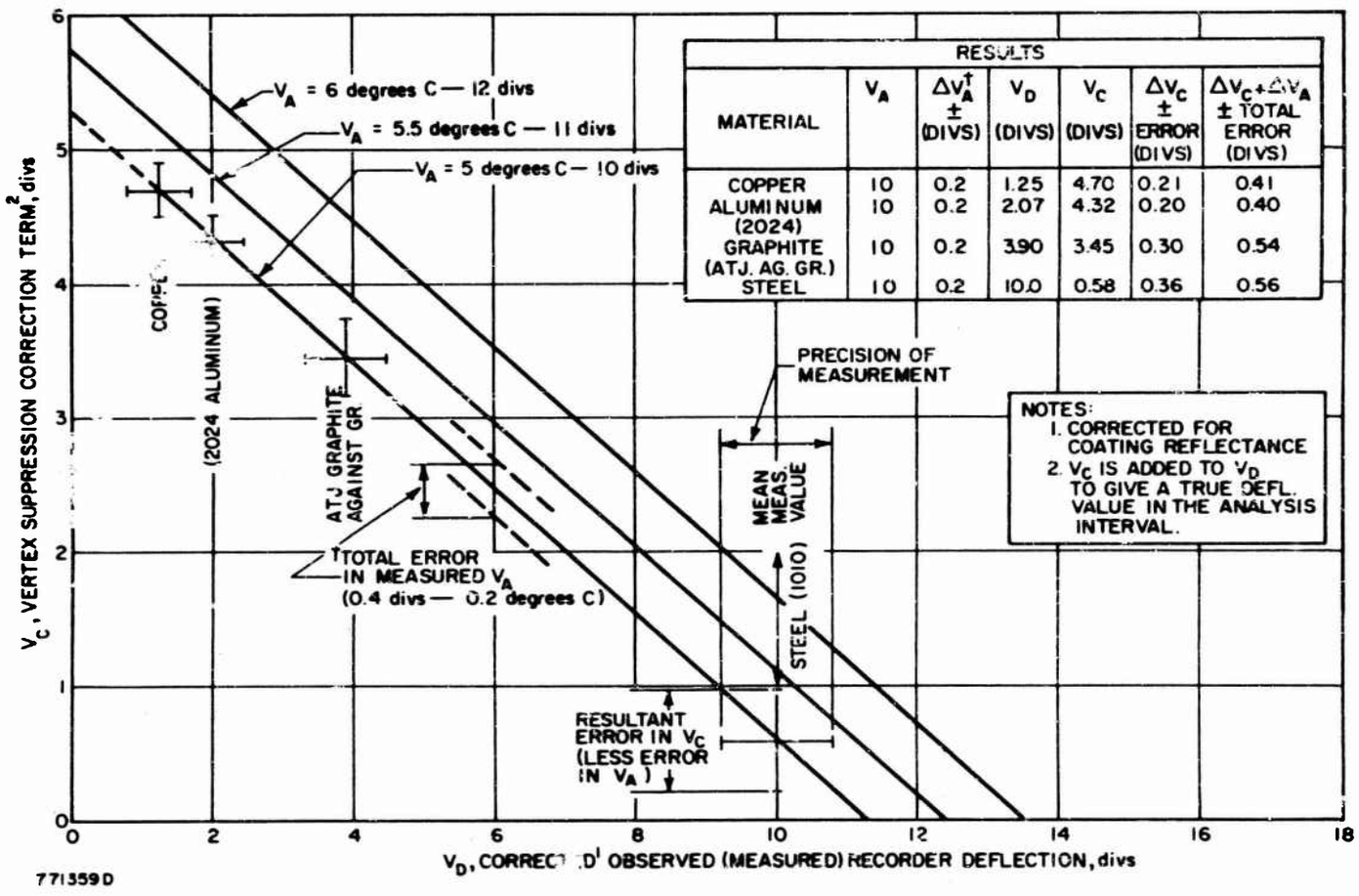

Figure 24. CORRECTION TERMS FOR RADIOMETER REFERENCE SOURCE-AMBIENT TEMPERATURE DIFFERENCE AS A FUNCTION OF RECORDER DEFLECTION

TABLE II

RESULTS OF MEASUREMENTS FOR $(k\rho C_p)^{1/2}$ AND THEIR COMPARISON WITH SOME REPORTED VALUES.

① Material	② Mean Deflection (Divs) (Corrected for Emissivity)	③ Precision of Measurement For ② (± divs)	④ Correction Term for Vertex Suppression and Signal Noise (div)	⑤ Precision of Measurement For ④ [3] (± divs)	⑥ Corrected Deflection: Mean Value ②+④ (divs)	⑥ Corrected Deflection: Precision [4] ③+⑤ ± %	⑦ Ratio of Corrected Deflection ⑥ to Armco Iron [5]	⑧ Measured [6] $(k\rho C_p)^{1/2}$ (Mean ± Error)	⑨ Reported $(k\rho C_p)^{1/2}$ (Mean ± Error)	⑩ Difference Between Extremes of ⑧ and ⑨ $\frac{⑧-⑨}{⑧} \times 100$ (Percent)
Copper	1.25	0.45	4.70	0.41	5.95	14.4	0.56 ± 0.07	0.68 ± 0.09	0.86 ± 0.05	-5.2
Aluminum (2024)	2.07	0.39 [2]	4.32	0.40	6.39	12.4	0.60 ± 0.07	0.63 ± 0.08	0.50 ± 0.03	+3.6
Graphite (ATJ, AG Grain)	3.90	0.60 [2]	3.45	0.54	7.35	15.5	0.70 ± 0.09	0.54 ± 0.07	0.35 ± 0.02 0.25 ± 0.02	+21.2
Steel (1010)	10.0	0.80	0.58	0.56	10.6	13.2	1.00 ± 0.13	0.38 ± 0.05	0.36 ± 0.02	0
Armco Iron	10.0	0.80	0.58	0.56	10.6	13.2	1	0.38 ± 0.05	0.38 ± 0.02	0
Lead 96 Pb-4Sb	20.7	0.95	0	0	20.7	4.6	1.95 ± 0.18	0.20 ± 0.02	0.16 ± 0.01	+5.6

1. This deflection value obtained by normalizing Armco specimen deflection to that for (1010) steel for the semi-infinite case.
2. The actual measured values of precision used and not the smoothed data.
3. Includes both the error in determining ④ due to measured error in ① and that in measuring the radiometer reference to ambient temperature difference, V_A.
4. It is to be noted that vertex suppression contributes approximates one-half the error in the corrected deflection column. A smaller value of V_A, higher radiometer sensitivity, and/or greater flux density will therefore diminish this error.
5. The error reported in ⑦ is the ratio-decimal-equivalent of the probable percent error obtained by taking 0.67 of the square root of the sum of the squares of each error. For example, for copper: Error = $0.67\ [(0.144)^2+(0.132)^2]^{1/2} \times 0.56 = 0.073$, so that ⑦ is stated as 0.56 ± 0.07
6. Obtained by dividing 0.38, the $(k_p C_p)$ reported value for Armco Iron, by ⑦. Consequently, a mean deflection of 10.6 divs. is equivalent to 0.38 and the test technique is calibrated.
7. This error is obtained by assuming that typical errors in measurement for k, C_p and ρ are 10, 5, and 1 percent, respectively, so that the probable error = $0.67\ [(0.10)^2+(0.05)^2+(0.01)^2]^{1/2} \times 100 = 11.2$ percent for $(k\rho C_p)$. The error does not include that arising from differences in values of k reported by different investigators; this being noted to exceed 50 percent for many materials including those tested.

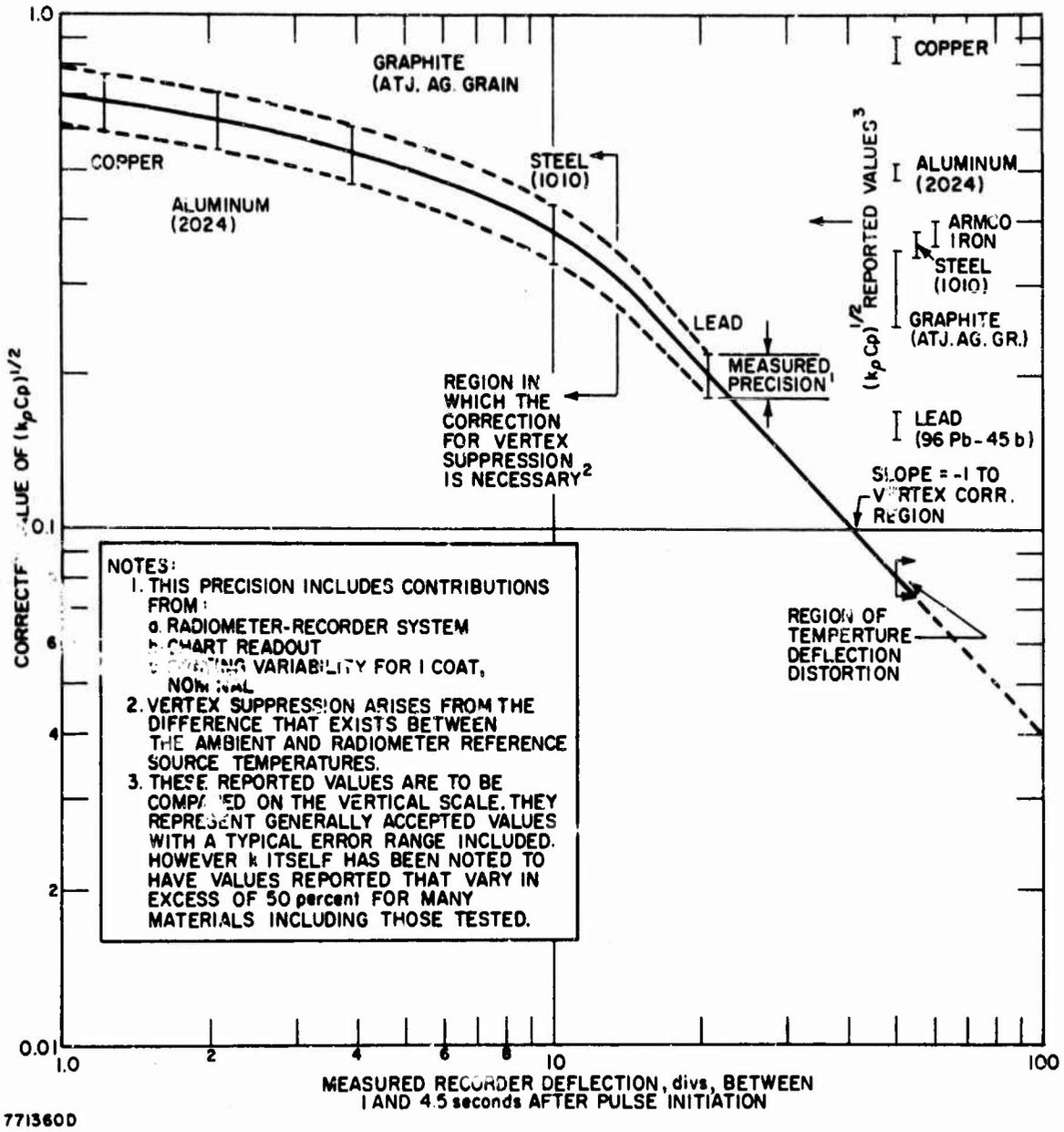

Figure 25. $(k_p C_p)^{1/2}$ AS A FUNCTION OF RECORDER DEFLECTION

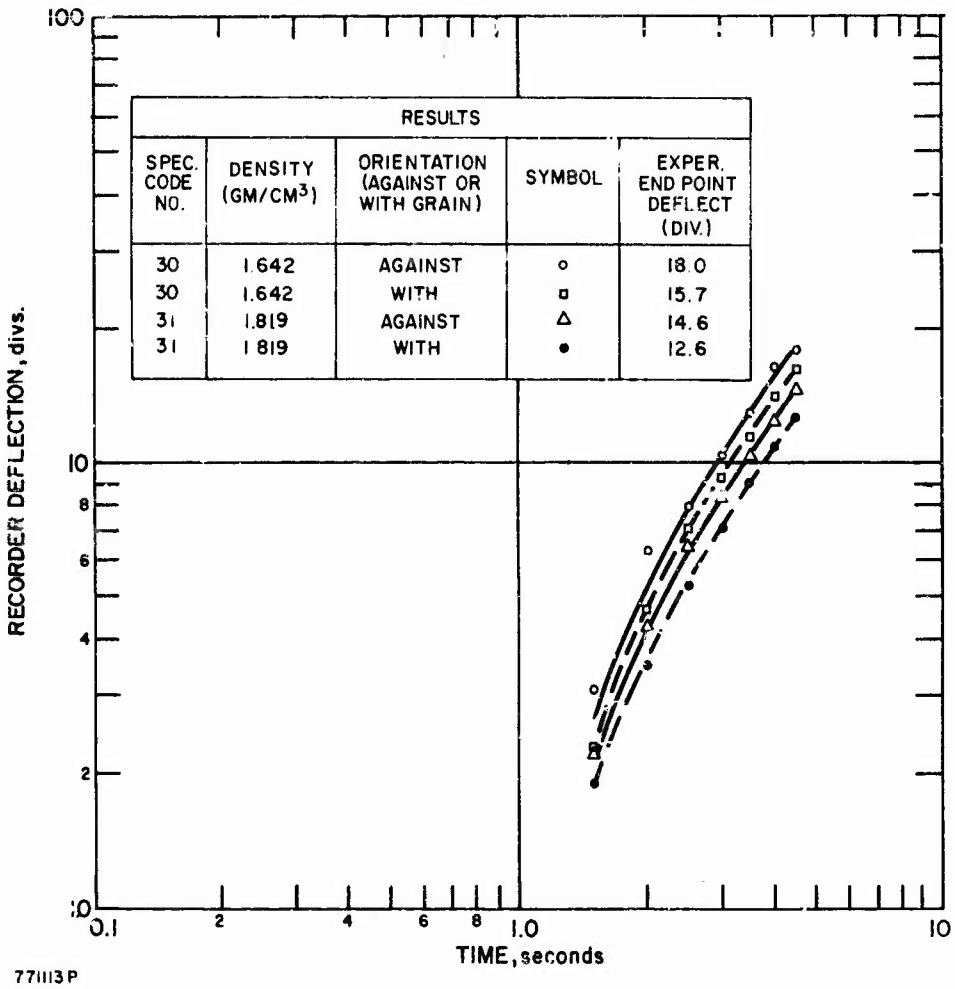

PARAMETERS:

1. LAMP VOLTAGE = 120 V
2. COATING: 3M VELVET BLACK
3. NO. COATS = 1
4. SPEC. DIMENSIONS: 1-INCH CUBES
5. TIME BASE AFTER PULSE INITIATION = 1.0 SECOND

NOTE:

1. BOTH THE SOLID AND DASHED LINES ARE CURVE SHAPES DERIVED FROM A STRAIGHT LINE FUNCTION FOR A TIME BASE = 1.0 SEC.
2. THE SOLID LINES INDICATE AGAINST-THE-GRAIN ORIENTATION OF THE CUBES.
3. THE DASHED LINES INDICATE WITH-THE-GRAIN ORIENTATION OF THE CUBES.
4. CORRECTION FOR REFLECTANCE LESS THAN 0.5 PERCENT FOR EACH CUBE

Figure 26. ILLUSTRATIONS OF THE ABILITY OF THE TECHNIQUE TO DISTINGUISH BETWEEN ORIENTATIONS AND DENSITY VARIABILITY OF ATJ GRAPHITE (FOR FINITE GEOMETRY)

TABLE III

RECORDER DEFLECTION VERSUS DENSITY AND CONDUCTIVITY RATIO OF 1-INCH CUBES OF ATJ GRAPHITE ORIENTED WITH AND AGAINST THE GRAIN

Graphite (ATJ) Cube Specimen Code No.	Density (gm/cm^3)	End-Point Deflection[5] (at 4.5 secs) against grain (divs)	End-Point Deflection[5] (at 4.5 secs) with grain (divs)	Thermal Conductivity Ratio[6,7] with and against grain k_W/k_{AG}	Ultrasonic Longitudinal Velocity (in/microsec)		
					V_{AG}	V_W	$\frac{V_W}{V_{AG}}$
29	1.649	18.5 ± 0.02^3	16.3 ± 0.02^3	1.28 ± 0.03^4	0.0766	0.0915	1.19
30	1.642	18.0 ± 0.02^3	15.7 ± 0.02^3	1.32 ± 0.03^4	0.0768	0.0911	1.18
13	1.700	16.9 ± 0.02^3	15.1 ± 0.02^3	1.26 ± 0.03^4	0.0787	0.0969	1.23
11	1.737	16.0 ± 0.02^3	15.1 ± 0.02^3	1.12 ± 0.03^4	0.0824	0.0971	1.18
26	1.818	15.4 ± 0.02^3	14.0 ± 0.02^3	1.21 ± 0.03^4	0.0839	0.1032	1.23
31	1.819	14.6 ± 0.02^3	12.6 ± 0.02^3	1.34 ± 0.03^4	0.0832	0.1026	1.23

1. Orientation of cubes determined using ultrasonic velocity techniques.
2. Cubes coated with 1 coat (nominal) 3M velvet black paint.
3. This error is associated with ability to read deflection on chart.
4. This is the probable reading error, obtained by taking the product of 0.67 and the square root of the sum of the errors for each deflection.
5. It is to be especially noted that the recorder deflections are for finite specimens. Their magnitudes will necessarily be greater than for the semi-infinite case, and require no vertex.
6. The thermal conductivity ratio: $k_W/k_{AG} = [\text{DEFL. AG. GR/DEFL. W. GR.}]^2$, where ρC_p is the same in either direction for a cube, and C_p is assumed constant for all 6 specimens.
7. For highly oriented type ATJ graphite, the ratio k_W/k_{AG} equals 1.33 from published data.

using ultrasonic velocity techniques. The degree of orientation is evidenced both by the thermal conductivity ratio and the velocity ratio in orthogonal directions. These ratios are to be compared to the generally accepted, published ratio of 1.33 for highly-oriented, type ATJ graphite. It is noted from the data that the degree of orientation is not related to density. Plotting the recorder deflections, with and against the grain direction, against density results in the straight line functions shown in Figure 27. Scatter in the data is attributed to coating thickness variability and to density variability. The approximate recorder deflection-density change sensitivity ratio is 1 division per 0.06 gm. per cu. cm. If this sensitivity is incorporated into a mathematical development, described in Appendix V, for determining the effect of density on the thermal conductivity of graphite, it can be said that a 1 percent increase in density will give rise to approximately a 2.5 and a 2.9 percent increase in conductivity for ATJ graphite in directions against and with the grain, respectively.

The effect of density variability on recorder deflection can be eliminated so that only thermal conductivity as a function of density is observed. This is accomplished by computing an equivalent conductivity, k_E, equal to $M/\rho(\Delta D)^2$, where M is a proportionality constant that includes the constant C_p for graphite, and ΔD is recorder deflection. Using the data from Table III, k_E is plotted against density in Figure 28. Estimated straight line fits to the data agree with the mathematical result, in Appendix V, that a 1 percent increase in density gives rise to about a 3 percent increase in conductivity for ATJ graphite.

These results for finite graphite specimens can be related to ideal, semi-infinite specimens to provide a means for determining the limitations of the technique in measuring $(k\rho C_p)^{1/2}$, and hence thermal conductivity variability. Assuming that a 1 percent change in density is determinable by other nondestructive test methods, this change gives rise to a 3 percent change in k, a 2 percent change in diffusivity, α, a 2 percent change in $(k\rho C_p)^{1/2}$, and consequently, a 2 percent change in recorder deflection. Ideal graphite produces a recorder deflection of approximately 3.9 divisions ±15 percent using this technique; this error being largely due to coating thickness variability. Thus, a $0.67 \times (15 \times 100/2) = 5$ percent change in density is necessary to produce a recorder deflection difference great enough to be considered minimally significant. Furthermore, this 5 percent minimum observable density change implies that the corresponding minimum observable conductivity change is equivalent to 15 percent, and the diffusivity change is equivalent to 10 percent.

V. Discussion

Because of the novel character of this technique, much detail has been presented in an effort to substantiate each step taken in its development. Considerable attention has been given to determining the magnitudes of errors arising from the several facets of the technique. By accounting for and preserving the separate sources of these errors, areas where improvements

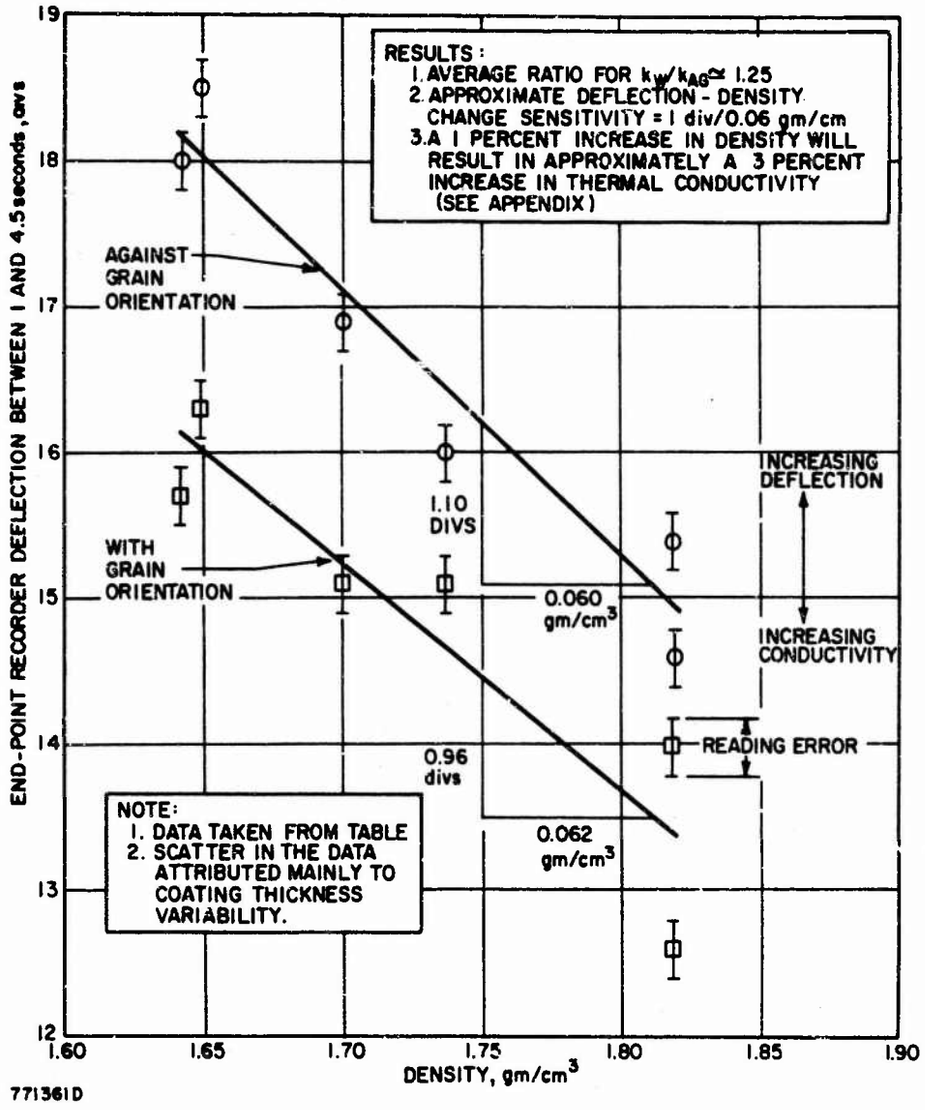

Figure 27. RECORDER DEFLECTION VERSUS DENSITY FOR FINITE SPECIMENS OF ORIENTED ATJ GRAPHITE

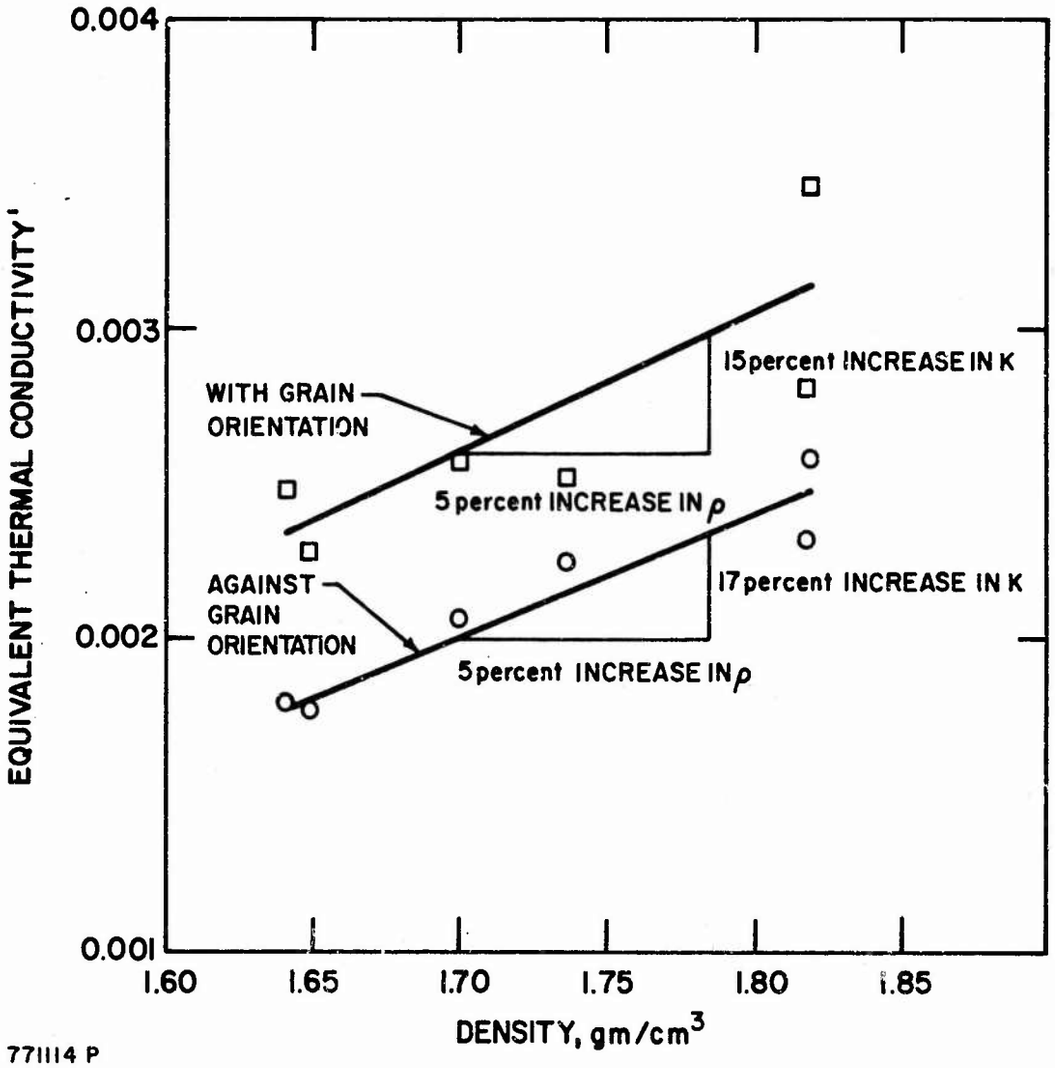

RESULTS:

1. THE AVERAGE RATIO FOR $k_w/k_{ag} \simeq 1.3$ AT $\rho = 1.7$ GM/CM^3
2. A 1-PERCENT INCREASE IN DENSITY GIVES RISE TO APPROXIMATELY A 3-PERCENT INCREASE IN THERMAL CONDUCTIVITY

NOTES:

1. THE EQUIV. THERM. COND.

$$k_E = \frac{M}{\rho(\Delta D)^2}$$

WHERE M IS A PROPORT. CONST. WHICH INCLUDES THE CONST. C_p FOR GRAPH. AND ΔD IS DEFLECTION.

Figure 28. EFFECT OF DENSITY ON THE THERMAL CONDUCTIVITY OF ATJ GRAPHITE

can be significantly made are readily apparent. Moreover, since an evaluation of the method relies essentially on these errors, a comparison of its results with those from other sources must necessarily consider the errors involved in the latter. Agreement between $(k\rho C_p)$ -values generated in this study and those obtained elsewhere must then be regarded in terms of reasonableness. Exact agreement cannot be expected for any case, because of intrinsic property variability that always exists between so-called typed materials, such as ATJ graphite, or even a specific grade of aluminum or steel.

The overall results are essentially summarized in terms of the differences in extremes between these and reported results that are tabulated in Table II. Graphite is seen to be the only material tested that is in apparent disagreement with these test results. The other four materials are each within a few percent of being in agreement with their corresponding reported values; agreement being considered to obtain when precisions of measurement overlap. These small differences, and even the large difference for graphite, are to be viewed as more ficticious than real. In support of this, it is first remarked that the reported values for $(k\rho C_p)^{1/2}$ were obtained by calculating the product of the k -, ρ -, and C_p -values listed in Table I; each value having been separately measured either by the same, or by different investigators, and having been selected by this author as representing an average, or a reasonably consistent value. Each listed value is also subject to a generally unknown experimental error, in itself, so that estimates of 10, 1, and 5 percent were used for the errors to be associated with the k -, ρ -, and C_p -values, respectively, in order to perform calculations for the errors to be associated with the reported $(k\rho C_p)^{1/2}$ -values; these estimates of accuracy being regarded as typical for measurements performed on similar type materials. Moreover, k -values, in particular, have been found in the literature to differ by as much as 50 percent for supposedly identical materials; materials similar to those used here. Furthermore, k -, ρ -, and C_p -values are normally measured and reported for average materials, where it is usual to presume that property variability in a material is averaged for specimen sizes used in standard measuring techniques. In this method, results are more influenced by material variability, as exists in ATJ graphite, for example, then they would be, say, in steady-state conductivity measurements. This is apparent because of the localized nature of the technique, such as the small area undergoing observation during heating. Lastly, the results for copper, aluminum and graphite are each affected by vertex suppression which creates additional error by producing "weak" signals. With these arguments providing a basis and the only guide for forming a judgement of the reasonableness of the agreement between the extreme differences, the method is then regarded to yield satisfactory results.

Validation of the method is not only supported by the reasonable over-all results it yields for inertia, but is evidenced particularly by the excellent agreement seen between the experimental and theoretical curve shapes for the history segments of semi-infinite materials in the 1 to 4.5 second time

interval. In addition, the magnitudes of measurement precision are sufficiently small, so that a good degree of confidence can be placed in the measurements. This confidence is borne out by the results for the finite graphite specimens, wherein density differences and grain orientation were easily distinguishable.

Translation of the finite results for ATJ graphite to semi-infinite graphite indicates that the present technique is capable of minimally discerning $(k\rho C_p)^{1/2}$ differences equal to 0.67 x15% = 10 percent, conductivity differences equal to 15 percent, and diffusivity differences equal to 10 percent. This conductivity measurement capability is to be compared with a typical error of 10 percent for steady-state conductivity measurements using standard destructive test methods. This 10 percent error would permit 0.67 x 10% = 6.7 percent k-differences to be minimally observable. It is important to realize that finite-size sections of graphite can be measured for $(k\rho C_p)$ -, k -, and α - differences less than those for the semi-infinite case; that is, to greater degrees of precision.

Since the present technique necessarily employs coatings, and coating thickness variability has been determined to constitute the principal source of precision error, it follows that control of thickness to better than about 15 percent will increase measurement precision. Using a higher conductivity coating material that still exhibits a high emissivity will also increase precision. Precision can further be improved by increasing the radiant flux incident to a surface and, of course, by eliminating the need for a coating entirely. A flux increase would tend to reduce the need for correcting the effect of vertex suppression and would provide a more favorable signal-to-noise level for high inertia materials. This correction for vertex suppression can be very nearly eliminated if a radiometer reference source is used that has a temperature equal to, or less than, that of the surroundings; there existing always a finite response character for any radiometer which must be exceeded before a signal is recognizable. Trade-offs between these interacting variables are necessary to optimize a technique for a particular situation.

It must be appreciated that the coating used here caused a time interval to be selected which was considerably delayed after pulse initiation, in order that the retardation effect of the coating would be negligible. This delay made it necessary to employ ideal specimens that are larger than would be necessary if a shorter delay and time interval for analysis could have been employed, because of the criterion of semi-infiniteness. Thus, improvement in the coating material will permit the testing of smaller ideal specimens.

The accuracy of the present technique can only be assessed in terms of the standard used for comparison. Assuming that standard measuring techniques on high-k materials are accurate to 10, 1, and 5 percent for k -, ρ -, and C_p -values, respectively, the probable error in calculating their product is

11.2 percent. The corresponding calculated error for a $(k\rho C_p)^{1/2}$-value is 5.6 percent, which is the "book-value" accuracy assigned to the value used for the Armco iron standard employed here. The probable error of measurement for $(k\rho C_p)^{1/2}$ for Armco iron in this study was 0.67 x 0.05 x 100/0.38 = 8.8 percent (from Table II). The accuracy of this technique is then considered to be 8.8 percent, of which approximately 70 percent is attributed to variability in coating thickness. Thus, exact control of coating thickness, or its elimination, would conceivably increase measurement accuracy for the technique to at least 5.6 percent and to probably about 3 percent if better standards can be found; this being considered a most favorable comparison between this technique and present standard test methods.

Extension of this comparative method to include other materials is, of course, entirely feasible. A natural consequence of the present technique is to extend it to materials having inertias less than that for lead (or, almost in general, to materials having lower conductivities), since measurement precision increases as thermal inertia decreases. For dielectric materials, emissivities are uniformly high, so that the use of coatings would probably not be as necessary as for metals. A further extension of the method to include elevated temperature measurements is possible, but the present technique would probably require considerable modification.

VI. Conclusions

A transient technique has been developed and validated for nondestructively measuring the near-room-temperature thermal inertia of semi-infinite solid materials by comparison with a reference standard, so that knowledge of heat flux is unnecessary. The thermal conductivity and diffusivity of a solid can also be determined if its density and specific heat are known. Variabilities in conductivity and diffusivity are then determinable, for solids having a uniform chemistry, if only density is known. The typical period of time required to generate an inertia measurement is about 10 seconds. The probable accuracy of the technique is estimated to be approximately 9 percent when calibrated against Armco iron, while the probable-precision error will increase as thermal inertia decreases; the present range being about 9 percent for copper to 7 percent for lead. Derived thermal conductivity values will have a precision error range approximately twice the error range for inertia, while diffusivity values will have an error range about equal to this. Coating thickness variability is estimated to contribute about 70 percent of the error to these precision values. These errors can be compared to a calculated accuracy of about 6 percent for $(k\rho C_p)^{1/2}$ values derived from typical measurement errors for k , ρ , and C_p using standard destructive test techniques.

Application of this transient technique to semi-infinite, coated, ATJ graphite sections indicates that it is capable of discerning $(k\rho C_p)^{1/2}$-differences equal to 10 percent, conductivity differences of 15 percent, and diffusivity differences of 10 percent. Typical standard steady-state measurements can determine conductivity to an accuracy of about 10 percent. For finite graphite specimens, conductivity differences of about 7 percent are minimally observable; this increased precision resulting from the apparent effect of a decrease in inertia, and hence stronger signal generated.

Extension of the technique in its present form to include materials having inertia values less than that for lead is entirely feasible. Measurement precision could ultimately be expected to increase to about 3 percent for low inertia values comparable to that typical of many dielectric materials. Further extension of the method, itself, to elevated temperature measurements of inertia is possible, although the present technique would probably require considerable modification.

VII. REFERENCES

1. H. S. Carslaw and J. C. Jaeger, "Conduction of Heat in Solids," Oxford, London, 2nd Edition, 1959, p. 75.

2. J. V. Beck and H. Hurwicz, "Study of Thermal Discontinuities and Associated Temperature Disturbances in a Solid Subject to a Surface Heat Flux, Part II," Avco Technical Report, TR-9-59-14, April 28, 1959, p. 9.

3. The Industrial Graphite Engineering Handbook, Union Carbide Corp., 1964, p. 5B.05.01.

PART III

INFLUENCE OF ATTENUATION UPON THE FREQUENCY CONTENT OF A STRESS WAVE PACKET -- S. SERABIAN*

I. INTRODUCTION

The use of plused ultrasound in the frequency range of 1/2 to 25 MHz for evaluating materials is well established. The three useful characteristics of ultrasound for such activities are velocity, attenuation, and the inability of ultrasound to completely traverse a discontinuity of mechanical properties. In the latter, some amount of energy is always reflected at the discontinuity, and accounts for the detection of such flaws as cracks and foreign inclusions.[1-3] Velocity measurements have been used to nondestructively determine density, modulus, and ultimate tensile strength of brittle materials.[4-6] Attenuation in conjunction with velocity measurements has significantly contributed to such studies as the behavior of dislocations in the metallic state,[7,8] magnetic wall domain[9] motion, and radiation damage.[10]

All the propagation parameters of ultrasound cited above are functionally dependent upon frequency. In highly attenuating materials, the frequency content of a pulse packet is altered or distorted during propagation.[11] This is particularly noticeable for the highly attenuating materials, such as bulk graphite, produced for the aerospace industry to meet the unique ablative and strength requirements. For such materials, it is necessary to understand frequency distortion and the resulting implications of such behavior upon the current uses of ultrasound for material evaluation. The purpose of this paper is to consider the measurement criteria for frequency distortion and, in particular, to study these effects in relation to attenuation and velocity measurements in graphite.

*Faculty member Lowell Technological Institute, Lowell, Mass.

II. PRELIMINARY CONSIDERATIONS

A stress wave propagating in the x direction in its simplest form may be typified as

$$y = A\,Cos\,(ct - x) = A\,cos\,2\pi(ft - ax) \quad , \tag{14}$$

where y is the displacement imparted to a particle of the medium being traversed, A is the maximum amplitude, f is the frequency, and a is the wave number or reciprocal wavelength. This relationship may be used to describe the propagation either of continuous waves or pulses. For pulses, it must be understood that the constant A is the maximum amplitude of the pulse packet. From this point on, the paper will be concerned only with the propagation of pulses. At any given instant of time (t), the above equation will give the total displacement (x) of the stress wave along the path of propagation. Also, at any given position, the equation will indicate the particle displacement that occurs as the wave passes through the position in question. The velocity (c) is known as the phase velocity, since it can be used to indicate the relative phase of two neighboring particles or positions along the path of propagation; velocity is related to the material constants of the propagating medium by

$$c_l^2 = \frac{E}{\rho}\,\frac{1-\sigma}{(1+\sigma)(1-2\sigma)} \quad ; \quad c_s^2 = \frac{G}{\rho} \quad ; \tag{15}$$

where c_l is the longitudinal velocity and is characterized by a particle motion in the direction of propagation; c_s is the shear velocity and has

a particle motion perpendicular to the direction of propagation; ρ is the density of the medium; σ is Poisson's ratio; and E and G are the tensile and shear moduli, respectively.

It should be noted that the above expressions for velocity are void of any frequency notation. In the usual sense, one associates a particular frequency with a stress wave, i.e., as governed by the characteristics of the excitation applied to the transducer. If the excitation is of a given frequency, then, the particle motion and velocity of propagation are defined by Equations (14) and (15). The stress wave will also experience an exponential decay in amplitude in accordance with a factor $e^{-a_f x}$, where a_f is the attenuation constant at the frequency f, and x is the distance that the wave has travelled in the medium. In other words, Equation (1) must be modified to read

$$y = A e^{-a_f x} \operatorname{Cos}(ct - x) = A e^{-a_f x} \operatorname{Cos} 2\pi(ft - ax) \quad . \tag{16}$$

In the strict interpretation of Equations (15) and (16), the only effect of a change in frequency is found in the particle motion and in the attenuation constant.

A transducer excitation that produces a pulse having a single frequency is of academic value only. The excitations usually involve a finite spectrum of frequencies as indicated in Figure 29. With such an excitation spectrum

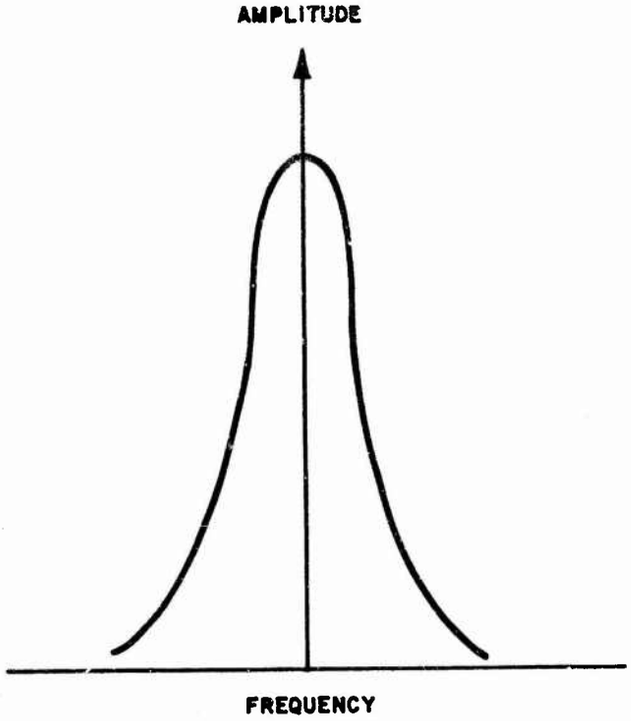

770349 D

Figure 29. DIAGRAMATIC REPRESENTATION OF THE FREQUENCY SPECTRUM OF THE TRANSDUCER ACTIVATION PULSE; f_o IS THE CENTER FREQUENCY

The total stress wave propagated into the medium is an additive effect of all the frequency components; i.e., Equation (16) must be further modified to read

$$\gamma_T = G(f_1)\, e^{-a f_1 x} \cos 2\pi(f_1 t - a_1 x) + G(f_2)\, e^{-a f_2 x} \cos 2\pi(f_2 t - a_2 x)$$

$$\ldots\ldots\ G(f_n)\, e^{-a f} \cos 2\pi (f_n t - a_n 2)$$

$$= \sum_f G(f)\, e^{-a f x} \cos 2\pi (ft - a_f x) \quad , \tag{17}$$

where $G(f)$ is the amplitude of the excitation at any given frequency, and may be mathematically defined by Fourier analysis techniques of the frequency spectrum typified by Figure 29. The wave number (a_n) is the reciprocal wavelength (λ_n) associated with the frequency (f) through the equation

$$\frac{f_n}{a_n} = c_n = f_n \lambda_n \quad . \tag{18}$$

If the material is dispersive in nature, such that the velocity is a function of the wavelength, then all the individual components would travel with their own phase velocity (c_n). Since the total stress wave is a composite of all such individual waves, it would have its own velocity, i.e., the group velocity. If we now consider the effect of attenuation, we find that the components at the higher frequencies are being preferentially attenuated with path length; thus, the pulse shape is being continuously distorted and the group velocity is continuously changing in magnitude as it propagates

through a medium. Thus, the group velocity under these conditions is not a useable material constant and is essentially undefinable unless the attenuation is well known.[12] For most materials, however, the velocity is nondispersive; i.e., the phase velocity is not dependent upon frequency. Thus, all the individual component waves illustrated in Equation (17) travel with the same velocity as defined by Equation (15) and

$$\frac{f_n}{a_n} = f_n \lambda_n = c \text{ (a constant)} \quad . \tag{19}$$

Therefore, once the total stress wave is formed, it will travel through the medium with the same velocity as the individual component waves; i.e., in a nondispersive material, the group velocity is equal to the common phase velocity (c) of Equation (19). Under this condition, the velocity of propagation of nondispersive materials is well defined and can be measured without ambiguities.

If the attenuation is negligible or essentially constant within the range of frequencies of the transducer excitation (Figure 29), then the total stress wave will travel undistorted in shape through the medium. If the effect of the attenuation constant cannot be considered negligible, however, then the higher frequency components will be attenuated with path length relatively more than will the lower frequencies. Thus, the total stress wave will continuously change its shape as it propagates through the medium.

III. EXPERIMENTAL WORK

Graphitite G was selected as the material for this study for two prime reasons: First, its attenuation is sufficiently high to produce the desired effects; second it is relatively homogeneous in material constants to ultrasound for the frequency range considered. The basic apparatus of

the experimental setup is shown in Figure 30. Figure 31 shows the actual equipment. The pulse oscillator activates the transducer to produce a stress wave pulse in the specimen; only the longitudinal mode of vibration will be considered. Following transmission through the specimen, the pulse is detected by another transducer on the opposite side, suitably amplified and displayed on the oscilloscope to facilitate a measurement of the shape and periodicity characteristics. A frequency spectrum analyzer was incorporated into the apparatus to display the frequency spectra both of the activation pulse applied to the transmitting transducer of the "received" pulse. Figure 32 shows typical displays for the activation pulse (Point A), the received pulse (Point B), and the frequency spectrum of either transducer (Point C).

In demonstrating the effects of attenuation, we are essentially concerned with the $e^{-\alpha_f x}$ term of Equation (17). For Graphitite G, it was found that a transducer excitation with a center frequency of 1.8 MHz allowed measurements over an extensive range of specimen thickness. The lower frequencies, with their lower attenuation constants, required specimens longer than those available in order to note the desired effect; the attenuation at the higher frequencies, however, was too high to allow the required measurements for noting the effect of propagation distance. The results at 1.8 MHz are shown in Figure 33. It should be noted that the frequency content of the

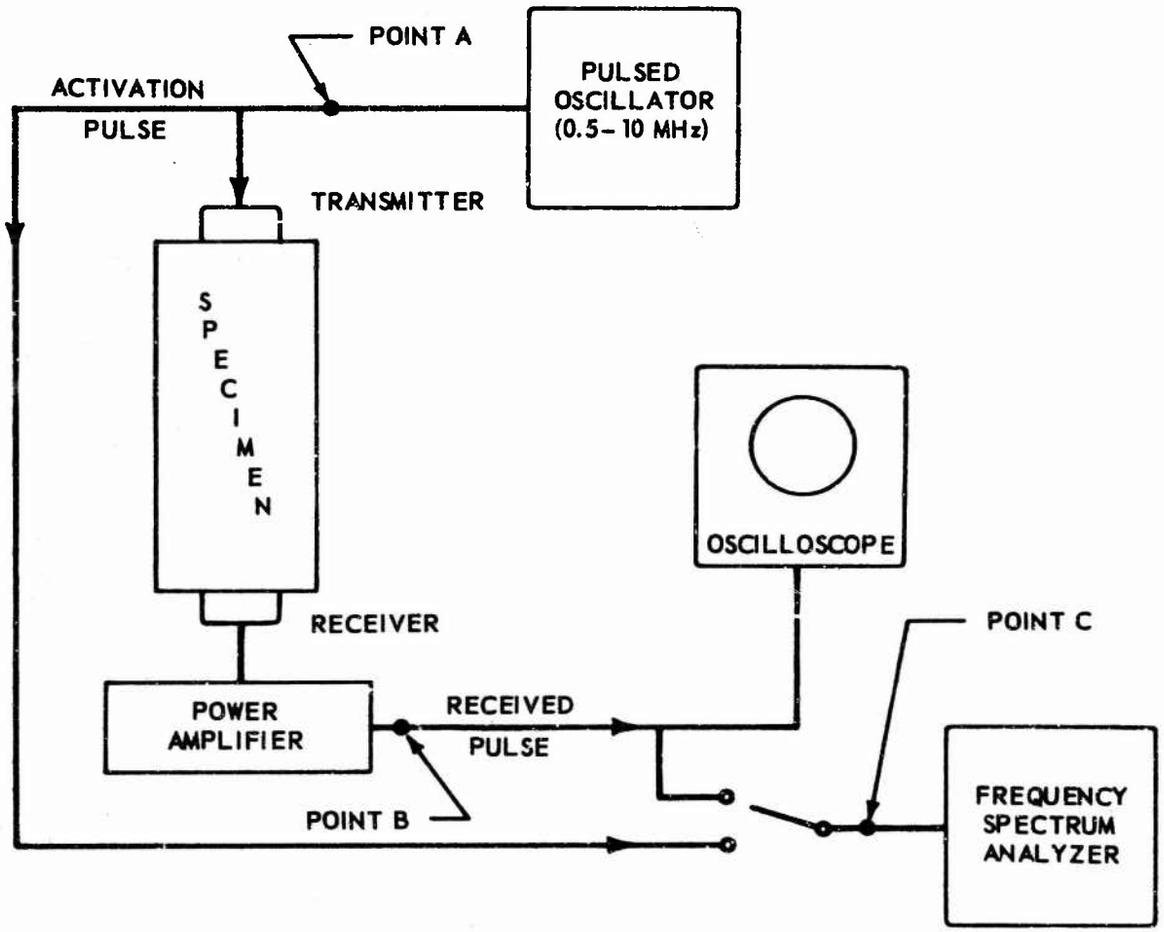

770350 D

Figure 30. BLOCK DIAGRAM OF MEASURING SYSTEM

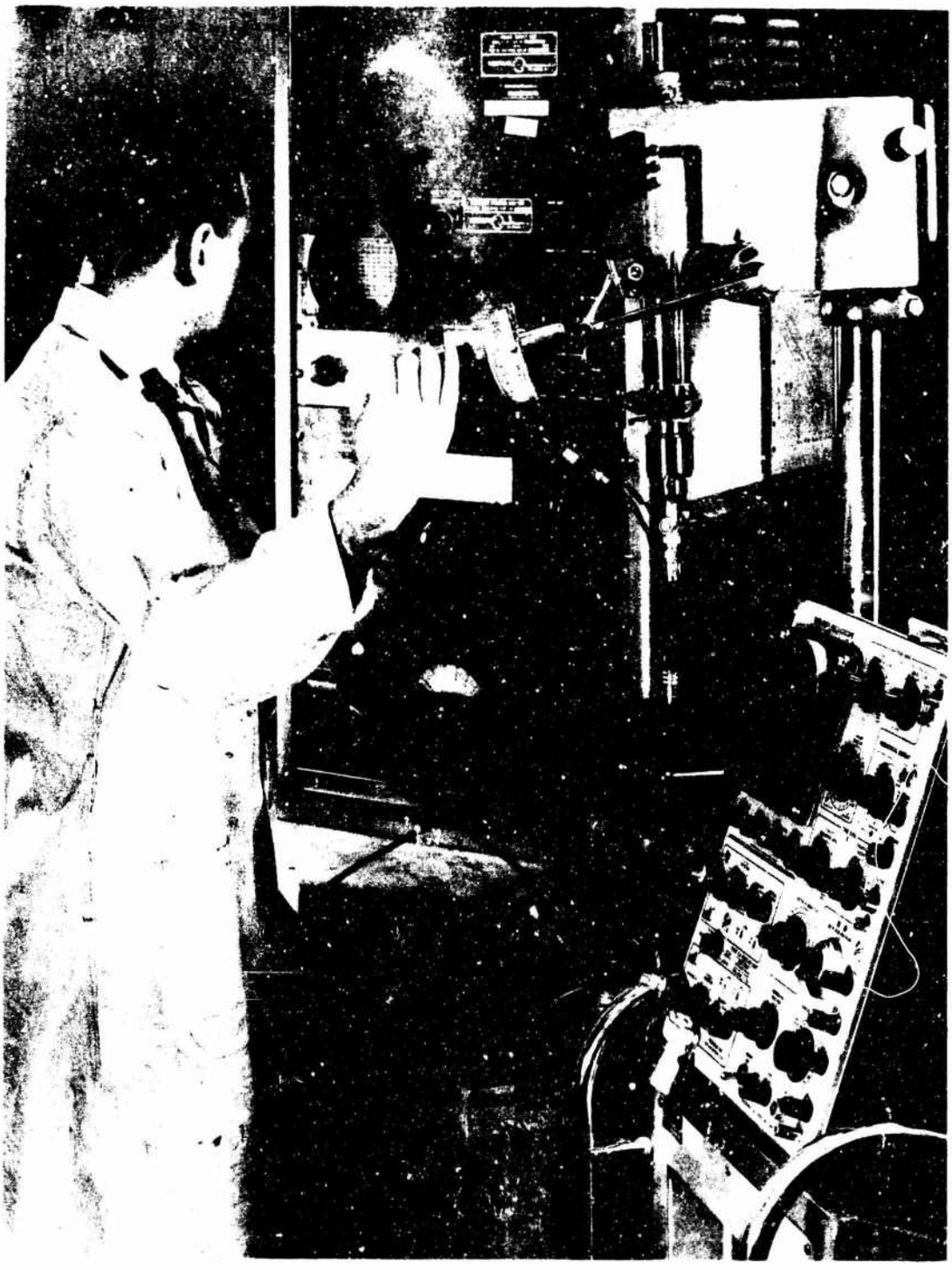

Figure 31. TEST EQUIPMENT. DRILL PRESS AND TORQUE WRENCH APPLY CONSTANT PRESSURE TO TRANSDUCER

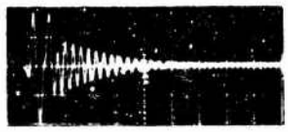

POINT A ACTIVATION PULSE

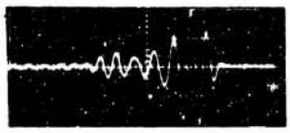

POINT B TOTAL STRESS WAVE

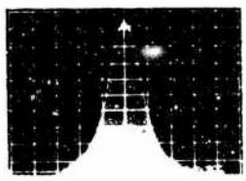

POINT C FREQUENCY SPECTRUM

770351 D

Figure 32. TYPICAL PULSE CHARACTERISTICS (REFER TO FIGURE 31 FOR LOCATION WITHIN THE MEASURING SYSTEM)

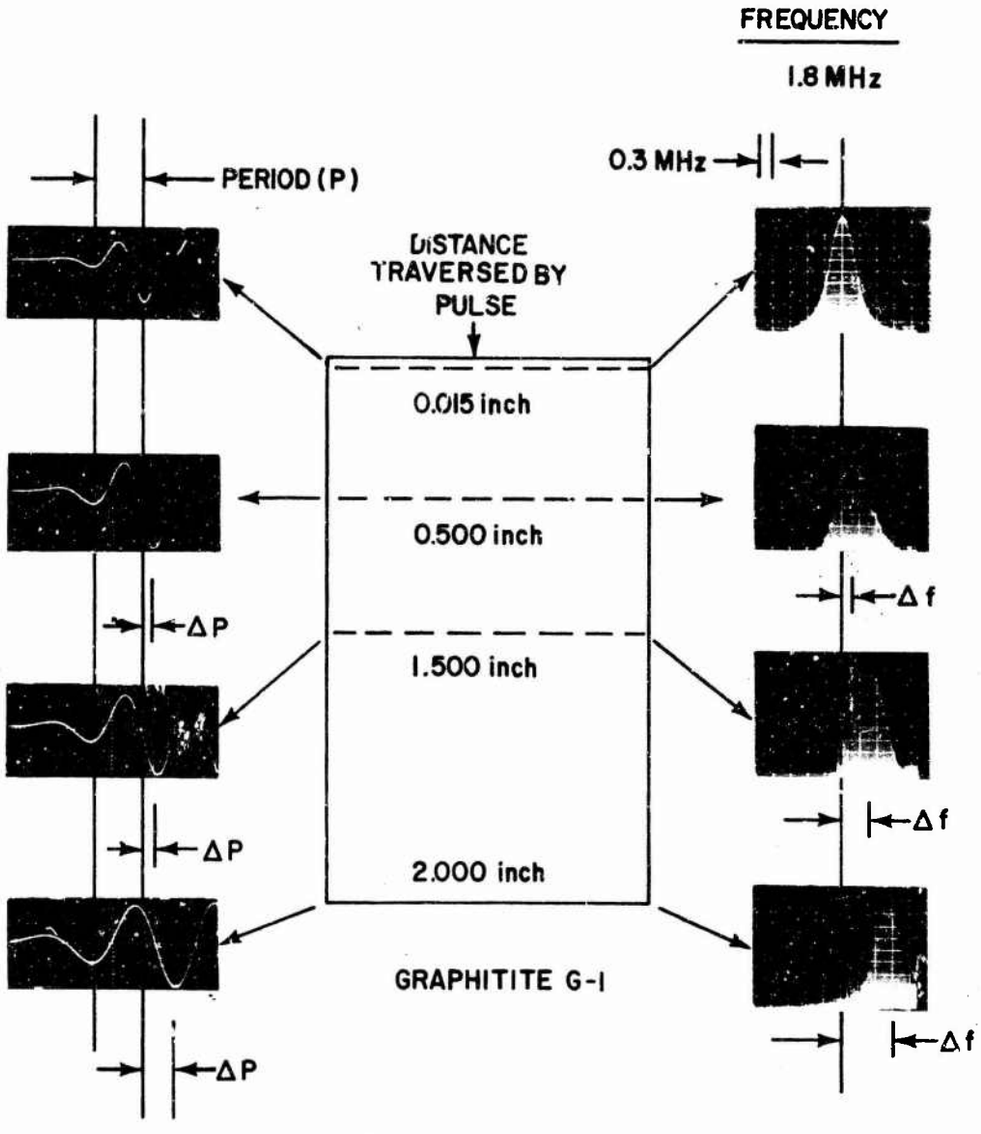

Figure 33. PERIODICITY AND FREQUENCY SPECTRA OF TRANSMITTED PULSES AS A FUNCTION OF PATH LENGTH

stress wave is continuously shifting to the lower frequencies as it propagates down the length of the specimen. The frequency shift is evident from the spreading of the received pulse in time, as noted by the continuous increase in the period of oscillation (ΔP) with specimen thickness. The wave forms indicated are those of Point B of Figures 30 and 32, expanded in time to facilitate measurements. Horizontal gain of oscilloscope was maintained constant for all measurements. The shift to the lower frequencies can also be observed in the frequency spectrum displays in Figure 33. Δf is the change in the center frequency. The instrument settings governing the horizontal component of the displays were held constant during measurements. Starting with a center frequency of 1.8 MHz at a thickness of 0.015 inch, the frequency spectrum has shifted to a center frequency of 0.9 MHz after a propagation distance of 2 inches, i.e., a frequency distortion of approximately 50 percent. For ease of interpretation, the frequency spectrum displays have been superimposed in Figure 34.

It should be mentioned that all the amplitudes of the displays of Figures 33 and 34 have been normalized; i.e., in each instance the gain was adjusted to provide the same amplitude. If we maintain a constant instrument gain throughout the experiment, the results would appear as diagrammed in Figure 35. The dotted line is the locus of the maximum amplitudes of the frequency spectrums and is indicative of the over-all attenuation experienced

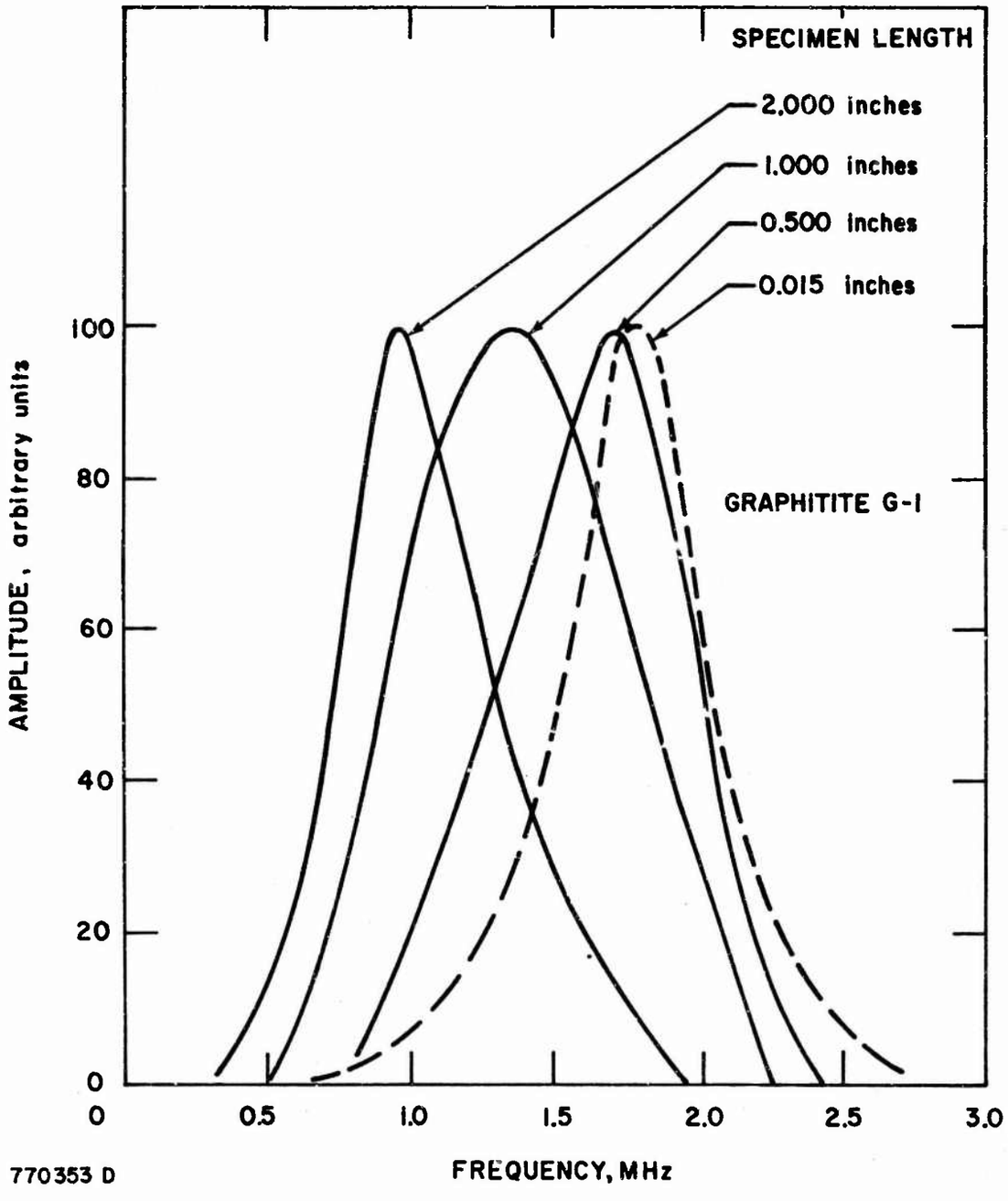

Figure 34. NORMALIZED FREQUENCY SPECTRA AT RECEIVER TRANSDUCER FOR SPECIMEN LENGTHS UP TO 2 INCHES (1.8 MH. CENTRAL FREQUENCY TRANSMITTED)

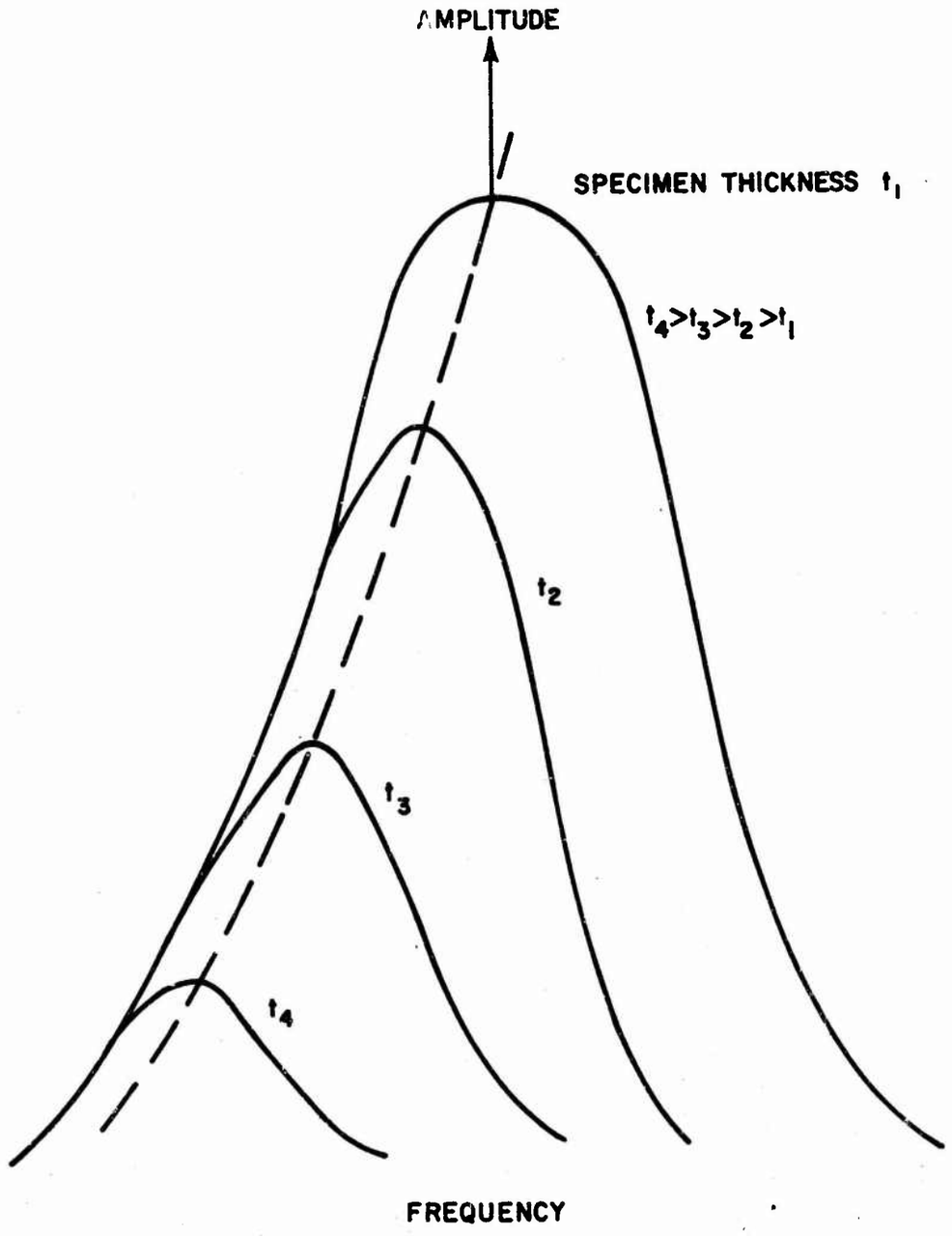

Figure 35. THE FREQUENCY SPECTRAL SHIFT TO THE LOWER FREQUENCIES, WITH AMPLITUDE DECREASE IN ACCORDANCE WITH ATTENUATION

by the stress wave. It must be appreciated that if the gain is now altered we do not revert back to the frequency spectrum of the initial stress wave. This may be further demonstrated by the fact that the frequency of the received pulse, as determined by a period measurement on the oscilloscope display, is always the center frequency of the particular frequency spectrum display.

IV. ANALYSIS OF EXPERIMENTAL DATA

Of prime importance in any discussion of the experimental data is a measurement of the attenuation of the medium, i.e., Graphitite G. The apparatus used is the same as indicated in Figure 30. The technique used was to note the amplitude of the total output pulse as the specimen length was varied. Throughout the experiment the instrument gain was maintained constant, and the transducer coupling conditions were duplicated each time by applying the pressure to the transducer by a torque wrench. (See Figure 31.) The attenuation at each specimen length was determined in the conventional manner from the slope of the semi-log plot of the amplitude-distance data. Figure 36 shows a typical result. The fact that the data form a straight line indicates the homogeniety of the specimens. A composite of such plots for the frequency range of 0.4 to 3.5 MHz is displayed in Figure 37.

Noting the attenuation frequency plot of Figure 37, we can derive one requirement for an appreciable frequency shifting or stress-wave distortion during propagation. It is not entirely a question of the magnitude of

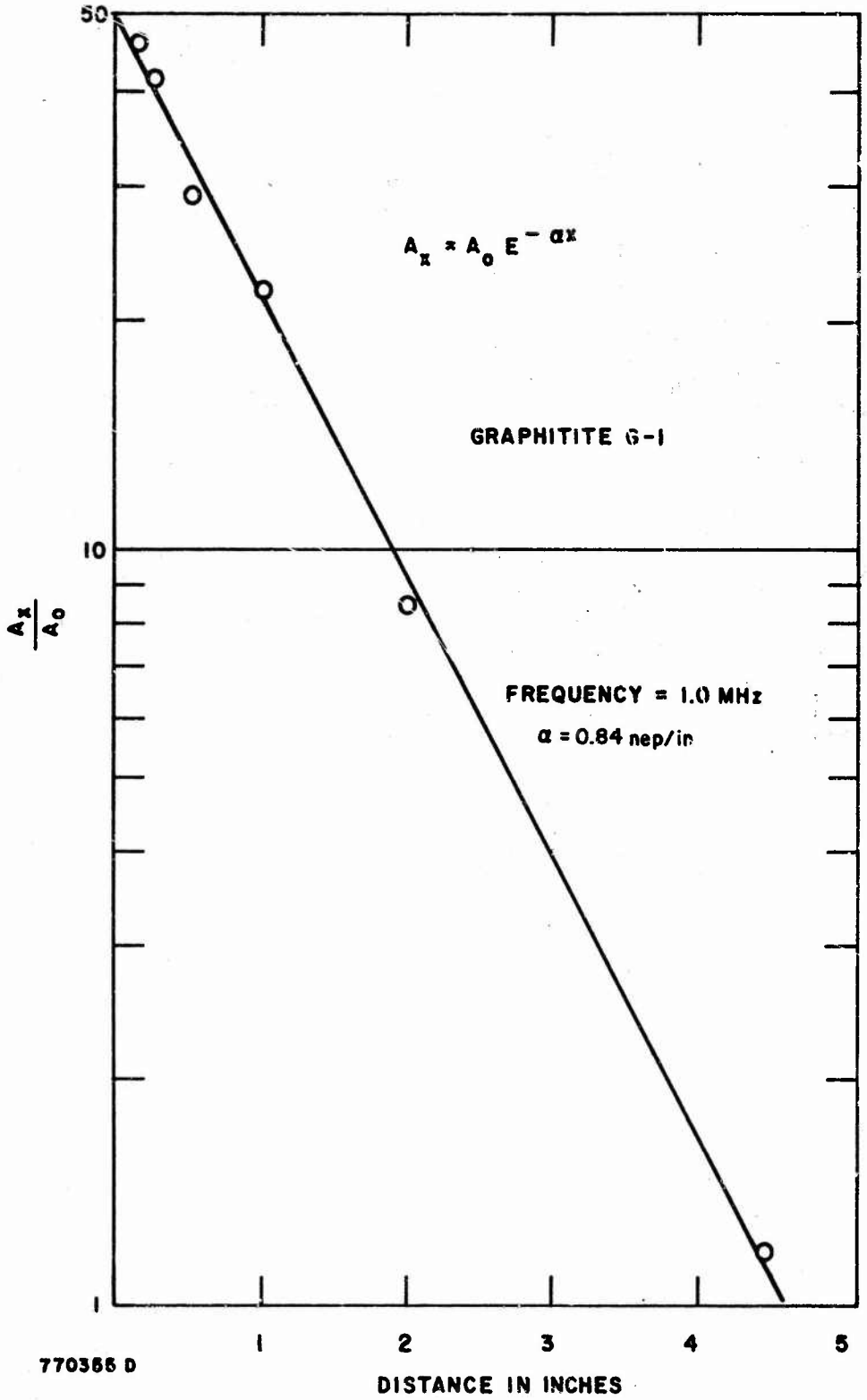

Figure 36. MAXIMUM AMPLITUDE OF A STRESS WAVE AS A FUNCTION OF SPECIMEN LENGTH (TRANSMITTER CENTER FREQUENCY OF 1.0 MHZ)

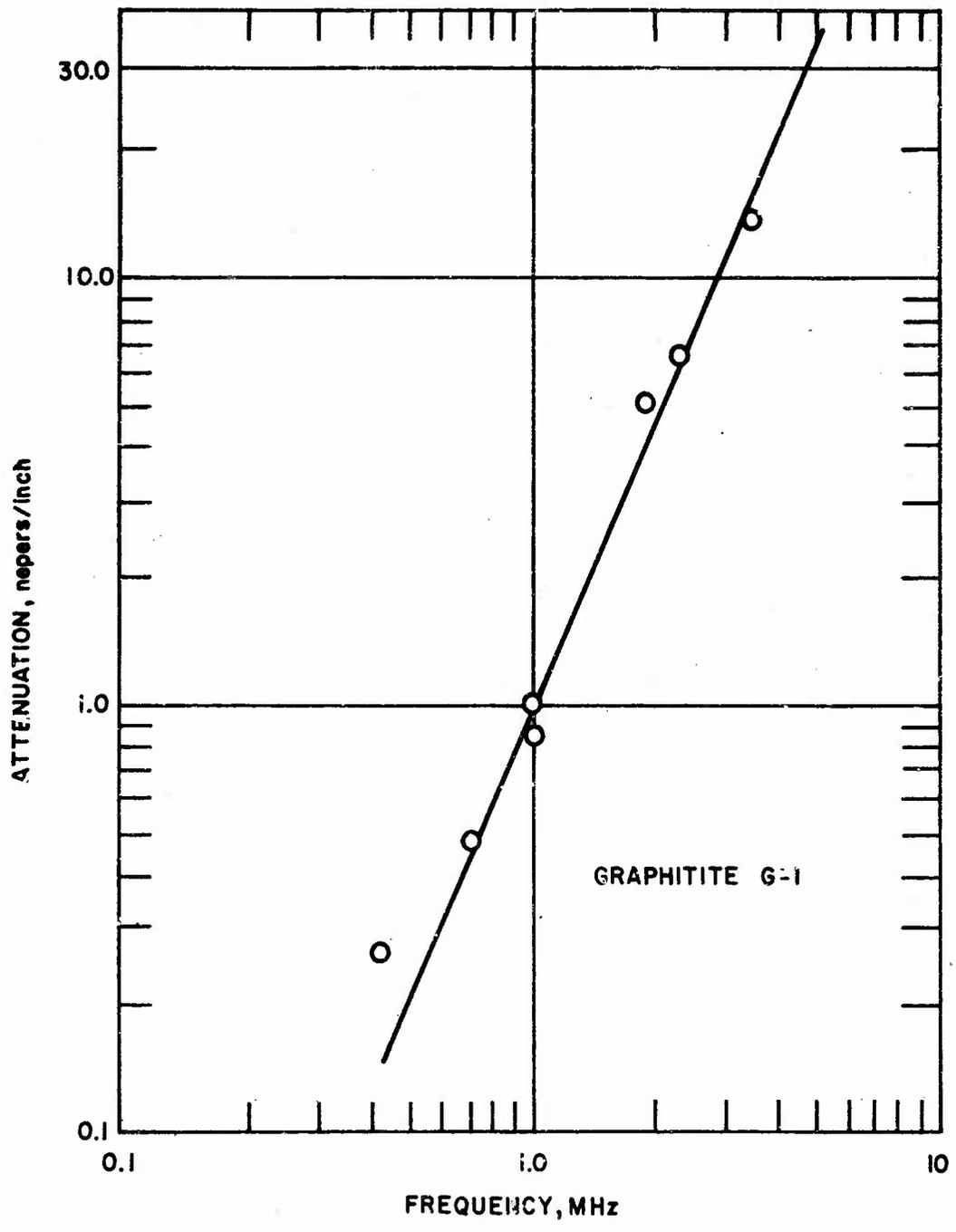

Figure 37. ATTENUATION-FREQUENCY PLOT OF GRAPHITE G-1 SPECIMEN GROUP

the attenuation: the important characteristic is the rate of change or the slope of the attenuation with frequency within the range of the frequency spectrum of the activation pulse to the transducer. The greater the slope, the greater the selective absorption (hence distortion) the pulse will experience. The effect of selective absorption may be illustrated by Figure 38, which shows the situation where two Graphitite G specimen groups have essentially the same attenuation at the center frequency but have different slopes. It should be noted that the Graphitite G-1, by virtue of its greater slope, produced the most frequency distortion (50 percent). After traversing 2 inches of specimen, the center frequency of the pulse of the Graphitite G-1 had shifted from 1.8 MHz to 0.9 MHz (Figure 34); while, for the Graphitite G-2, for the same propagation path length, the center frequency was only shifted to 1.26 MHz -- a frequency distortion of 30 percent.

The effect of the magnitude of attenuation can be realized by considering the aluminum specimen of Figure 38. Although the slope of the attenuation-frequency plot of the aluminum is the same as that of the Graphitite G-2 specimen, the pulse, after traveling an equivalent path length, produced no frequency distortion. In other words, the condition for selective absorption was present; but insignificant changes were produced, due to the low magnitude of attenuation. For the pulse to experience a notable frequency

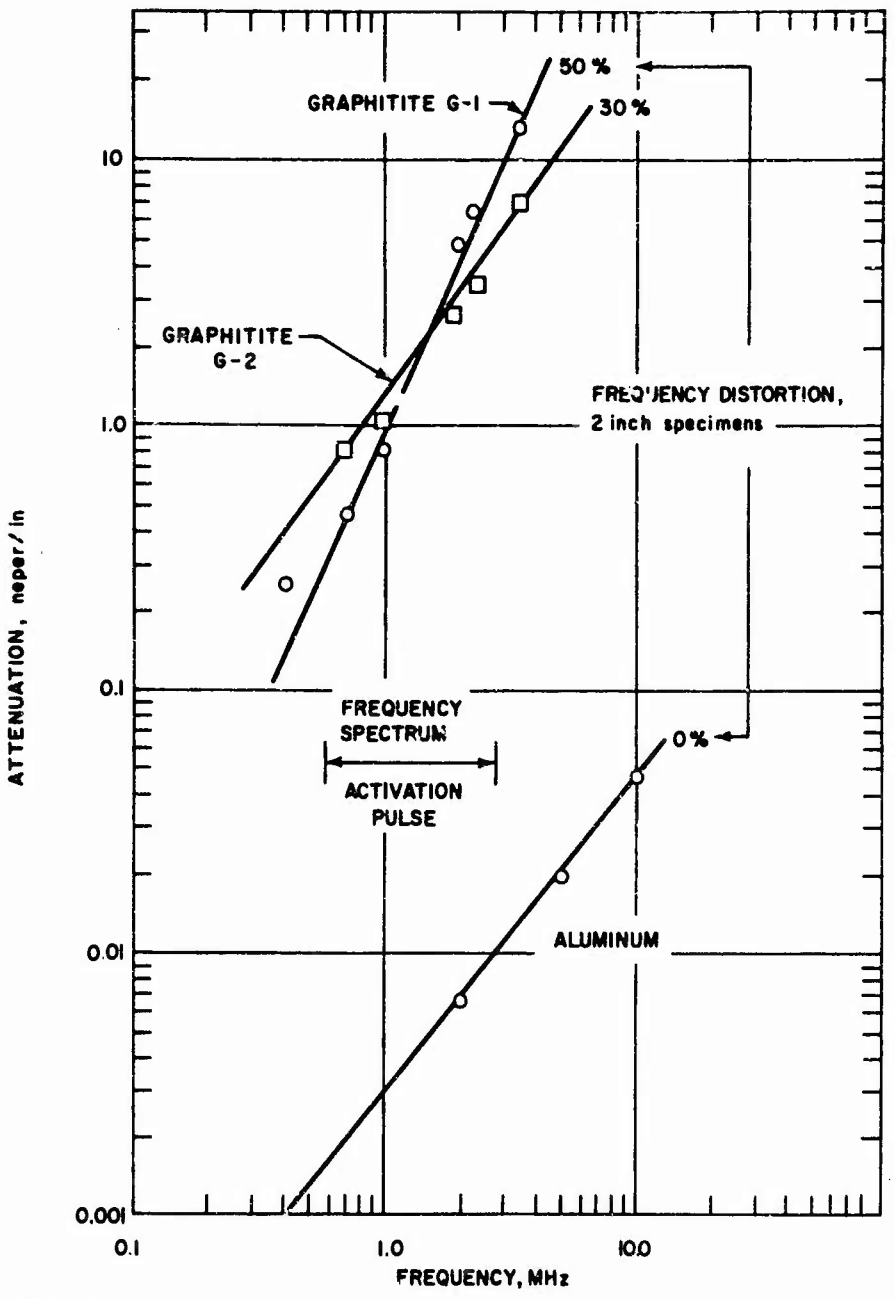

Figure 38. SPECIMEN ATTENUATION CHARACTERISTICS AND THE RESULTING FREQUENCY DISTORTION FOR PATH LENGTH OF 2 INCHES

distortion in the aluminum specimen, either a very long specimen or a much higher frequency activation pulse must be used, as dictated by the exponent $e^{-a_f x}$ of Equation (17).

It is possible to note the effect of attenuation upon the frequency content of a stress wave by analytical techniques. Assuming that the stress wave propagating through a specimen of 0.015 inch has essentially no frequency distortion, we may consider the frequency spectrum involved as characterizing the stress wave at the transmitting transducer. Since the attenuation as a function of frequency is known (Figure 38), the amplitude of any portion of the frequency spectrum after traversing a given specimen length may be evaluated according to the $e^{-a_f x}$ term of Equation (17). If the initial amplitude at a given frequency is taken as A_f°, then the amplitude of the stress wave after traveling x distance (A_f^x) is given by

$$A_f^x = A_f^{\circ} \; e^{-a_f x} \; . \qquad (20)$$

These quantities are diagrammed in Figure 39. Performing the necessary calculations at a sufficient number of frequencies produces an agreement with the experimental data noted (Figure 34). Typical results for Graphitite G-1 are shown as Figure 40.

To be complete, it should also be mentioned that it is possible to approximate A_f° as a function of frequency in a closed form by a Gaussian or error distribution. In adapting the constants of the Gaussian distribution, the mean

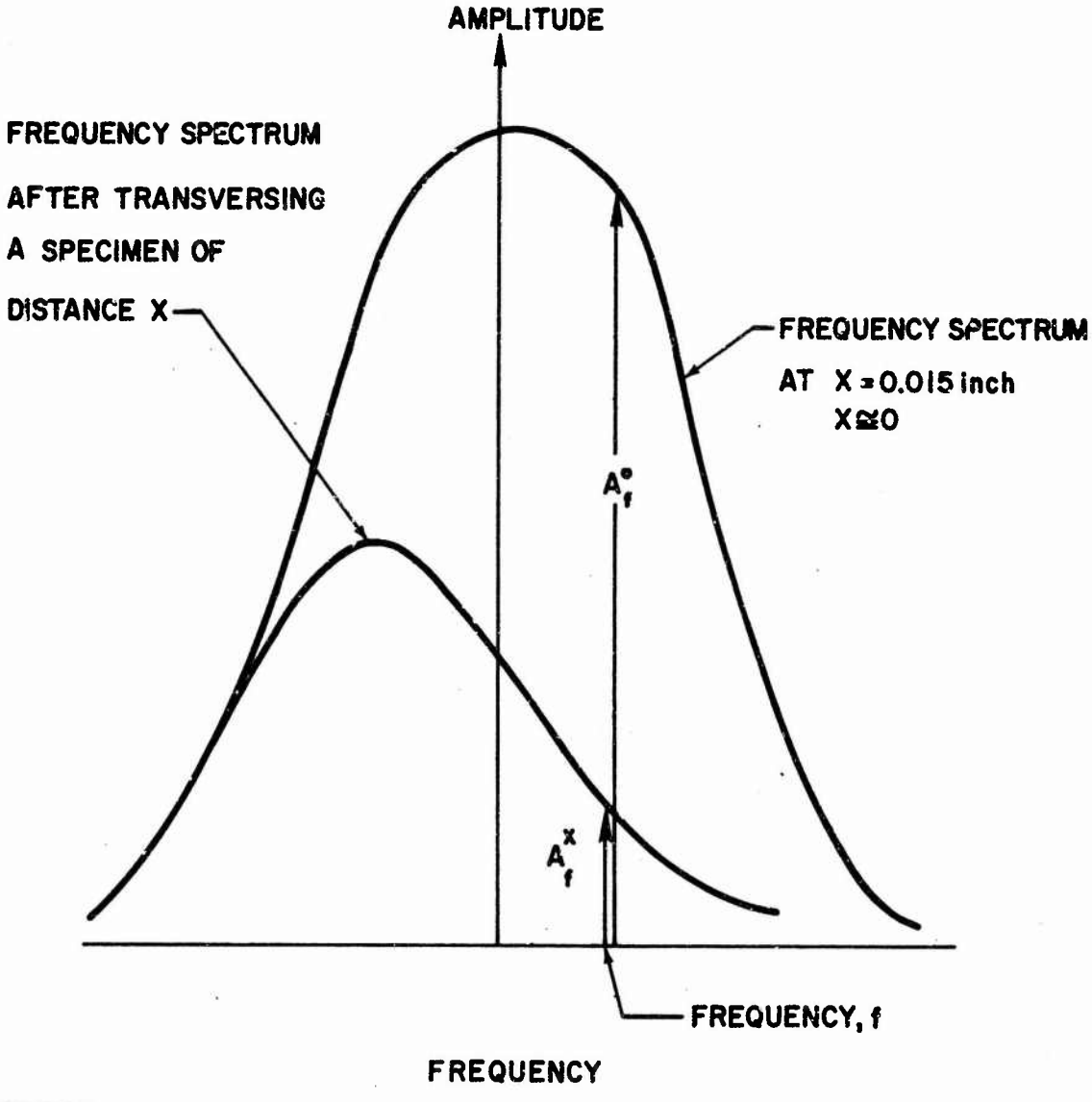

770358 D

Figure 39. GRAPHICAL DISPLAY FOR EQUATION (20)

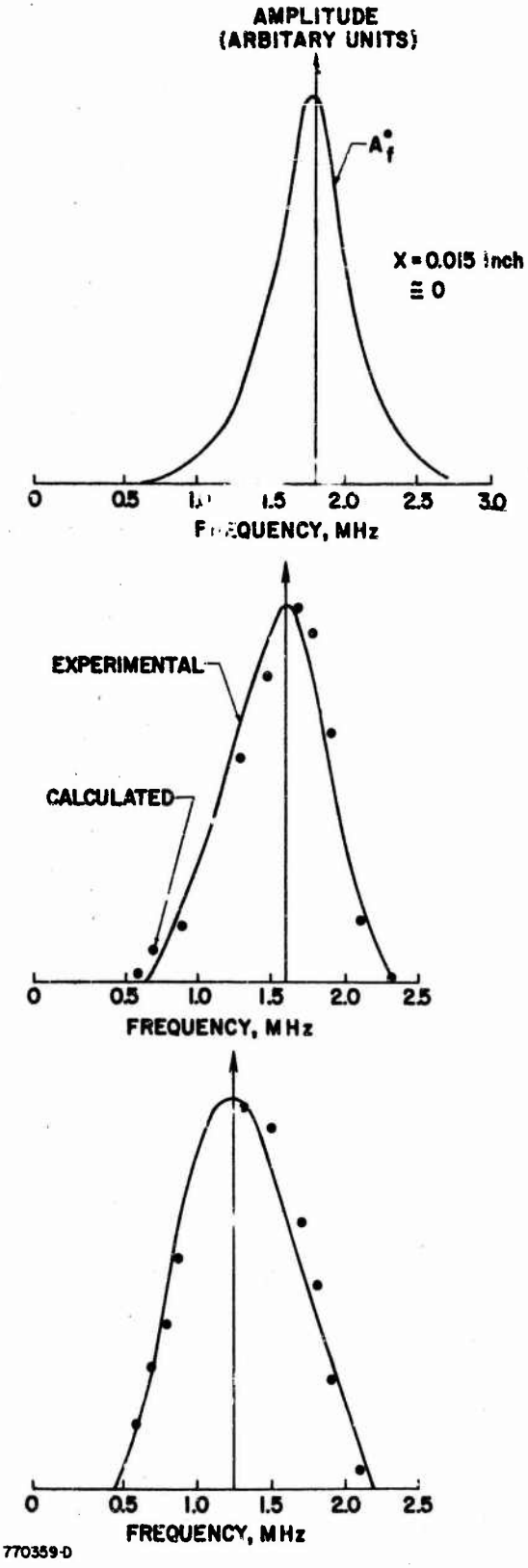

Figure 40. COMPARISON OF THE ANALYTICAL AND EXPERIMENTAL OBSERVATIONS OF FREQUENCY DISTORTION FOR DISTANCES OF 1/2 INCH AND 1 INCH

becomes the center frequency, and the standard deviation is representative of the decay in amplitude for the off-center frequencies and can be calculated by standard procedures.

V. SUMMARY

The attenuation of a material can significantly influence the frequency content of a propagating stress wave. The over-all effect is that the frequency content is continuously shifting to the lower frequencies as the high-frequency components are attenuated with propagation distance. There are two prime factors that are responsible for this action. First, there must be a high rate of change of attenuation with frequency within the frequency spectrum of the activation pulse. This condition produces the selective attenuation necessary for frequency distortion. Second, the magnitude of the attenuation must be high enough that the relative difference produced by selective attenuation is appreciable. It should be noted that a high attenuation without the required high rate of change of attenuation with frequency within the transducer activation spectrum would produce no frequency distortion. The high attenuation would merely account for a general or overall attenuation of the pulse at all frequency components. Of course, the frequency distortion becomes more pronounced at longer propagation distances, since the effect is represented by an $e^{-\alpha f x}$ term.

The implications of highly selective attenuation conditions are many and varied. Without going into great detail, we may enumerate some of the consequences. In ultrasonic flaw detection, the detecting ability of a particular inspection scheme is predicated upon the frequency of the interrogating beam.[13] In general, the higher the frequency, the greater the detecting ability, as dictated by the wavelength to flaw diameter ratio. If the stress wave is continuously experiencing a shift to the lower frequencies with thickness, then some regions of the part being inspected are not being viewed with the same detecting sensitivity. This is of prime concern, since the difference in detecting ability is in the direction of less-sensitive flaw detection. The low-frequency content of a distorted pulse would also present a pulse having a slower rise time, thus presenting an interrogating beam having less resolving ability.

In the measurement of velocity, one procedure measures the time of transit through a specimen of known thickness by noting the location of the first positive swing of an extended radio frequency display.[14] The apparatus used is that shown in Figure 30. The time axis of the scope is calibrated by a material of known velocity. Figure 41 shows the effect of frequency distortion upon such a velocity measurement. With this procedure, the error in time produces a lower velocity, and the full impact of this error upon a velocity determination is found while working with the lower frequency

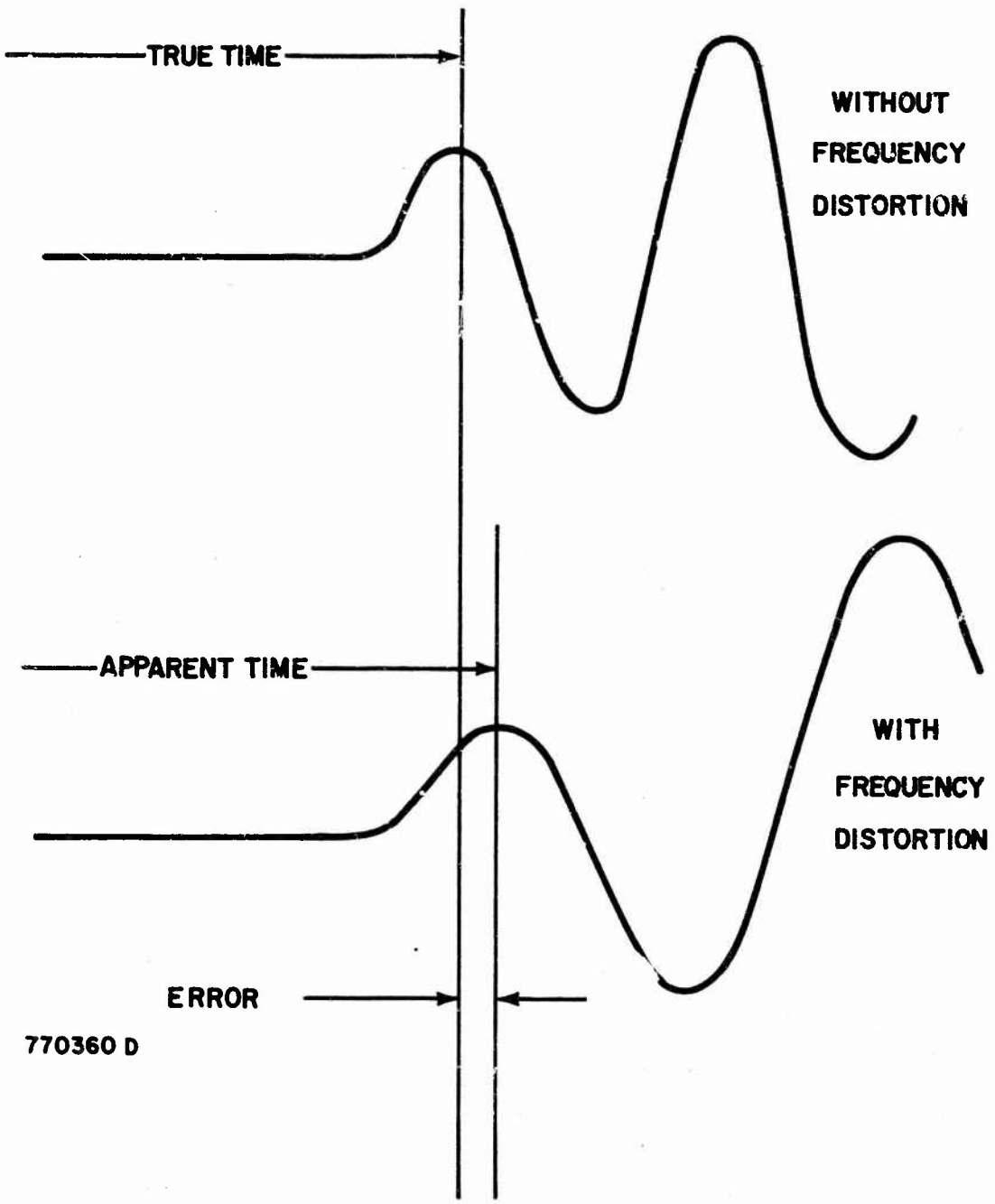

Figure 41. FREQUENCY DISTORTION ERRORS FOR VELOCITY USING FIRST POSITIVE COMPONENT OF THE PULSE

transducers and thinner specimens. One approach to eliminate the error would be to consider a single frequency activation scheme employing a continuous wave, e.g., resonance techniques.

An analysis of the effects of frequency distortion on velocity measurements in relation to properties determination is important. However, in regard to graphite, it is to be noted that the errors in velocity have been assessed to be insignificant in relation to their use for determining mechanical properties as discussed in References 6 and 14. This results primarily from the fact that, for the relatively low frequencies used (1 MHz or below) to establish the mechanical properties correlations, the attenuation is essentially constant within the activation pulse of the transducer. Therefore, the effects of frequency distortion errors in velocity measurements are negligible. It is particularly significant to note that values of modulus of elasticity calculated from velocity data in graphite agree quite well with destructively determined results.

Attenuation measurements are perhaps most directly influenced by the pulse distortion as discussed in this paper. The very concept of pulse distortion leads to an uncertainty in the actual frequency being used; at best, we can only speak of an average frequency. Since the shift in frequency is to the low side of the frequency spectrum, where, in general, the attenuation is less, apparent determinations of attenuation would be lower in magnitude than actual. One method of relieving this situation is to work with narrow band activation pulses, such that the necessary condition for selective attenuation is minimized or eliminated. In any event, a frequency spectrum analyzer should be incorporated in the measurement system in order to know the extent of frequency pulse distortion.

REFERENCES

1. Firestone, F. A., and J. R. Fedrick, J. Acoust. Soc. Am., 18, 200–209 (1946).
2. Desch, C. H., D. O. Sproule, and W. J. Dawson, J. Iron and Steel Inst., 1, 319–328 (1946).
3. Van Valkenberg, H. E., Nondestructive Testing, 21, 178–180 (1963).
4. Lockyer, G. E., Materials Evaluation, 23, 144–148 (1965).
5. Smith, J. T., and S. A. LoPilato, Trans. AIME, 236, 597–598 (1966).
6. Lockyer, G. E., and E. A. Proudfoot, "Nondestructive Determination of Mechanical Properties of Refractory Materials," to be published in J. Am. Ceram. Soc.
7. Hikata, A., R. Truell, A. Granato, B. Chick, and K. Lucke, J. Appl. Phys., 27, 396–404 (1956).
8. Granato, A., and K. Lucke, J. Appl. Phys., 27, 583–593 (1956).
9. Bratina, W. J., U. M. Martius, and D. Mills, J. Appl. Phys., 31, 2415–2426 (1960).
10. Truell, R., J. Appl. Phys., 30, 1275–1278 (1959).
11. Kolsky, H., Phil. Mag., 8 693–697 (1956).
12. Brillouin, L., Wave Propagation in Periodic Structures (McGraw-Hill Book Co., 1946), p. 76.
13. Serabian, S., "Ultrasonic Testing of Large Rotor Forgings -- Criteria for Detecting Ability," Paper 57-A-279, ASME (1957).
14. Lockyer, G. E., AFML-TR-65-113 (1965).

Page 94 is intentionally blank

PART IV.

NDT APPLICATION ANALYSIS - S. W. CARTER

I. Scope

This discussion has been developed to provide an analysis of nondestructive testing as an applied tool of quality and reliability programs concerned with aerospace applications of graphite. The sources of information used in preparation of this discussion were the efforts and developments evolved during the past several years under AFML contracts with Avco Corporation, Space Systems Division, and titled "Nondestructive Methods for Evaluation of Graphite Materials" and the varied background and current disclosures by others in the field which were pertinent to the Avco interest.

II. Introduction

Efforts to obtain graphite which is suitable for aerospace application have encountered three basic areas of frustration:

- the lack of specific knowledge relating measurable materials properties or condition to service performance
- the wide point-to-point variation in measurable properties which is inherent to graphite stock
- the technological difficulty in obtaining relevant information regarding the integrity of graphite on a macro-level

The problems underlying these frustrations stem from materials and design engineering sources and extend into the quality and reliability field. The full impact of the situation becomes evident when attempting to establish specification requirements and apply verification test methods. To facilitate understanding of the over-all problems, the following brief explanations are appropriate.

A. Design Dilemma

The unusual property of graphite which makes it an interesting candidate material for aerospace use is its increase in strength with increasing temperature. The design information concerning graphite, i.e., its physical properties, is currently available in the form of handbook data for the various grades manufactured. This information has been generated from results obtained from the destructive testing of numerous test units,

the averaging of these results and the presentation of average values and the range over which the averaging was conducted. Design models for critical service applications have not always functioned satisfactorily when developed upon this information. The resultant uncertainty surrounding graphite has led to overdesign. However, because of this same uncertainty, the exact amount of overdesign cannot be accurately estimated and a realistic evaluation of testing results is not possible. Therefore, the testing of prototype designs is failing to generate corrective design information with the consequence that a vicious cycle exists.

B. Quality/Reliability Dilemma

As a starting point, quality assurance and reliability engineering require realistic information as to the relevant materials properties, their values and tolerances. From this start, it is possible to establish test requirements and determine if fabricated design models meet the intended criteria. The correlation between design calculation and functional testing is then possible. Without this type of integrated program, the value of quality engineering remains in question and effective reliability predictions of either inherent or achieved nature cannot be determined. Without valid starting information, failures which occur evolve into chaotic post-mortum with Q/R interests applying all their test and review tools trying to assist the design interest in locating an unknown quantity. Cut and try methods of analysis are involved and direct suspicion is always cast upon the "overlooked irregularity". A witch hunt for cracks or flaws always ensues. If enough pressure prevails, it will eventually be recognized that a "missing link" condition exists. What is usually missing is knowledge as to which design requirements were actually relevant to the service undertaken.

C. NDT Application Considerations

The application aspects of nondestructive testing are concerned with optimizing the test machinery and instrumentation to effectively interface with manufacturing and to meet the requirements of the test program. This is the quality planning and engineering activity concerned with the when, where and how to verify the quality characteristics which at this stage should be at least preliminary drawing and specification requirements. Ideally, application presupposes that NDT capability has been fully developed and test relevance determined as an orderly and interrelated part of the materials and design engineering. This supposition in turn assumes that the material is well understood with respect to its properties and that the material manufacturing technology is reliably controllable. Actually, such is seldom the case and a smooth transition from feasibility to practice is seldom realized. An overlap of development and application generally occur in both materials and testing areas. Experience therefore indicates the advisability of early and constant surveillance of development programs by quality and

reliability interests. Periodic analysis of progress in specialized Q and R facets such as NDT will provide guidance to all concerned. Effective analysis of applied NDT must involve an objective evaluation of test relevance and capability. The results of such an evaluation will be the highlighting of inadequacies that forecast problems. This information will have the twofold benefit of correctly orienting test development and concurrently permitting the application of existing capability to the most realistic advantage.

III. Problem Analysis

It appears wise when dealing in aerospace design to recognize that graphite per se is not a new material (although some grades are recent innovations) and that the basic quality/reliability problems now being considered are born of extension of use into new areas which have increased service demands. This is not to imply that prior testing difficulties did not exist or that improvement in NDT capability would not benefit the graphite industry for control of their conventional products. Rather, it is to emphasize that precedents exist in manufacturing and testing technologies which can be helpful as starting points but dangerous if not analyzed in light of the new requirements. One obvious starting point has been to attempt to use commercially available grades of graphite for certain specific items of aerospace hardware. Of particular interest here is the material specification exercises that have evolved. Faced with an existing material and new service requirements, three immediate alternative specification approaches are possible:

- Buy to the existing commercial specification - This approach will guarantee that material can be obtained. It also poses the need for and presumes the willingness to perform extensive test development and materials evaluation studies to obtain correlation with service performance.
- Develop new specification based upon new requirements - This approach is self limiting since the vendor will be reluctant to supply material to unproven criteria and without material testing of design models is not possible, hence, realistic proven requirements are not generated.
- Develop a compromise specification incorporating as much in the line of new requirements as the vendor will accept - This has the potential advantage of requiring the vendor to screen and attempt to upgrade the material supplied. He will, however, use existing test and verification methods. This alternative also requires the user to justify each demand -- a fact that radically curtails what can be accomplished with limited starting knowledge. Disadvantages are the slowing of delivery and substantial increase in cost.

Argument pro and con for each alternative is possible depending upon point of view and the contingencies (economic, schedule and technical) involved. Nevertheless, from the basic quality standpoint, one common denominator can be noted; initially, either of the three alternatives will result in delivery of essentially the same material, manufactured and tested by the existing methods. From this, one may draw some rather direct conclusions:

- Although the final objective can be an improved material, such will be evolved by developing a better understanding of existing available graphite.

- The route to better understanding of graphite is via investigation of the relationship between properties and service performance.

- Test means must be provided to support correlation studies.

- The test means used must be based upon a thorough understanding of the failure modes and mechanisms involved.

From the foregoing alternatives and conclusions, we can develop the following rationale:

For the present and immediate future, the quality and reliability concern with aerospace graphite will be with the capability and relevancy of testing performed in the following two areas:

- Structural integrity -- defined as the presence or absence of macro-level discontinuities.

- Material properties -- defined as the individual engineering characteristics which collectively establish the fundamental, physical nature of the material.

In the following sections, we shall evaluate the status of nondestructive testing as it now applies in these two areas.

A. Structural Integrity

Structural integrity considered jointly from the nondestructive test and graphite material standpoints deals with tangible anomalies generally known better as unsoundness. The various conditions of unsoundness are for the greater part process induced. When unsoundness is an economically or technically uncorrectable but predictable characteristic, its effect upon material service can usually be determined and factored into design. When, however, unsoundness is randomly generated it cannot be individually compensated in design calculation and

from this uncertainty the "safety factor" is born. Aerospace design where weight consideration and reliability demands are stringent can afford neither this calculated luxury nor its low confidence alternative. Accordingly, graphite intended for such application must be screened free of random conditions of unsoundness. Now the graphite producers and the aerospace design engineer will agree with this reasoning in principle. They will, however, argue vehemently concerning the relative and appropriate levels of significance. Essentially, the obligation to prove significance lies with the designer and the obligation to minimize incidence lies with the producer. Neither can fulfill their obligation without test means by which to detect unsoundness. Insofar as this problem concerns a random event, the sampling system must involve extensive testing to obtain high confidence inspection results. Nondestructive testing theoretically affords this sampling capability. Now let us examine its actual test capability in order that we can ascertain how NDT "flaw detection" can best fit into the Q/R program.

1. Radiography

Several investigations have been conducted to determine the capability of the radiographic process to determine the presence, size and location of macro-flaws in graphites.[1, 2, 3] A brief summary of these works and findings at Avco SSD is as follows.

Radiography utilizes the process of differential absorption of penetrating (x or gamma) radiation to disclose variations in material. A void or concentration of foreign material in a general matrix will absorb radiation differently from the matrix material and thereby is detectable. The degree of detectability, i.e., the sensitivity of the process, can be explained in terms of contrast, the relative difference in radiation quantity created as the radiation passes through a material containing an anomaly (subject contrast) and the relative difference in film darkening as the anomaly and surrounding material cast their radiation shadow (radiographic contrast). Also necessary to an evaluation of sensitivity is the definitive capability of the process which may be defined as the trueness or exactness by which the object being radiographed is portrayed in the shadow induced film image. Without involving the numerous details of the technology, it can be stated that graphite (carbon) presents problems in the following areas:

a. At the energies where differential absorption is greatest, graphite, due to its low Z number, is a more effective scatterer than absorber of radiation. Since scattered radiation does not contribute information to the inspection process, the phenomena of scatter and absorption are in conflict and the contrast sensitivity of the process if degraded.

b. At higher energies which are used to penetrate greater thicknesses of material the scatter problem is reduced by self absorption between graphite and other material including air (void) is also reduced again limiting the contrast sensitivity of the process.

c. The differential absorption of radiation effective between graphite and air is very small thereby presenting a technical difficulty to the detection of voids.

d. Fractures which present small volumes except in the direction of their principle dimensions (cracks for instance) are not reliably detected by radiographic means.

e. Inherent graininess of graphite establishes a lower level of definitive sensitivity for the radiographic process.

There are several techniques which are applied to reduce the aforementioned problems encountered in graphite radiography. Assuming the application of the best state-of-the-art radiography, i.e., selection of optimum energy, minimizing scatter and employing optimum film characteristics, the general void sensitivity (contrast and definition) that can be expected for graphite radiography is illustrated in Figure 42.

It can be assumed that metallic inclusions in graphite are more easily detected than are voids. The probability of radiographically detecting a randomly oriented crack having a small thickness dimension is very poor. It is generally safe to state that for thicknesses of graphite above six inches, radiation energies of 1000 KV or above are preferred.

When attempting to evaluate what can be detected radiographically in graphite in terms of the functional engineering value, attention is invited to the difficulty and complexity of results encountered by Southern Research Institute as related in report AFML-TR-65-142 dated May 1965. This attempted correlation involved relatively thin sections of graphite and standard destructive tests. The difficulty in assessing the influence upon serviceability of flaws radiographically detected in bulk graphite or in fabricated hardware is evident. The use of radiography is advocated to evaluate process starts and for spot-check monitoring of production. Both cases permit sectioning of the product to sizes convenient for inspection. Inspection is confined to process induced discontinuities of a macro size and for which corrective action is technically feasible. No issue can be taken with the radiographic screening of destructive test specimens to eliminate conditions of gross and obvious structural irregularity and thereby reduce testing cost and time. The value of radiography for screening of bulk graphite and for the analysis of flight hardware is subject

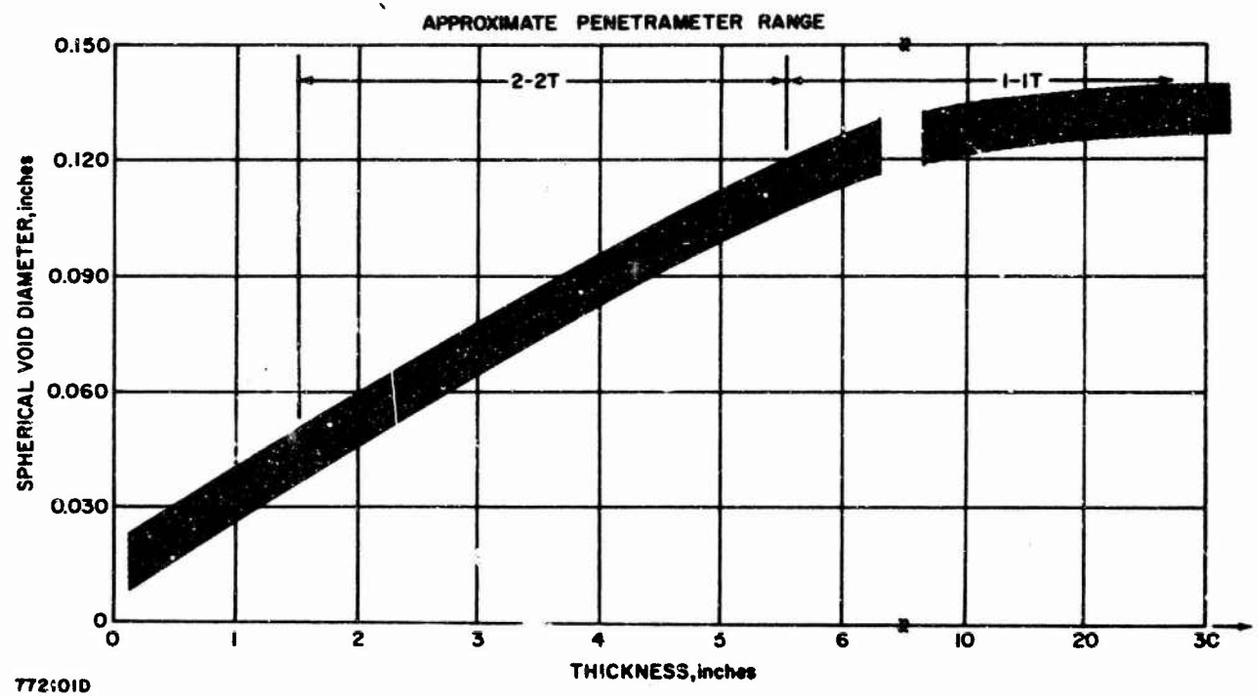

Figure 42. GENERALIZED PRESENTATION OF VOID DETECTABILITY

to question. The engineering significance of what remains undetected can negate any value in the former case, whereas the lack of complete and valid criteria for acceptance poses a quality problem in the latter case. This last statement must be qualified in cases where any valid criteria exists. For instance, where the presence of voids or included foreign material of radiographically detectable size can be cited quantitatively and specifically as deleterious to the product, a benefit does exist. Far better, however, to reduce the incidence of such discontinuities via more determined process controls, since these are process induced variables. Better also to examine the blank (not bulk) stock prior to costly fabrication. This entire area will be summarized under recommended NDT quality procedures.

2. Ultrasonic Flaw Detection

The application of ultrasonics to the detection of macro flaws involves the propagation of an acoustic energy wave within a material and the detection of the reflected or attenuated wave after it has encountered material anomalies which are of different acoustic properties (impedance). Fractures or voids present solid to gas interfaces with grossly different impedance. Acoustic energy impinging upon such anomalies is reflected almost totally. Foreign material included within a generally homogeneous matrix presents a similar condition. The general premises applied to ultrasonic flaw detection are: (a) the highest frequency (shortest wavelength) possible will provide the best acoustic beam directivity and best test resolution; (b) the lower the frequency the less the scatter and attenuation and the better propagation within the material. Since these two features conflict all testing is conducted upon a compromise basis predicated upon the acoustic properties of the material being tested. Graphite unfortunately presents an acute problem in that attenuation of acoustic wave energy is high. Attenuation in graphite varies from grade to grade and is influenced by the grain size involved.

However, regardless of the grade, graphite differs in acoustic attenuation from other materials normally inspected ultrasonically by many orders of magnitude. The following table indicates this difference for Graph-i-tite G (maximum grain size .033 inch) and worked aluminum and steel.

Table I: Relative Acoustic Attenuation

	.5 mHz	1 mHz	2.25 mHz	5 mHz
	Attenuation db/inch			
Graph-i-tite G	2.58	8.686	44	250
Aluminum (worked)	.011	.026	.112	.174
Steel (worked)		.1	.2	1.-

Translated into the generalized capability the high acoustic attenuation exhibited by graphite means:

a. At 1 mHz, propagation is limited to distances on the order of 12 inches. Using pulsed echo, reflection techniques this means that a discontinuity lying at a maximum of 6 inches from the surface is within test range. However, one must appreciate that conventional ultrasonic test equipment provides but a few milliwatts per cm^2 of power at the transducer. The attenuation after 12 inches of travel for a 1 MHz frequency will reduce this power by a factor of 10^{-10}. Accordingly, the reflected power seen at the receiving transducer (provided the reflecting surface is normal to the acoustic beam path) is on the order of less than 10^{-13} watts per cm^2. The area of the resolvable discontinuity would be in the vicinity of 3/8 to 1/2 square inch if we apply the rule of thumb that reflecting areas equal to one-half that of the transmitting transducer can be resolved. This would be somewhat optimistic since the reflecting surface is seldom either smooth or totally perpendicular to the transducer. The amplification of 100 db required to detect these weak levels of signal is subject to considerable noise and the resultant signal degradation which also reduces test capability. While through transmission of acoustic energy will extend the test range to path lengths up to 12 inches, this technique encounters its own unique problems. Through transmission relies upon changes in signal strength as the means for identifying discontinuities lying in the acoustic beam path. The inherent variability of graphite will itself cause wide fluctuations in signal strength. Therefore, to maintain confidence in the test, it is generally necessary to require near complete loss of signal to indicate a true macro flaw. Under such conditions, the test resolution is degraded by at least a factor of two less than that of the pulsed reflection technique.

b. Reduction of the ultrasonic frequency to 0.5 mHz will in theory increase the test range by a factor of roughly 3.5 but will degrade the resolution capability by near the same amount. Effectively, because of other influencing factors, it is more correct to assume that a 0.5 mHz frequency will extend the useful propagation path to on the order of 24 inches and at the very best will resolve discontinuities having on the order of 1 square inch in circular area or greater.

In conjunction with the foregoing, the reader must keep certain other facts in mind. A reduction in the maximum grain size of the graphite will result in improved test capability, i.e., less attenuation. Unfortunately, the smaller maximum grain sizes usually apply to the smaller size billets of graphite rather than the larger and it is in the latter case that extension of test capability is needed. Because of the highly divergent reflection from spherical discontinuities, such as voids or inclusions of foreign material, the sizes necessary here for detection

by the pulsed reflection technique are several orders greater than for the plane type discontinuities previously discussed. For the through transmission technique, shape has little influence upon resolution since it is the defiladed area behind the discontinuity which is of importance. Not all discontinuities present in a graphite billet, even though they lie within the test range (distance), will be detected. For instance, the scattering effect of localized porosity can disperse the reflected signal to undetectable levels. Fractures under compressive loading could at the lower (.5 mHz) frequencies transmit a sufficient amount of energy to go unnoticed. It is conceivable that an intermittent fracture condition, i.e., one constituted alternately of small areas of rupture and sound material, would not be detected -- again, due to scattering or low reflected signal strength.

At Avco, ultrasound has been applied successfully to detect the presence of gross fracture in 12 inch diameter Graph-i-tite G billets. Pulsed echo testing was conducted radially at .4 mHz with complete circumferential scanning. Fractures involving a number of square inches were mapped and confirmed. In several cases, spurious reflected signals indicated suspect areas later found to be local volumes of small (lace curtain) ruptures. As a consequence of widely differing signal strength noted during velocity measurements (through transmission technique), an end section of a 17 inch H205-85 billet was considered suspect. Subsequent sectioning disclosed that the end volume for a distance of several inches was approximately .10 gm/cc lower in density than the remainder of the billet. On numerous other instances while measuring acoustic velocity the radical position to position changes in transmitted signal strength (acoustic energy absorption) raised questions as to the actual structural integrity of the material. Unfortunately, in most of the instances so noted, the material was destined for machining into destructive test specimens and as yet test results and scrap material are not available for a more rigorous investigation. It should be noted here that no apparent correlation exists between such acoustic attenuation and measured velocity. Further, least the reader be confused, it should be pointed out that for velocity measurement the thickness and acoustic attenuation can be considerably greater than for flaw detection. This situation arises because for velocity measurement the acoustic energy need only be detected whereas in flaw detection it is necessary to evaluate and compare the received signal.

3. Penetrant Liquid Test

The use of various liquids to reveal or emphasize surface conditions has proven helpful to the general macro flaw analysis effort. When combined with other test results, penetrant liquid examination can often provide additional information to confirm or elaborate upon suspected

conditions of discontinuities. It has been the practice at Avco to examine graphite blanks and finished machined parts using alcohol and relying upon differential evaporation to reveal discontinuities at the surface. This "alcohol wipe" technique (a saturated lint free swab is wiped across the surface) has revealed porous areas, stringer type porosity, cracks and has confirmed and detailed radiographic evidence of striated layers of varying density. While alcohol wipe does provide a rather transient indication, it is considered adequately sensitive for the conditions of interest (including tight cracks) and it effectively precludes contamination of the graphite. Elusive indications can be rechecked several times without intermediate processing steps. Aside from the obvious limitation to surface testing, the lack of objective evidence of test results presents the most serious drawback to this testing technique.

The fluorescent and dye penetrant systems commonly used in the metals field have limited application in graphite inspection since these liquids are retained in the porous material and are difficult or impossible to completely remove. Obviously, question can be raised regarding the significance of the retained material; but until a test program is undertaken to settle this issue, the only sound Q and R attitude is "no contamination". These penetrant systems are useful in instances where the material is not destined for further test or use, i.e., to supply information on a post mortum basis. The detail provided generally is superior to that possible by alcohol wipe techniques and test results can be photographed or sketched for record. An example of such an application is shown in Figure 43. Here, a graphite billet was found by visual and ultrasonic test to be substandard. The billet was sectioned to verify these findings and dye penetrant test applied to the sectioned surface. In addition to the major cracking, the dye penetrant disclosed an extensive small crack pattern and a porous (unimpregnated, dry core) area.

B. Materials Properties

Graphite has been available since at least 1895 and has found successful application in many areas. Obviously many attempted applications along the way must have led to disappointments which in turn initiated improvements in the material and consequent expansion in use. We are now faced with a potential area of application which is exceedingly demanding. The available information regarding the materials properties of graphite is being shown to be either inaccurate or incomplete since failures of hardware and test models are occurring. The only choice of action appears to be to obtain the knowledge necessary to either live with what we have or to generate an improved material. In the following discussion, we will assume that the graphite is "structurally sound" according to prior definition and will consider the accuracy and adequacy of existing properties information to the extent that nondestructive testing is involved.

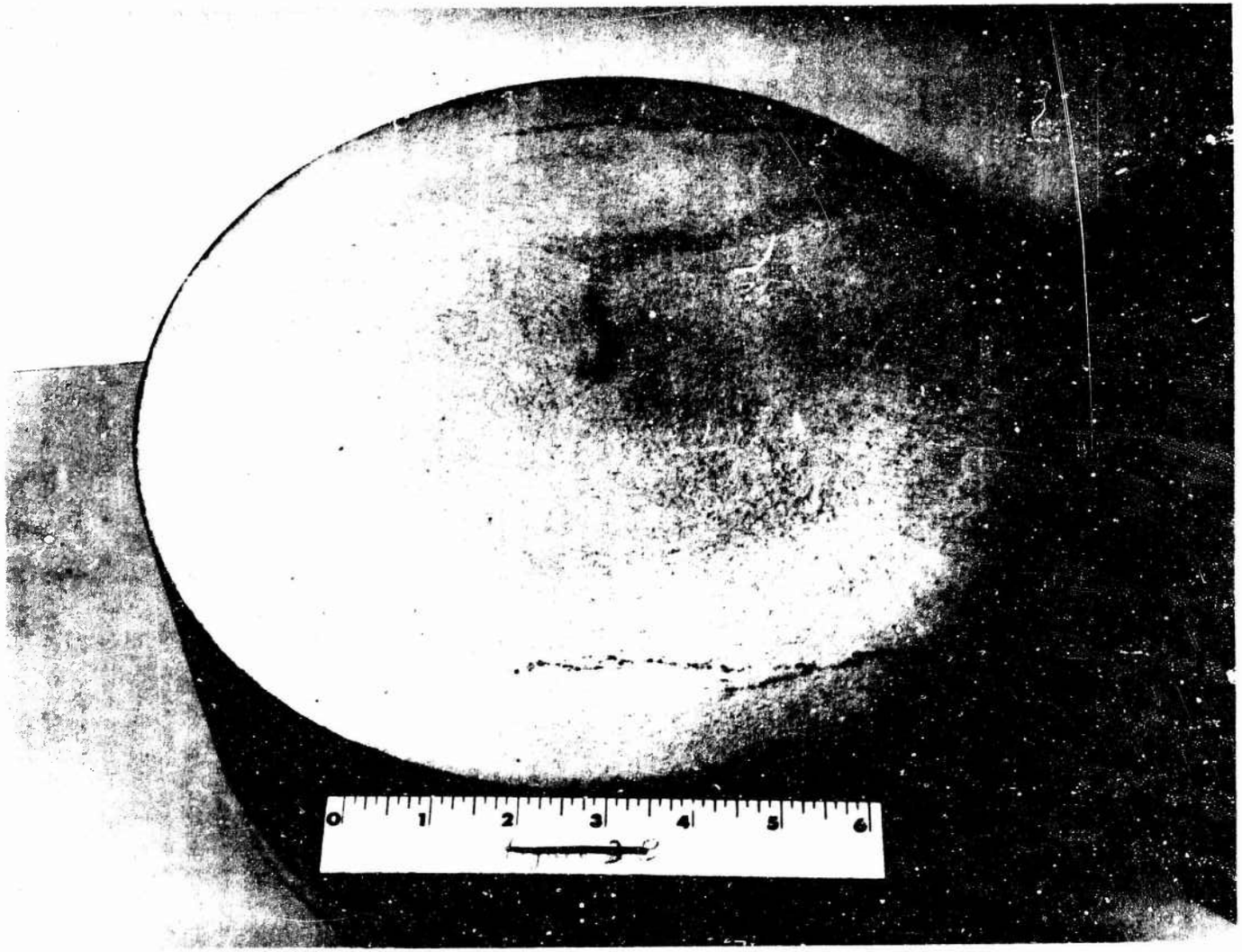

Figure 43. PHOTOGRAPH OF CRACKED GRAPHITE BILLET AS DETECTED BY PENETRANT INSPECTION

1. Accuracy of Design Information

Nondestructive testing is by nature an indirect method when used to obtain quantitative information. With few exceptions, nondestructive tests results must be correlated with destructive tests to obtain applicable meaning. This, of course, presupposes that the methods and techniques of destructive testing were valid in that the quantities evolved are directly relatable to service requirements. If this is not the case, any attempt to extend and improve the credibility of design information by NDT will likewise be inaccurate insofar as absolute values are concerned.

Because of failures, the accuracy of properties values now available from handbook sources has come under suspicion. What is being challenged as a potential source of error is the means of destructive evaluation. This is to say that knowledge is lacking and need exists for a better understanding of failure modes and mechanisms. It is both rational and significant that question be raised in this area since the impact upon design efforts of any novel information could be tremendous. It is, however, not necessary that current suspicions regarding existing absolute values of graphite properties cause any curtailment of effort to extend knowledge in such areas as ranges of properties variability and improved sampling methods.

2. Adequacy of Design Information

We have previously (Introduction) stated that existing design information was derived from the destructive measurement of numerous test units. The term, "sample", was purposely avoided in this phraseology and herein lies an important point of interest. A sample is by definition a portion or portions taken to represent a lot. The sampling operation is the selection of a part, convenient in size for testing, from a whole which is of much greater bulk, in such a way that the proportion and distribution of the quality to be tested are the same in both the whole and the part to be tested. Bear in mind the emphasis placed upon representativeness and sameness as we continue with this discussion of graphite.

One description of synthetic graphite given in a current encyclopedia is as follows: "Commercially produced synthetic graphite is a mixture of crystalline graphite and cross-linking intercrystalline carbon. Its physical properties are the result of contributions from both sources. Thus, among engineering materials, synthetic graphite is unusual because a wide variation in measurable properties can occur without significant change in chemical composition." Although this is an oversimplified explanation of why variation in properties exists, it does serve to illustrate the general acceptance of this condition. Many

investigations both by manufacturers and users have proven this point beyond a doubt, although disagreement will be found regarding the magnitudes involved. If we examine the basis upon which agreement regarding properties variation was reached and from which existing handbook averages are calculated, we will find that dimensions of the specimens and the sample selection procedure generally assumed a homogeneous material although anisotropy was recognized. The incremental variation on a sub-sample size has not been considered fully. For prior applications, this might not have been of importance. For aerospace applications involving thermal and complex physical stress, it could well be significant. It appears within the realm of possibility that not only are the basic averages values of physical properties (for instance dynamic modulus and tensile strength) important but the incremental gradient of these properties could be more significant. If this concept is correct, we are now confronted with several new factors. We can consider graphite similar to a non-homogeneous bulk material and exercise the necessary steps to obtain representativeness of samples. This possibly will lead to different averages and very probably to a wider range of measured veriability. We can reconstruct our testing techniques and evaluation procedure to generate specific incremental gradient values of properties. This will require that the relevant increment size be ascertained as a function of service performance. We must bear in mind that whatever action is undertaken our objective is to provide more credible design information and to improve material reliability (inherent) by extending testing and monitoring capability back into production.

3. Improvement in Test Adequacy

The program undertaken at Avco Corporation/Space Systems Division during the past several years has been directed (in one sense) toward increasing the sample number to improve the credibility of the test results. To accomplish this end with realistic economy of time and material, the methods of testing have necessarily been nondestructive. To acquire design engineering data as an end product of nondestructive testing has required extensive correlation between NDT and destructive test results. This correlation has been successfully accomplished because the fundamentals concerned with the interaction of materials and energy were carefully studied and congruent destructive and nondestructive tests were compared. Capabilities developed during the first year of contracted effort are summarized in the final report for that period. Briefly, a radiation gaging technique was developed which is capable of measuring density in the grades of graphite of interest to within ±1 percent, thereby facilitating the mapping of variations in this important property within and between billets. Combined use of ultrasonic

velocity measurements and radiometrically determined density were uniquely correlated to dynamic elastic modulus. Both with and against the grain measurements and correlations have been shown valid to within approximately $\pm 0.06 \times 10^6$ psi for the graphite grades examined. Further extension via correlation has provided ultimate tensile strength information to within approximately ±300 psi. Since the tests are rapid and the material tested is unaltered, the number of samples obtained can be greatly increased. Thus, the results are far more representative of the lot than were those previous obtained via spot check, destructive tests. To process the quantities of data collected by nondestructive means a computer program was established (see Figures 44 and 45). At this point in development, it has been possible to determine density, dynamic elastic modulus and ultimate tensile strength throughout entire billets having volumes from several cubic inches to well in excess of one cubic foot. The sample dimensions tested are at present dictated by the area of the ultrasonic transducer and the collimated radiation beam, which for work to date have been on the order of 1/2 to 1 inch. Sample volumes have therefore been this area (1 inch) multiplied by the thickness of graphite in the direction of test. Since test results are integrated over these areas and volumes, the gradients determinable are in increments of one inch.

This development program has succeeded in improving the representativeness of sampling simply by increasing the number of test units evaluated. The extended sampling has provided a means for generating a figure of merit for variability gradients. The nondestructive feature of the test methods does permit evaluation of the actual graphite which is to be used. These factors appear to be significant advancements in improving the adequacy of design information. Unfortunately to date, the very limited feedback of functional test data in combination with the need for better understanding of failure mechanisms does not permit effective evaluation of the full impact of this approach.

Although full value analysis cannot yet be undertaken, test surveillance in combination with reliability considerations does indicate that further test refinement might prove valuable. Recent nondestructive test examination of a series of graphite blanks destined for fabrication into test cones, revealed a lack of specific correlation between the qualitive structural integrity examinations and the quantitative materials properties testing. For example, radiographic and penetrant tests indicated a striated area of alternate (with the grain) strips of different density. Radiometric and ultrasonic velocity measurements did not indicate this local variability as a function of density, modulus or tensile properties. The reason for the differing test results is obvious -- the volumes of material being evaluated in each instance are different. The important point, however, is the question regarding significance of the gradient of variability. Is the more abrupt gradient observed and qualitatively evaluated worthy of concern? How does this gradient relate to function?

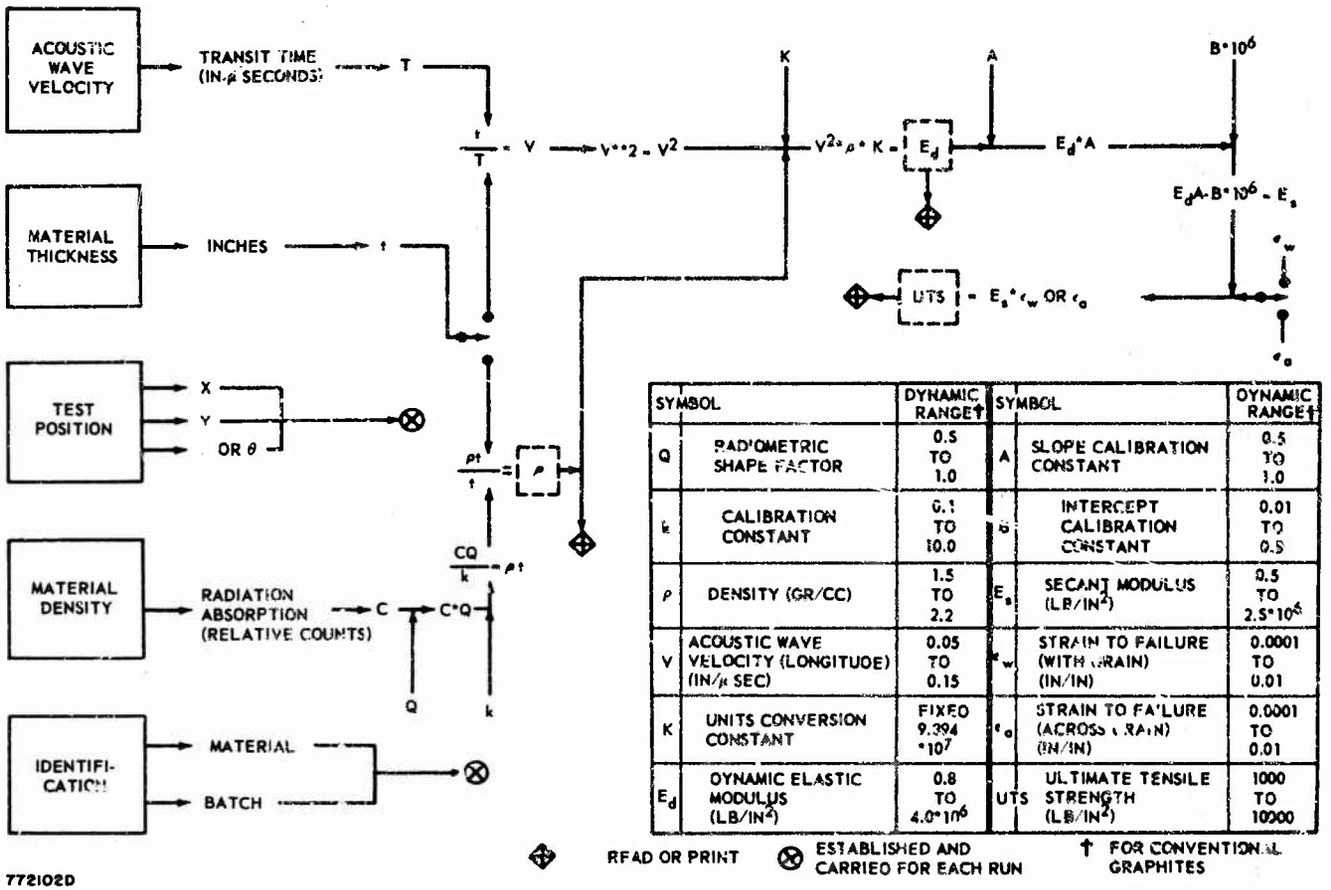

SYMBOL		DYNAMIC RANGE†	SYMBOL		DYNAMIC RANGE†
Q	RADIOMETRIC SHAPE FACTOR	0.5 TO 1.0	A	SLOPE CALIBRATION CONSTANT	0.5 TO 1.0
k	CALIBRATION CONSTANT	0.1 TO 10.0	B	INTERCEPT CALIBRATION CONSTANT	0.01 TO 0.5
ρ	DENSITY (GR/CC)	1.5 TO 2.2	E_s	SECANT MODULUS (LB/IN^2)	0.5 TO $2.5*10^6$
V	ACOUSTIC WAVE VELOCITY (LONGITUDE) (IN/μ SEC)	0.05 TO 0.15	ε_w	STRAIN TO FAILURE (WITH GRAIN) (IN/IN)	0.0001 TO 0.01
K	UNITS CONVERSION CONSTANT	FIXED $9.394*10^7$	ε_a	STRAIN TO FAILURE (ACROSS GRAIN) (IN/IN)	0.0001 TO 0.01
E_d	DYNAMIC ELASTIC MODULUS (LB/IN^2)	0.8 TO $4.0*10^6$	UTS	ULTIMATE TENSILE STRENGTH (LB/IN^2)	1000 TO 10000

Figure 44. COMPUTER PROGRAM -- FLOW DIAGRAM

ST-18 I.B.M. 704 CODING FORM

PROPOSER M. "ERIALS PROPERTY OFFICE SECTION 8210 TEL. EXT. 105/697 DATE 16 January 1967

TITLE SONIC MODULUS for TENSILE PROPERTIES SET UP Temporary Form SHEET 1 OF 1

PROBLEM NO. MEMO NO. WORK ORDER NO.

MATL	BATCH	POSN	TIME	FACTOR	THICK.	Rho T	K	SF	Epsilon	A	B	DATE
1 2 3 4 5 6	7 8 9 10 11 12	13 14 15 16 17 18	19 20 21 22	23 24 25 26 27 28	29 30 31 32 33 34	35 36 37 38 39 40 41 42	43 44 45 46 47 48 49 50	51 52 53 54 55 56 57	58 59 60 61 62 63 64	65 66 67 68 69 70	71 72 73 74 75 76	77 78 79 80

OBJECT

Program will carry out the following equations:

TTIME = TIME + FACTØR

VELOCITY = THICKNESS/TTIME

RHØ = DENSITY FACTOR/(2.54 * THICKNESS * SF)

E_D = (VELOCITY)^2 (RHØ) (K) (10^7)

E_S = A * (VELOCITY)^2 (RHØ) (K) (107) - B * 10^6

UTS = E_S * EPSILØN

OUTPUT

MATL, BATCH, PØSN, RHØ, ED, UTS

772103D

Figure 45. IBM CODING FORM

Expressed in another manner, the homogeniety of a material is a relative characteristic which depends upon the level of analysis one desires to consider. From the standpoint of aerospace application of graphite, the rate of application and magnitude of the thermal and physical stresses which might be anticipated indicate that the gradients of significance might be one or two orders of magnitude smaller than measurements being taken with present NDT procedures.

IV. Recommended Application of NDT

The following are recommendations based upon the capabilities and relevance disclosed in the foregoing discussions and intended as guidelines for immediate application of existing NDT methods in support of current aerospace graphite programs. It must be appreciated that as a quality and reliability tool, NDT correctly should be evaluated as part of the total quality program if maximum effectiveness is to be realized. Unfortunately, however, the scope of the investigations to which this analysis is related was limited and did not allow for the comprehensive materials and process studies necessary for total quality program coverage. Sufficient insight into the graphite industry was obtained to recognize the presence of unique quality engineering problems involving economics, schedules, product varieties and information gaps common to an expanding field. Accordingly, the recommendations developed are general, are based upon obvious oversimplification, and will definitely be altered as both materials and test technology improve. The following breakdown of catagories and elements shows their interrelated interest factors and is presented to illustrate the underlying considerations which were employed here. The term, "producer", is meant to represent the manufacturer of the graphite while the term, "user", is employed to designate the organization responsible for design (and/or fabrication) of flight hardware from the graphite.

NDT Constraints

Capability Relevance Availability	Producer User	Interest

Inspection Levels

Receiving Process Final	Producer Interest
Receiving Intermediate Final	User Interest

Material Levels

Raw Material, Billet	Producer Interest
Blank, Part	User Interest

Specification Levels

Raw Material, Process	Producer Interest
Billet, Flyable Hardware	User Interest

NDT Inerrogation Level
- Structural Integrity
  - Voids
  - Fractures
  - Inclusions
- Materials Properties
  - Density
  - Dynamic Modulus
  - Ultimate Tensile Strength

NDT Methods
- Radiography
- Ultrasonic Flaw Detection
- Penetrant Liquid
- Radiometric
- Ultrasonic Velocity

A. Radiography

Application of radiographic testing is recommended as follows:

1. By producer as process evaluation tool: Most effective would be application to pilot run, process evaluation wherein all graphite produced by new equipment, procedure or from unproven raw material is examined for unpredictable discontinuities, such as voids and inclusions. Examination is continued until the incidence of such discontinuities is reduced to an acceptable level whereupon a sampling procedure is substituted to monitor production. This application of radiography requires that rejectable size and distribution limits for voids and inclusions be established as a function of service requirements. The discontinuity size so determined will dictate the thickness that the graphite must be to permit effective radiography. Accordingly, the pilot lots and subsequent samples will either be inspectable as

produced or will need to be destructively sectioned to permit radiography. Attention is invited to the cases where basic stock is reprocessed such as by hot working or impregnation. Under such conditions, it is logical that production of the basic graphite stock would be subject to radiographic process evaluation and monitoring and this same procedure applied to the reprocessing.

2. By producer and user as screening test for all destructive test specimens: Radiographic examination of all destructive test specimens is advocated to improve the credibility of test results. It is not specifically intended that any correlation between discontinuities (voids and inclusions) and destructive test results be attempted, rather, this examination is performed to screen out specimens which contain discontinuities of a rejectable size (as cited above for process evaluation) and thereby preclude the inclusion of nonrepresentative test results in final properties analysis.

3. By user as for acceptance test of part: The inspection level at which radiography would be applied would be either the intermediate or final, i.e., either the blank or the finished machined part. Selection of inspection level would be dictated by the size and geometry of the graphite involved. For instance, it is preferable from an economy standpoint to radiograph the blank prior to machining, if the dimensions allow for detection of significant discontinuity size. In such instances where the graphite dimensions of both the blank and part preclude radiographic detection of significant discontinuities, the radiographic test requirement should not be applied and reliance upon process control with the consequent acceptance of a lower confidence in reliability and contingent adjustment in design parameters.

B. Ultrasonic Flaw Detection

Application of ultrasonic flaw detection is recommended on essentially the same basis as was advocated for radiographic inspection, i.e., process evaluation, specimen screening and acceptance test of part (or blank). The objective of ultrasonic testing is to locate fracture type discontinuities, a function which radiographic inspection cannot perform with confidence. As with radiographic inspection, the size and geometry of the graphite introduces limitations in test capability which will, in many cases, necessitate destructive sectioning at the process evaluation level and will guide selection of either part or blank for acceptance test. Since designers are prone to reject all fracture type discontinuities and because the capability of ultrasonic techniques to locate such flaws is limited, the burden at the process evaluation level is increased. Increased also is the need for early NDT test engineering (at the process level) to ascertain the test capability and thereby permit early decision regarding the merit of application to final acceptance testing.

C. Penetrant Liquid Test

Penetrant liquid testing is recommended as follows:

1. By producer as process evaluation tool: The process evaluation procedure discussed under radiography is again applicable here. Where sectioning is required for radiographic or ultrasonic testing, penetrant examination of the cut sections will supplement the information provided by the other NDT. Where sectioning is not required to effectively perform other testing, it is advisable that such be performed to substantiate the prior test results. In either case, sectioning to provide information in several planes and with due respect to the processing method is advocated. Where material is not destined for test specimens, the use of dye or fluorescent techniques is preferred.

2. By producer and user as screening test for all destructive test specimens: Penetrant liquid testing here will specifically supplement or replace ultrasonic testing where the latter proves to be infeasible or technically inadequate. Since the effect of any absorbed material upon the results of certain destructive tests is unknown, the use of alcohol (or similar low vapor pressure liquids) as a penetrant and observation of the differential evaporation pattern is recommended.

3. By user for acceptance of final machined part: Again, the use of alcohol is recommended to preclude contamination of the graphite. This test is specifically advocated as a means of overcoming the limitations of radiographic and ultrasonic testing as regards small fracture type discontinuities at the surface. Further, when either radiography or ultrasonic test is applied at the intermediate level, penetrant liquid test of the final part provides the inspection coverage necessary to detect fracturing which might be induced by final machining.

D. Radiometric Gaging

Application of radiometric gaging to determine density is recommended as follows:

1. By producer as a process evaluation tool: Since density is a discrete property of graphite and is influenced by process variables, and since current spot check procedures for density determination have been shown to be nonrepresentative, the application of radiometric gaging to permit realistic sampling is advocated. The "introduction" of this technique at the process level appears most appropriate. Immediate application to pilot lot evaluation and extension into a process monitoring program using a statistical sampling procedure is a logical approach. Equipment and test technique have not been

sufficiently developed and evaluated to recommend "on line" application at this time. For instance, density determination through the diameter of cylindrical billets is feasible, however, determination in an axial direction could present problems. For the present, the most effective use of radiometric density gaging requires that the material be cut to size and the necessary sample selection made with due regard to processing characteristics.

2. By user for intermediate level inspection: Prior to machining of critical flight hardware, it is advocated that the graphite blanks be inspected by radiometric gaging to verify local density and density gradients. This recommendation assumes that such blanks are of simple geometric form (cylinder, cube, rectangular block) and that the actual flight hardware is of a more complex geometry. It is assumed also that the design interest can establish tolerance limits for density or that the information gained at this inspection stage will be utilized for correlation with performance test results.

E. Ultrasonic Velocity

Application of ultrasonic velocity determination is recommended on essentially the same basis as was radiometric gaging, i.e, process evaluation by the producer and intermediate level inspection by the user Ultrasonic velocity is relatable to dynamic elastic modulus and is influenced by process variables thereby providing a process control tool. The general limitations cited for radiometric gaging also apply here. The utilization of test results gained at the intermediate inspection level is also dependent upon design interest using the published literature to obtain the velocity/modulus correlation and establishing tolerance and gradient limits or, seeking ultimate correlation with service performance. Obviously, both producer and user can combine radiometric density and ultrasonic velocity test results and, as explained earlier in this analysis, extend the correlation to obtain ultimate tensile strength. Although equipment and techniques are in a stage of continued refinement, this should not be a basis for delaying application of this test method.

F. Test Duplication and Consonance

The newly developed NDT characterization system utilizing radiometric gaging and ultrasonic velocity measurement is designed to evaluate material properties and does not examine for macro-level conditions of structural integrity. The disclosure of discrete fractures or voids during radiometric density gaging or ultrasonic velocity measurement would be purely fortuitous. Such discontinuities to be detected would have to be of sufficient magnitude to radically alter the density or impede the transmission of the acoustic wave. At present, the detection of local pockets

of porosity, dry core, bursts or "lace curtain" cracking is strictly test technician dependent. Obviously, automated testing or the use of personnel not highly qualified in the NDT field will reduce to near zero the probability of macro-flaw detection. It is necessary, therefore, that inspection specifically for macro-flaws be conducted as separate testing.

G. Specifications

It is recommended that specifications for current use reflect the prevailing graphite and NDT technology as follows:

1. Procurement Specification: NDT requirements cited in procurement specifications placed by the user with the producer should continue to cite minimum allowable density. In addition, the specification should state that the production process or processes employed to produce the graphite material shall have been evaluated and shall be under a control system which has been shown capable of producing a material having the following criteria:

Voids: No single void to exceed ____ in maximum dimension. Voids having a maximum dimension between ___ and ____ shall be located no closer edge-to-edge than _____.

Inclusions: No single inclusion to exceed _____ in maximum dimension. Inclusions having maximum dimension between ___ and ____ shall be located no closer edge-to-edge than _____.

Fractures: There shall be no evidence of cracking.

Further, the specification should implement existing Specification MIL-Q-9858A or MIL-I-45208A to assure contractor compliance with established quality program requirements acceptable in other areas of material production. Note that, from the NDT standpoint, the advocated wording does not require that the delivered material be guaranteed free of discontinuities -- only that the process be shown to have the required capability and control means and that the material be traceable to the process.

2. Part Specification: A separate material specification should be developed by design interest for application to flyable hardware. This specification should contain as mandatory the structural integrity criteria cited in the procurement specification. In addition, and as soon as measurable materials properties are correlated with service performance, this specification should require minimum property values and maximum allowable property gradients.

V. Conclusions

Modern quality management concepts found effective and necessary in obtaining materials for aerospace use are applicable to graphite. Graphite producers must be prepared to implement such quality programs throughout the manufacturing cycle. They must be willing to refine process control procedures considerably beyond those now employed. Designers desiring to use graphite must first determine fully the relevant quality attributes and significant tolerances required for advanced applications before expecting producers to react efficiently to their needs. Both producer and design elements should recognize that the starting materials and those ultimately found satisfactory will be separated by a cooperative effort in which each element must study and appreciate the other's technical and economic problems.

The recent improvements in NDT of graphite will provide more of the tools necessary to implement a realistic quality program and to supply information in support of design reliability efforts. The application of these NDT tools should be undertaken with all the dispatch that economic considerations and engineering capability will permit.

REFERENCES

1. Radiographic Behavior of Graphite and Berylium, Elliot, D. E.; Stokes, J. L.; Tenny, G. H. nondestructive Testing, Vol XX, No. 3, May-June 62 pp 161

2. Research on Radiographic Techniques of Graphite Evaluation, Report No ML-TDR-64-277

3. Adaption of Radiographic Principles to the Quality Control of Graphite, WADD Tech Report 61-72 Vol IV

Page 120 is intentionally blank

APPENDIX 1

Outline of Seminar Plan

1. Technical Lectures

   A. Philosophy of NDT Materials Evaluation Approach (Graphite in Particular)

      1. Macroscopic flaw inspection

         a. Assurance of flaw-free material

      2. Identification of properties of interest

         a. Relate to intended application and design (singly and in combination)

      3. Definition of variables influencing properties

         a. Relate to physical composition (chemical if applicable)
         b. Analyze in relation to material processes

      4. Select NDT methods and techniques

         a. Relate to properties of interest, physical composition and influencing variables

         b. Analyse NDT energy/materials interaction

      5. Theoretically justify NDT selection

         a. Related theory and mathematical expressions

NOTE: Tables to be displayed relating properties to influencing variables, and NDT techniques and energy interaction with related material variables.

   B. Experimental Program for Graphite

      1. Program flow chart showing step-by-step approach

         a. Bulk material evaluation to identify level and range of NDT response (qualitative)

         b. Selection of specimen blanks to embrace level and range of NDT response

c. Quantitative measurements on selected specimen blanks

d. Selection and preparation of destructive test specimens

e. Quantitative measurements on destructive test specimens

f. Destructive testing

g. Correlation of quantitative NDT measurements and destructively determined properties

h. Statistical analysis of data as necessary

NOTE: Program flow chart to be displayed.

C. Nondestructive Methods and Techniques Discussion

1. Radiometric Gaging (Penetrating Radiation)

a. Property to be measured (density)
b. Theoretical discussion (related equations)
c. Equipment

1) Schematic diagram
2) Component description
3) Functional operation

2. Ultrasonic Velocity

a. Properties of interest (mechanical)
b. Theoretical discussion (related equations)

1) Direct properties relationship

2) Unferred properties relationship (empirical observations relative to tensile strength)

c. Equipment

1) Schematic diagram
2) Component description
3) Functional operation

3. Infrared Radiometry

a. Properties of interest (ther al)
b. Theoretical discussion (re ed equations)
c. Equipment

1) Schematic diagram
2) Component description

D. NDT Screening of Billets (Qualitative)

1. Radiometric Gaging (ρ)

a. Typical result showing variability

2. Ultrasonic Velocity (V_L)

a. Typical results with and against grain (anisotropy)

3. Analysis of level and range of NDT response (same discrete volumes for both measurements)

a. Select specimens to embrace minimum, maximum and intermediate NDT response

NOTE: Infrared not applicable here since it has been in developmental stage throughout program.

E. Specimen Blank Correlations

1. Verify radiometric density by gravimetric technique
2. Correlate V_L with dynamic modulus (E_D)

a. Describe E_D briefly (equation for)
b. Analyze V_L vs. E_D data

1) log-log expression
2) slope of curves
3) influence of ρ as intercept
4) both grain directions, all grades tested

3. Analyze Poisson's ratio (σ)

a. f (σ) versus σ for graphite

1) σ calculated and measured

b. V_L equation reduces to $V_L^2 = E_D$

4. Correlate ρV_L^2 vs. E_D

a. Identify the NDT parameter - significance in terms of discrete locations

b. Describe the curve and analyze

1) Best fit equation, slope, intercept, etc.
2) Statistical analysis - correlation coefficients, etc.
3) Both grain directions, all grades tested

c. Determination of E_D

1) confidence limits

F. Destructive Test Correlations

1. Ultimate tensile strength (UTS)

a. ρV_L^2, E_D, E_T (tensile modulus), and E_s (secant modulus)

1) Relative comparison graphically

2) $E_s = \frac{UTS}{E_T}$ = total strain to failure)

3) Significance of ratio $\rho V_L^2/E_s$ = constant for given grade and direction

2. Correlation of ρV_L^2 vs. E_s

a. Analysis of data

1) Best fit equation, slope, intercept, etc.
2) Statistical analysis - correlation coefficients, etc.
3) Both grain directions, all grades tested

b. Determination of UTS

1) $\bar{E}_T$ = constant for given grade and direction
2) Confidence limits

G. Infrared Thermal Properties Measurements

1. Uniqueness of Technique

a. Nondestructive, transient, one surface, etc.

1) Rapid measurement and economy compared to steady state technique

2. Applicability to components (geometry and size) still in experimental stage

H. Significance of Properties Measurements (NDT Characterization)

1. Design purposes

a. Single importance of each property
b. Combined importance of each property
c. Significance of level and range of variability

2. Performance

a. Behavior characteristics

1) Thermal shock

b. Thermomechanical stresses

1) Properties gradients

c. Properties threshold (failure limits)

1) Computer design of specimen for simulated environmental tests

2) Real service tests of selected material

d. Performance correlations

II. Demonstrations

A. Radiometric Gaging

1. Equipment display and readant
2. Typical measurements
3. Data computerization for properties calculations

B. Ultrasonic Velocity Measurem nts

1. Equipment display and readant
2. Typical measurements
3. Data computerization for properties calculations

C. Infrared Radiometry

1. Equipment display and readant
2. Typical measurements
3. Data computerization for properties calculations

D. Applications Analysis (Lectures)

1. Equipment implementation (each method)
2. Resolution and sensitivity
3. Procedural description (laboratory and field use)

    a. Billets
    b. Hardware components
    c. Specifications

4. Quality and reliability program considerations
5. User - producer considerations
6. NDT constraints

    a. Capabilities
    b. Relevance
    c. Availability

7. Inspection levels

    a. Receiving
    b. Intermediate
    c. Final

8. Etc.

APPENDIX II

Analysis of Data Relating Destructive and Nondestructive Tests for Certain Types of Graphite

by C. A. Lermond

Nondestructive test (NDT) data in the form of density (ρ) and longitudinal wave velocity (V_L) together with the corresponding destructive tensile test data as secant and dynamic moduli for a series of five grades of graphite (CFZ, ZTA, CFW, RVA and ATJ) were submitted for evaluation. All data was converted to punch cards for ease in manipulation. Each punch card contained complete identification and test data for a single specimen.

Experimental evidence indicates that there is a direct relationship between the NDT and destructive test results if the NDT values are expressed as the product of the density and the square of the longitudinal wave velocity ($K\rho V_L^2$). The raw mechanical data together with the product term for the NDT data are shown in Table I. There are a total of 132 specimens broken down as follows:

Grade	No. Specimens
CFZ	6
ZTA	16
CFW	36
RVA	25
ATJ	49

Data plots for each grade of graphite were obtained directly from the punch cards using a Benson-Lehner Plotter E. These are shown in Figures II-I–II-10. In all cases, data taken with and against the grain are shown in a single plot. It will be noted that the data does indeed fall on a straight line using the function for the NDT data.

Regression lines were obtained using the previously punched data as input. The resulting equations are shown below:

Grade				RMS
CFZ	$K\rho V_L^2$	=	$0.509 + 1.111 \; E_s$	0.210
ZTA	$K\rho V_L^2$	=	$0.322 + 1.432 \; E_s$	0.045
CFW	$K\rho V_L^2$	=	$0.321 + 1.418 \; E_s$	0.054
RVA	$K\rho V_L^2$	=	$0.488 + 1.193 \; E_s$	0.069
ATJ	$K\rho V_L^2$	=	$0.342 + 1.307 \; E_s$	0.077

TABLE I

Destructive And Nondestructive Test Data For Graphites

CFZ GRAPHITE

SPEC	RHO	ED	ES	RVL2
1AG001	1.877	1.21	0.93	1.24
1AG002	1.889	1.25	0.71	1.28
1WG003	1.893	2.00	1.26	2.18
1WG004	1.875	1.78	1.17	1.86
1WG005	1.876	1.73		1.77
1WG006	1.874	1.80		1.77

ZTA GRAPHITE

SPEC	RHO	ED	ES	RVL2
1AGA01	1.916	0.92	0.46	0.97
1AGA02	1.918	0.91	0.44	0.97
1AGA03	1.926	0.93	0.48	0.96
1AGA04	1.931	0.89	0.44	0.94
1AGC01	1.907	0.91	0.43	0.91
1AGC02	1.900	0.89	0.42	0.95
1AGC03	1.894	0.94	0.43	0.97
1AGC04	1.890	0.90	0.49	0.98
1AGC05	1.893	0.90	0.46	0.97
1AGC06	1.895	0.89	0.41	0.96
1AGC07	1.909	0.91	0.45	0.96
1WGB01	1.816	1.67	1.08	1.80
1WGB02	1.849	1.90	1.18	2.09
1WGB03	1.897	2.27	1.38	2.45
1WGB04	1.939	2.78	1.79	2.97
1WGB05	1.978	3.39	2.33	3.59

TABLE I (Cont'd)

CFW GRAPHITE

SPEC	RHO	ED	ES	RVL2
1AGA01	1.813	1.28		1.28
1AGA02	1.809	1.20	0.68	1.20
1AGA03	1.813	1.21	0.66	1.20
1AGA04	1.796	1.16		1.16
1AGA05	1.798	1.18	0.62	1.19
1AGA06	1.801	1.19	0.61	1.20
1WGW01	1.811	1.64		1.72
1WGW02	1.813	1.71		1.84
1WGW03	1.805	1.72	0.97	1.79
1WGW04	1.816	1.73	1.03	1.80
1WGW05	1.819	1.67	0.96	1.75
1WGW06	1.820	1.62	0.99	1.72
1WGW07	1.800	1.69	0.99	1.76
1WGW08	1.788	1.64	0.99	1.74
1WGW09	1.802	1.73	1.05	1.72
1WGW10	1.796	1.63	0.95	1.72
1WGW11	1.799	1.69	0.96	1.76
1WGW12	1.797	1.66	0.97	1.72
2AG 07	1.802	1.24	0.70	1.28
2AG 08	1.806	1.32	0.75	1.34
2AG 09	1.817	1.29	0.65	1.30
2AG 10	1.820	1.26	0.64	1.28
2AG 11	1.818	1.27	0.7[illegible]	1.29
2AG 12	1.837	1.28	0.69	1.29
2WGW13	1.819	1.70	1.06	1.79
2WGW14	1.812	1.66	0.99	1.71
2WGW15	1.812	1.63	0.93	1.57
2WGW16	1.812	1.64	0.95	1.69
2WGW17	1.799	1.65	0.94	1.70
2WGW18	1.809	1.70	1.05	1.78
2WGW19	1.802	1.63	0.95	1.71
2WGW20	1.806	1.67	1.05	1.75
2WGW21	1.817	1.76	1.09	1.82
2WGW22	1.820	1.70	0.97	1.79
2WGW23	1.818	1.70	1.02	1.71
2WGW24	1.837	1.73	1.09	1.76

TABLE I (Cont'd)

RVA GRAPHITE

SPEC	RHO	ED	ES	RVL2
1AGY01	1.853	1.19	0.71	1.25
1AGY02	1.849	1.23	0.78	1.26
1AGY03	1.854	1.23	0.71	1.29
1AGY04	1.835	1.28	0.79	1.30
1AGY05	1.836	1.27	0.73	1.33
1WGX01	1.833	1.44	0.88	1.51
1WGX02	1.840	1.45	0.88	1.54
1WGX03	1.841	1.46	0.87	1.54
1WGX04	1.860	1.53	1.01	1.63
1WGX05	1.859	1.56	0.95	1.66
1WGZ01	1.848	1.49	0.89	1.57
1WGZ02	1.847	1.49	0.93	1.58
1WGZ03	1.860	1.54	0.99	1.62
1WGZ04	1.851	1.55	0.96	1.64
1WGZ05	1.850	1.56	0.96	1.63
2AGRA1	1.820	1.35		1.35
2AGRA2	1.808	1.28	0.68	1.29
2AGRA3	1.828	1.32	0.67	1.33
2AGRA4	1.817	1.27	0.62	1.25
2AGRA5	1.818	1.27	0.60	1.27
2AGRA6	1.823	1.36	0.68	1.29
2AGRA7	1.817	1.31	0.60	1.31
2WGW01	1.831	1.65	0.95	1.74
2WGW02	1.828	1.64	0.93	1.72
2WGW03	1.824	1.69	0.92	1.65

TABLE I (Concl'd)

SPEC	RHO	ED	ES	RVL2
1AG101	1.726	1.02	0.59	1.08
1AG102	1.718	1.02	0.54	1.08
1AG103	1.714	1.03	0.53	1.09
1AG104	1.725	1.05		1.11
1AG105	1.761	1.14	0.60	1.21
1AG201	1.683	1.02	0.55	1.01
1AG202	1.686	1.00	0.55	1.01
1AG203	1.689	1.01	0.55	1.02
1AG204	1.706	1.02	0.54	1.04
1AG205	1.750	1.09	0.61	1.16
1AG210	1.746	1.09	0.58	1.13
1AG212	1.754	1.08	0.53	1.14
1WG106	1.798	1.81	1.11	1.88
1WG107	1.749	1.67	1.01	1.75
1WG108	1.729	1.57	1.00	1.64
1WG109	1.722	1.53	0.99	1.63
1WG206	1.721	1.51	0.93	1.62
1WG207	1.729	1.54	0.99	1.65
1WG208	1.743	1.54	0.96	1.63
1WG209	1.683	1.30	0.86	1.41
1WG211	1.672	1.22	0.75	1.37
1WG213	1.696	1.34	0.85	1.46
2AGA01	1.686	0.99	0.61	1.05
2AGA02	1.691	0.99	0.56	1.04
2AGA03	1.703	0.99	0.60	1.06
2AGA04	1.706	1.02	0.59	1.07
2AGA05	1.690	1.05	0.63	1.10
2AGA06	1.700	1.05	0.61	1.11
2AGA07	1.700	1.00	0.63	1.06
2AGA08	1.708	1.01	0.59	1.07
2WGW01	1.732	1.71	1.08	1.75
2WGW02	1.705	1.59	1.03	1.68
2WGW03	1.688	1.56	1.08	1.61
2WGW04	1.678	1.53	1.00	1.57
2WGW05	1.657	1.45	1.09	1.50
2WGW06	1.688	1.47	0.97	1.53
2WGW07	1.686	1.49	0.96	1.56
2WGW08	1.721	1.59	1.11	1.70
3AGX01	1.764	1.17	0.70	1.27
3AGX02	1.743	1.16	0.64	1.26
3AGX03	1.742	1.15	0.66	1.23
3AGX04	1.759	1.18	0.61	1.27
3AGX05	1.760	1.18	0.71	1.28
3WGY01	1.760	1.65	1.01	1.83
3WGY02	1.747	1.58	1.06	1.76
3WGY03	1.745	1.58	1.05	1.76
3WGZ01	1.755	1.63	1.04	1.79
3WGZ02	1.758	1.62	1.04	1.80

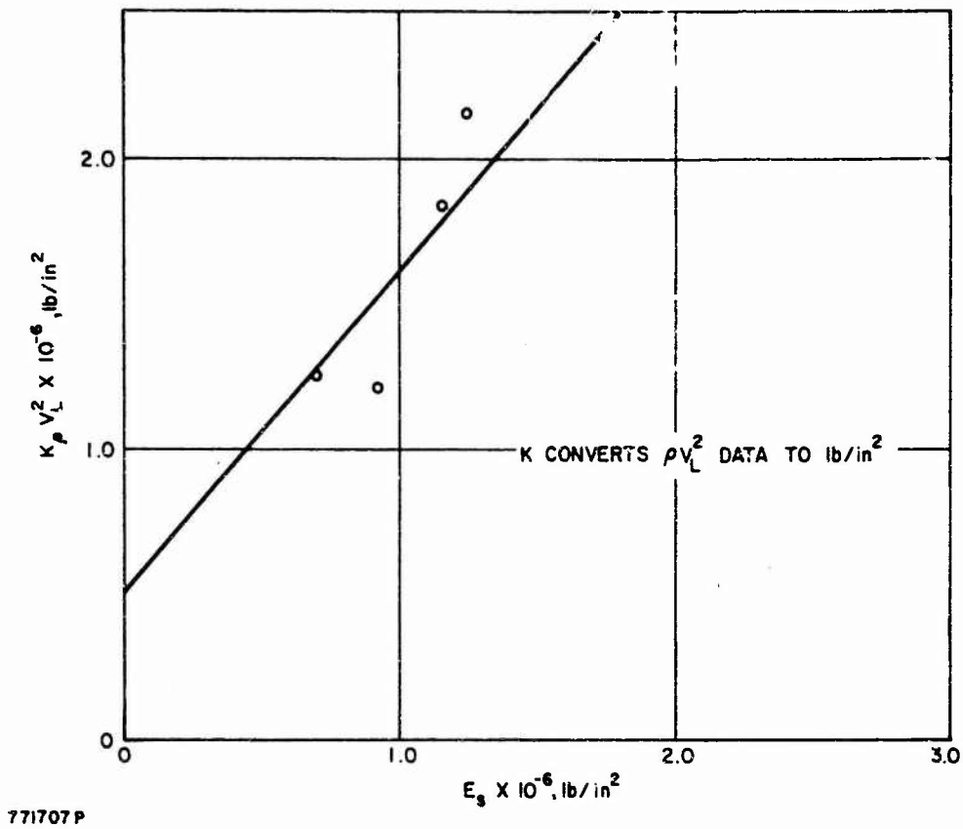

Figure II-1. RELATIONSHIP OF $K\rho\ V_L^2$ AND E_s FOR CFZ GRADE GRAPHITE

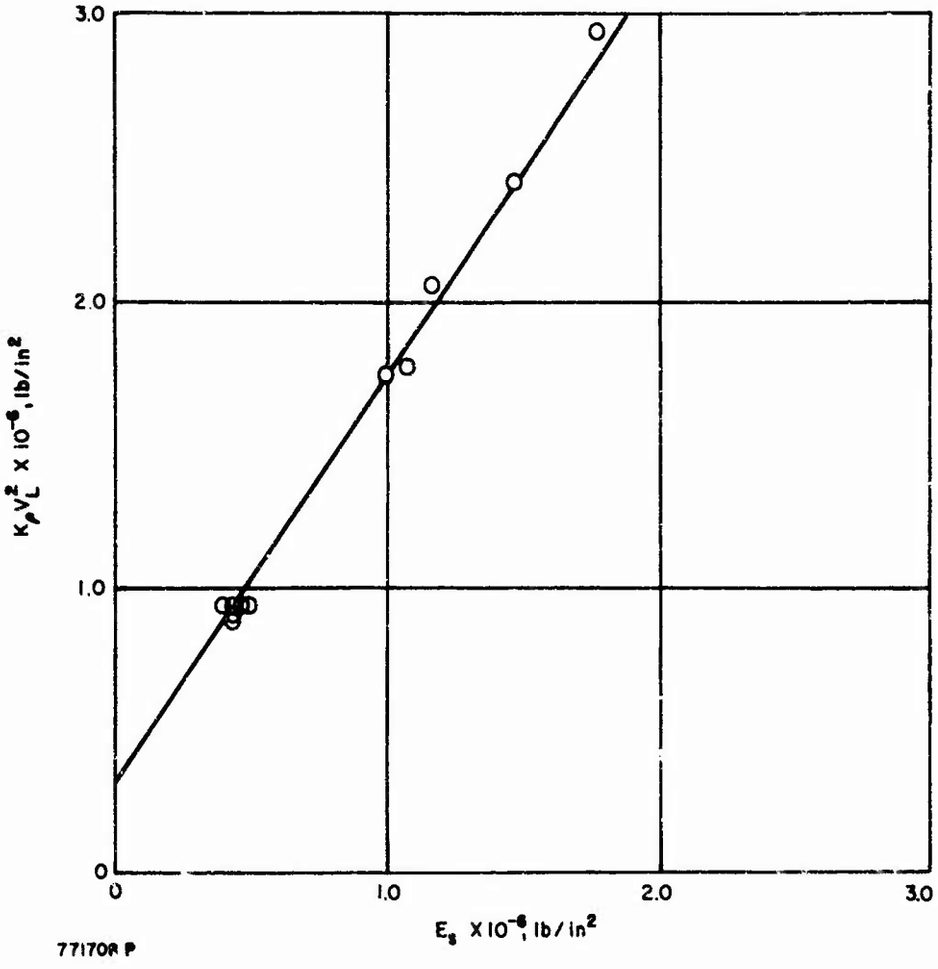

Figure II-2. RELATIONSHIP OF $K_\rho V_L^2$ AND ε_s FOR ZTA GRADE GRAPHITE

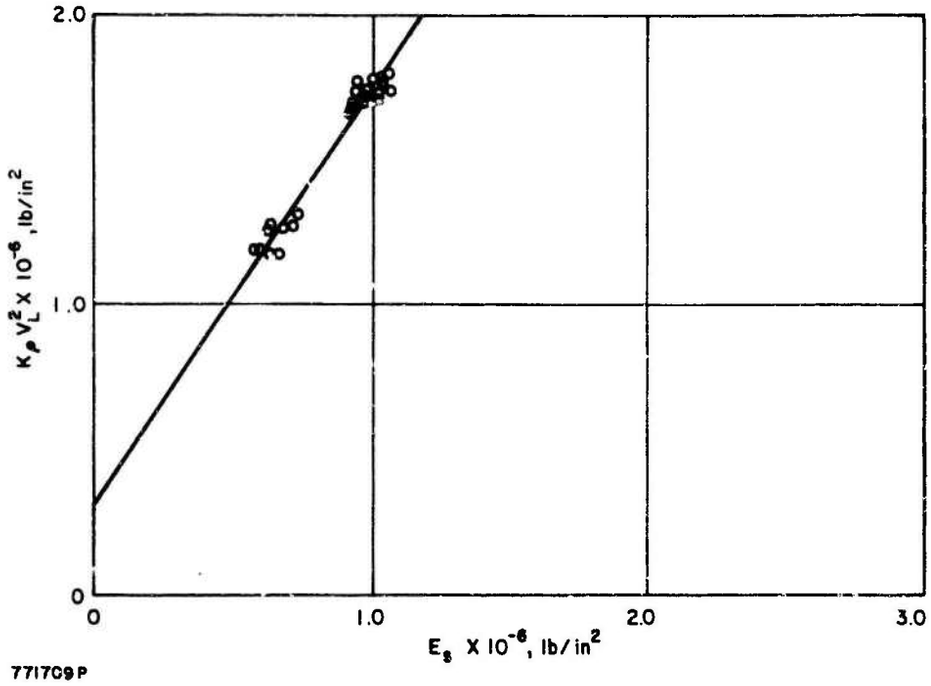

Figure II-3. RELATIONSHIP OF $K_\rho V_L^2$ AND E_s FOR CFW GRADE GRAPHITE

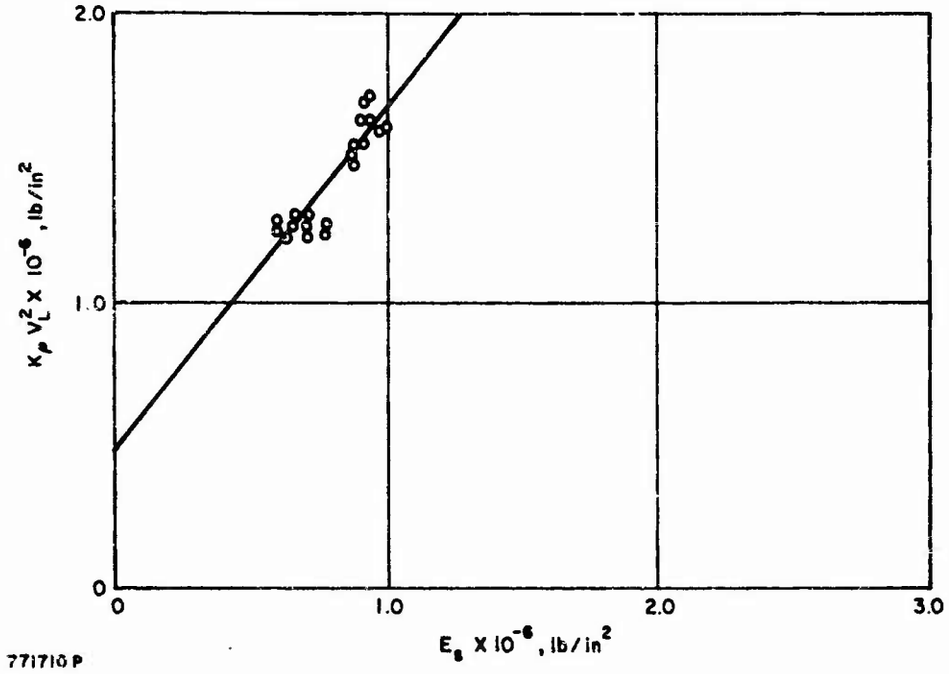

Figure II-4. RELATIONSHIP OF $K_\rho V_L^2$ AND ε_s FOR RVA GRADE GRAPHITE

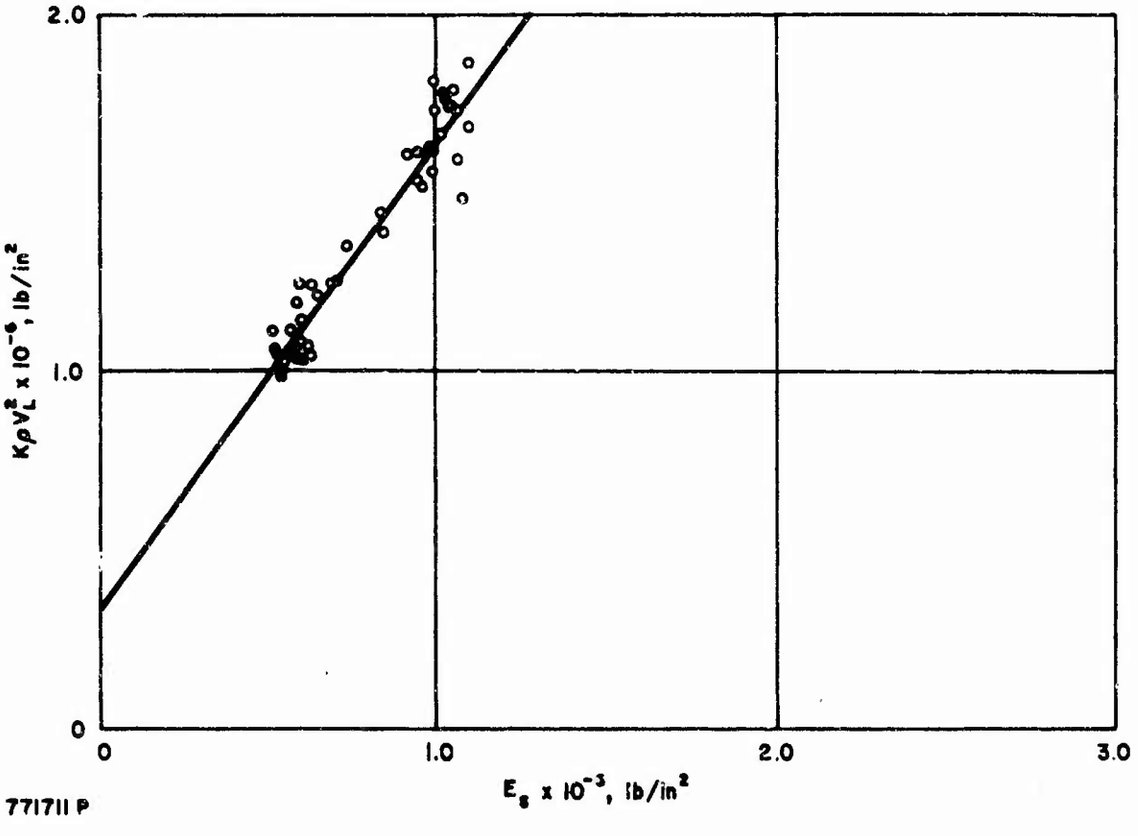

Figure 11-5. RELATIONSHIP OF $K_\rho V_L^2$ AND K_s FOR ATJ GRADE GRAPHITE

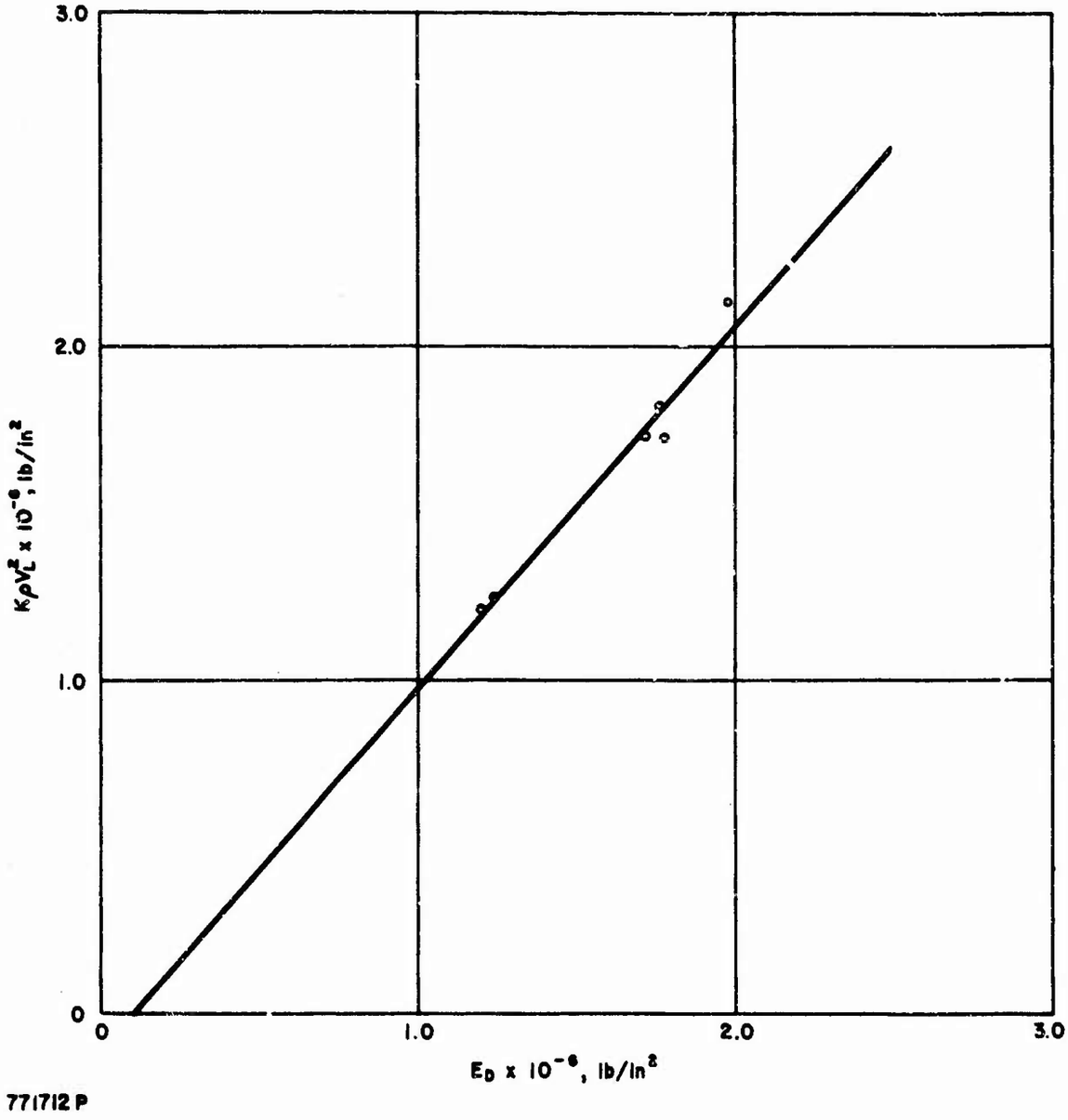

Figure 11-6. RELATIONSHIP OF $K_\rho V_L^2$ AND E_D FOR CFZ GRADE GRAPHITE

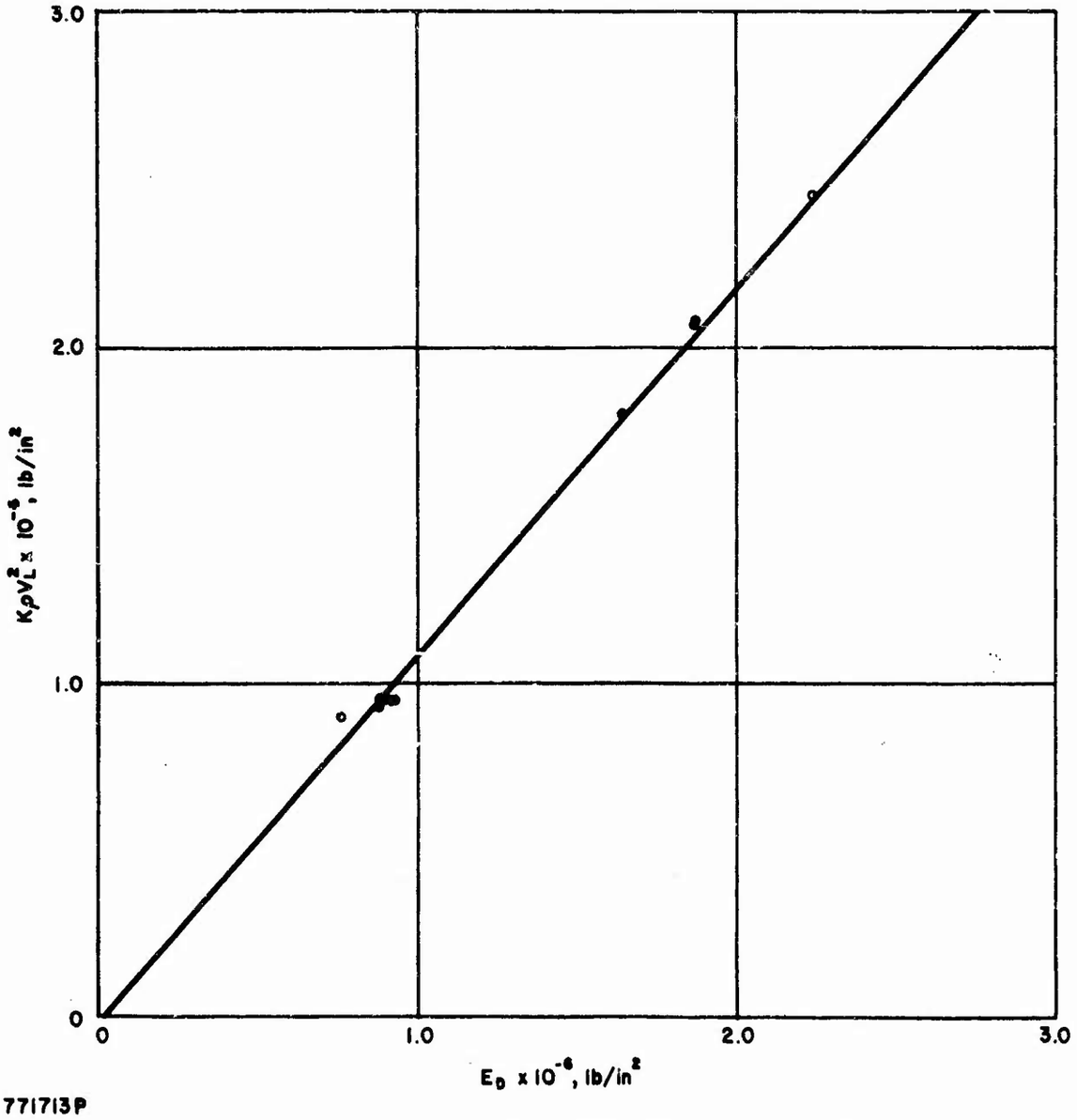

771713P

Figure II-7. RELATIONSHIP OF $K\rho V_L^2$ AND E_D FOR ZTA GRADE GRAPHITE

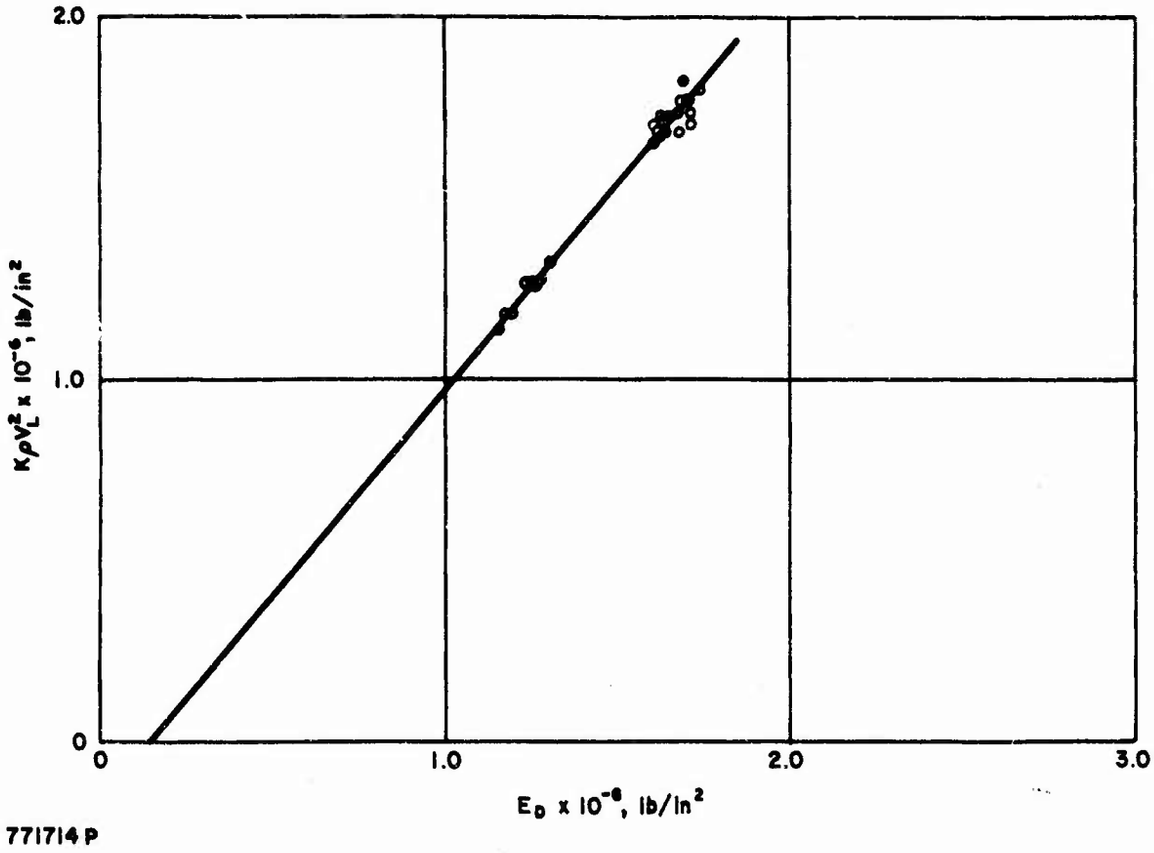

Figure 11-8. RELATIONSHIP OF $K\rho V_L^2$ AND E_D FOR CFW GRADE GRAPHITE

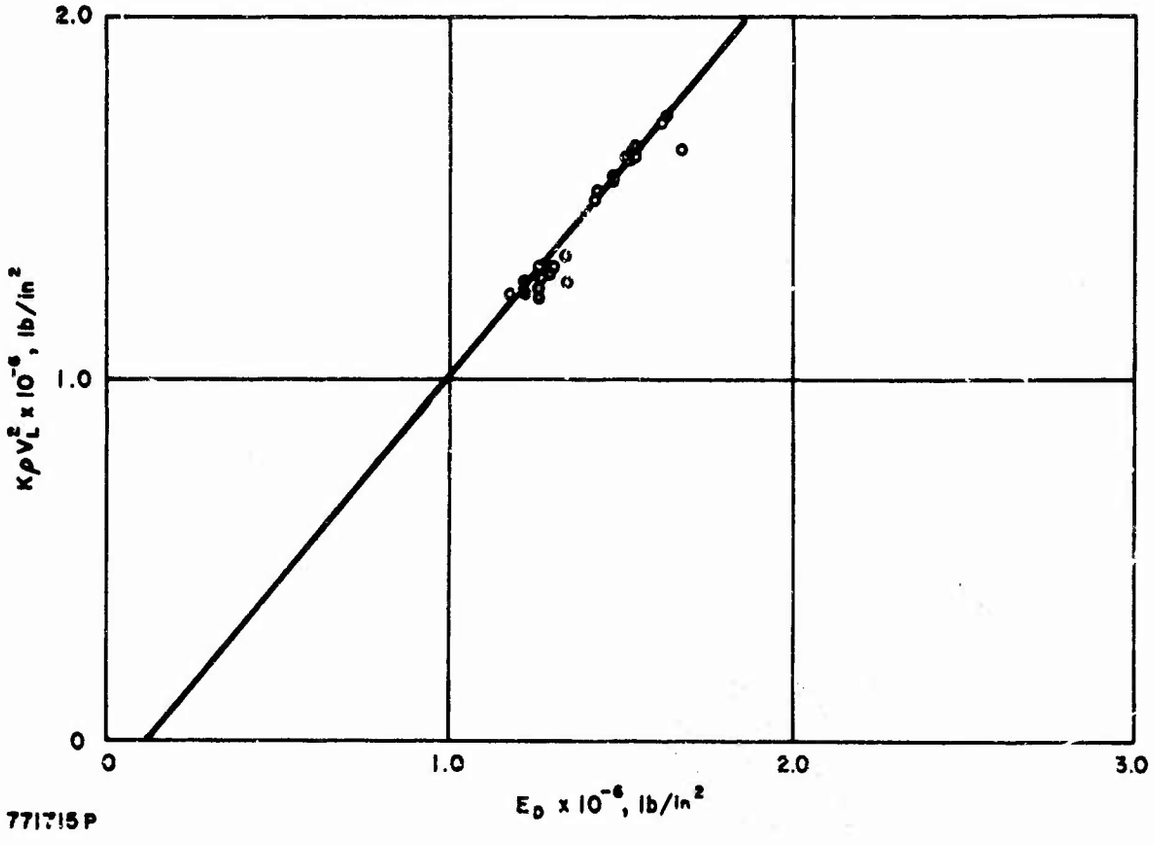

Figure 11-9. RELATIONSHIP OF $K_\rho V_L^2$ AND K_D FOR RVA GRADE GRAPHITE

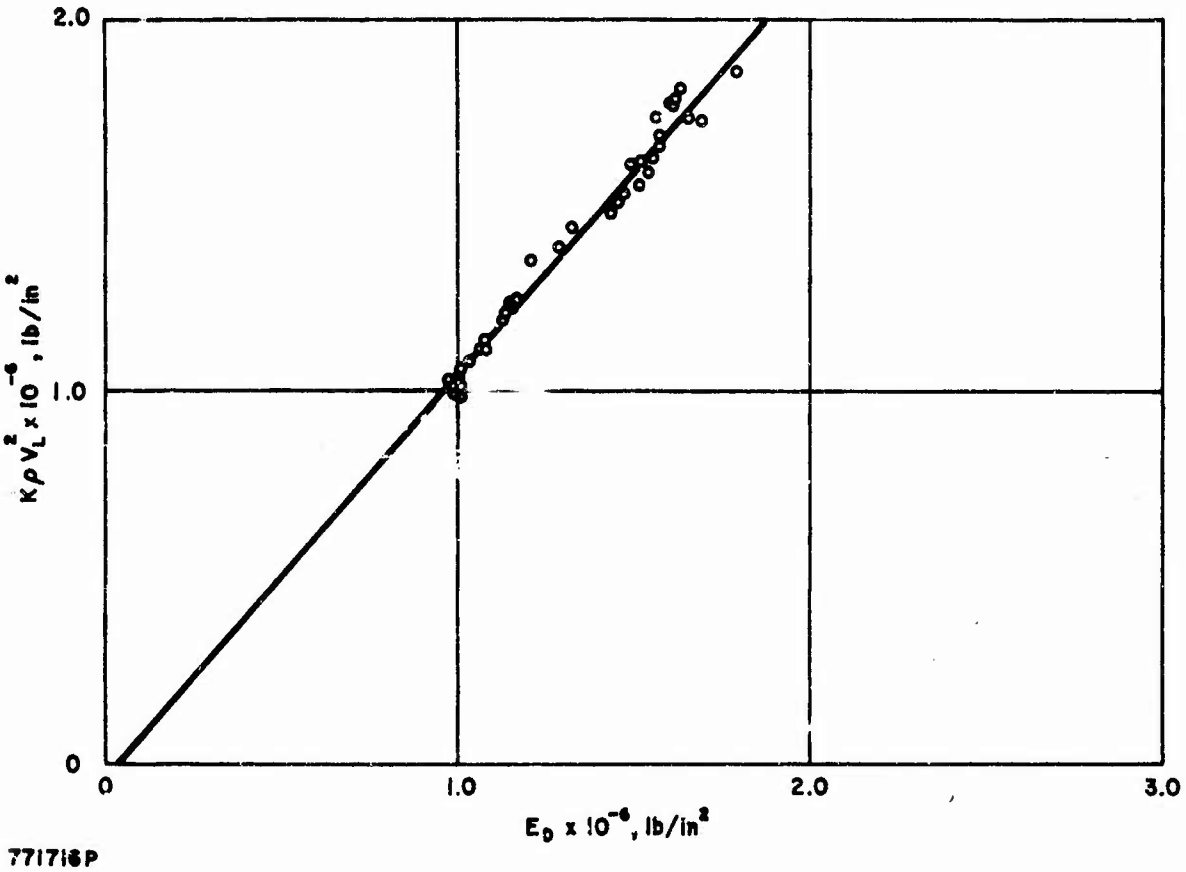

Figure 11-10. RELATIONSHIP OF $K_\rho V_L^2$ AND K_D FOR ATJ GRADE GRAPHITE

Grade			RMS
CFZ	$K\rho V_L^2$	= 1.104 E_D - 0.114	0.018
ZTA	$K\rho V_L^2$	= 1.066 E_D + 0.009	0.031
CFW	$K\rho V_L^2$	= 1.121 E_D - 0.137	0.026
RVA	$K\rho V_L^2$	= 1.129 E_D - 0.138	0.043
ATJ	$K\rho V_L^2$	= 1.095 E_D - 0.041	0.032

As part of the computer program which calculates the coefficients of the regression line, there is a print out of the root mean square (RMS) of the differences between the experimental $K\rho V_L^2$ value and that calculated from the best linear fit. These values have been included in the data above. The highest RMS value is that for the $K\rho V_L^2$ data for grade CFZ for which there are only four data points. Further testing should be done on this grade to confirm the relationships which have been indicated.

Correlation coefficients indicate the goodness of fit of the trend line for the data pairs. A value of "1" indicates a "perfect" fit while a value of "0" indicates no fit. The correlation coefficient is calculated from the coefficient of the modulus term and the standard deviations of the two variables as follows:

$$R = \lambda_{E_s} \frac{\sigma E_s}{\sigma K\rho V_L^2}$$

These values are tabulated below:

Grade	λ_{E_s}	σ_{E_s}	$\sigma_{K\rho V_L^2}$	R
CFZ	1.111	0.248	0.458	0.601
ZTA	1.432	0.599	0.832	1.000
CFW	1.418	0.161	0.240	0.951
RVA	1.193	0.135	0.175	0.920
ATJ	1.307	0.216	0.299	0.942
Grade	λ_{E_D}	σ_{E_D}	$\sigma_{K\rho V_L^2}$	R
CFZ	1.104	0.322	0.358	0.992
ZTA	1.066	0.806	0.832	1.000
CFW	1.121	0.214	0.240	0.999
RVA	1.129	0.149	0.175	0.961
ATJ	1.095	0.265	0.299	0.970

Again, only the $E_s/K\rho V_L^2$ relationship for the CFZ grade shows a poor fit which could be remedied by additional testing.

A similar analysis was performed for the composite population. Figures 11 and 12 show the two plots. It would appear that the relationship holds both for individual grades of graphite and the composite of the five grades evaluated. The two regression line equations are as follows:

$$K_\rho V_L^2 = 0.306 + 1.398 E_s \qquad \text{RMS} = 0.087$$

$$K\rho V_L^2 = 1.062 E_D \quad 0.210 \qquad \text{RMS} = 0.045$$

The correlation coefficients, which are 0.988 and 0.991, respectively, are indicative of good fits.

The graphs have been drawn to show not only the regression line but also the 98% data range based on σ and the factor 2.326. Using these graphs then, it is possible to predict E_D and E_s from the corresponding NDT test values within less than 10% and 15%, respectively, at the 98% confidence level. It should be noted that for random tensile data is on the order of 15 percent. Also, if one talks about 2.326 σ for a single grade the values are significantly lower than for all grades combined as above. For example, for CFW alone it is possible to predict E_d and E_s to within approximately 6 percent and 11 percent, respectively, at the 98 percent confidence level.

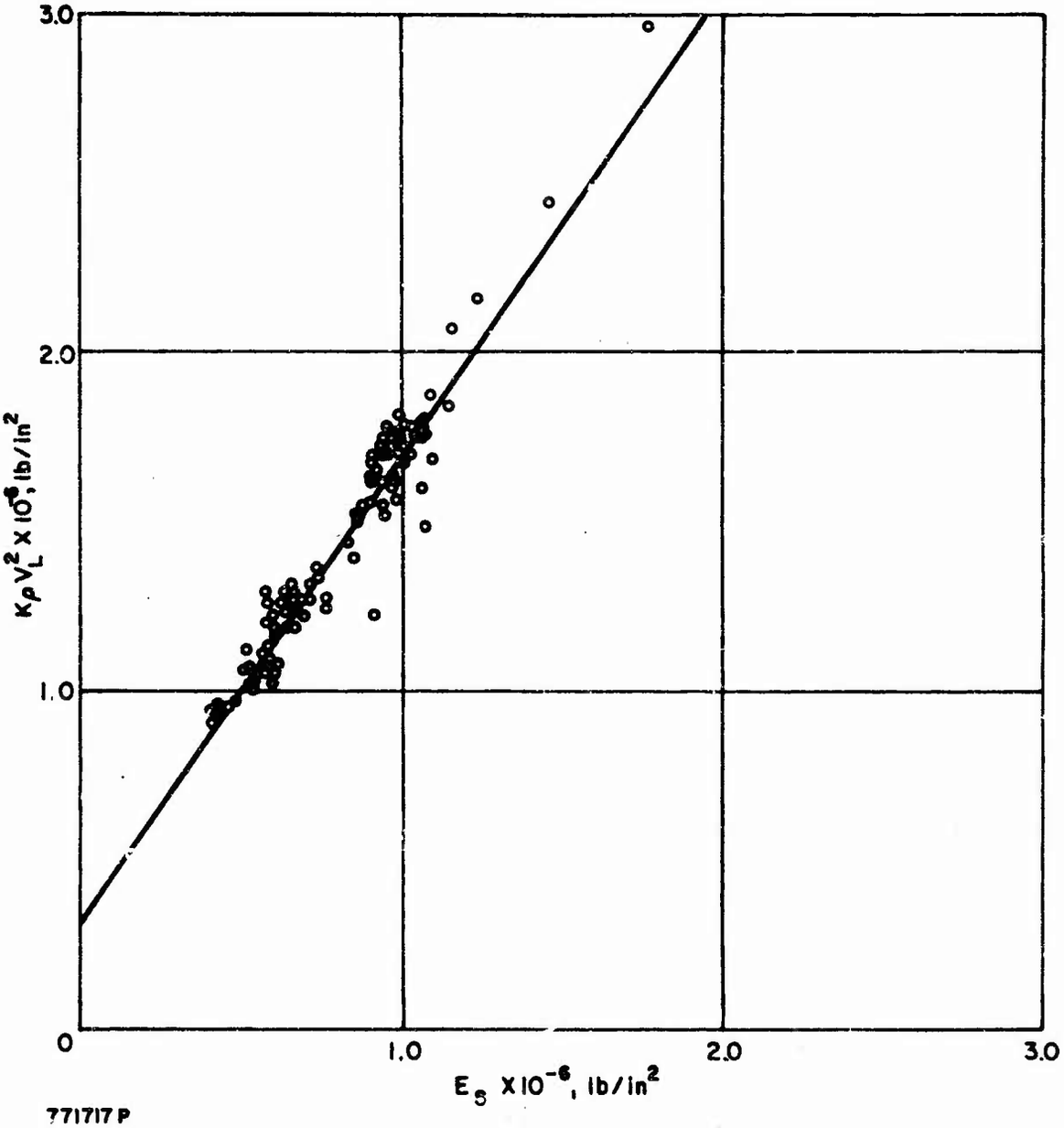

Figure 11-11. COMPOSITE PLOT OF ALL FIVE GRADES OF GRAPHITE SHOWING RELATIONSHIP OF $K\rho V_L^2$ AND E_s

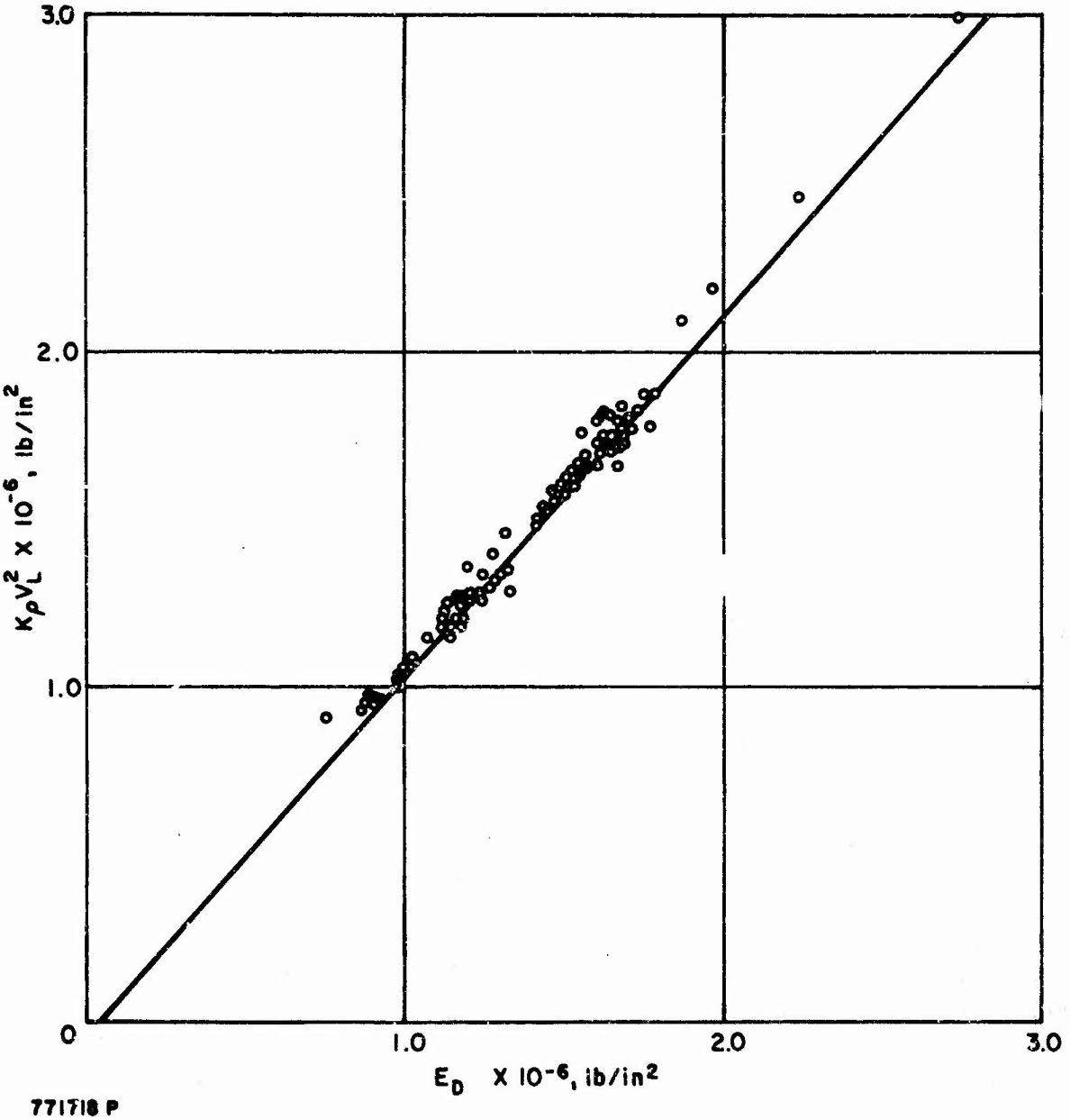

Figure 11-12. COMPOSITE PLOT OF ALL FIVE GRADES OF GRAPHITE SHOWING RELATIONSHIP OF $K_\rho V_L^2$ AND E_D

Page 146 is intentionally blank

APPENDIX III

Correction for Vertex Suppression Due to Radiometer Reference Source and Ambient Temperature Difference

A correction term must be added to the recorder deflection for a material when its parabolically-shaped temperature history is partially obscured during the time period of observation and subsequent analysis due to suppression of the vertex. To determine the magnitude of this correction only the difference between ambient temperature and the radiometer reference source temperature, and the relationship between recorder deflection and radiometrically measured temperature need be known. The radiation flux incident to a specimen's surface need not be known. The nature of this corrective term is illustrated graphically in Figure III-1.

As seen in the figure, V_o denotes the zero level of signal voltage, $-V_A$ denotes the signal level corresponding to ambient temperature, V_D denotes the observable signal level above V_o at t_2, and $-V_C$ denotes the correction term to be added to V_D to account for the magnitude of vertex suppression that occurs at t_1. The expression relating these quantities can be derived easily by recalling certain characteristics of a parabolically-shaped curve. The expression for a parabolic history, for a solid labelled "a", can be written as:

$$V_{t_a} = C_a t^{1/2} - V_A \quad , \tag{III 1}$$

where V_{t_a} is the signal level at time t, C_a is a proportionality constant, and V_A is the value of V_{t_a} at $t = 0$, if suppression exists. From the notations indicated in Figure III-1.

$$V_{t_{a_0}} = - V_A \tag{III 2a}$$

$$V_{t_{a_1}} = C_a t_1^{1/2} - V_A \tag{III 2b}$$

$$V_{t_{a_2}} = C_a t_2^{1/2} - V_A \tag{III 2c}$$

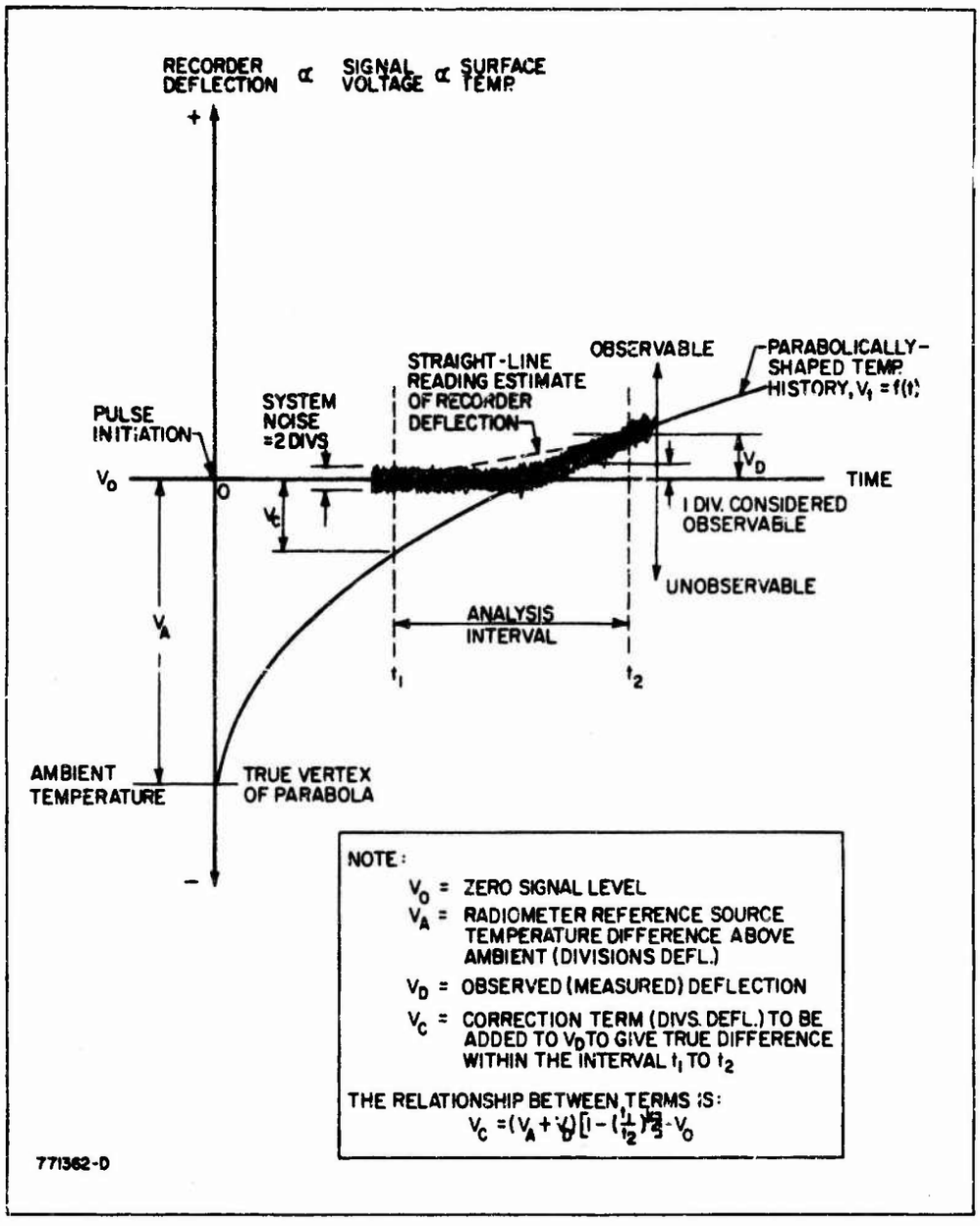

Figure III-1. ILLUSTRATION HISTORY CURVE PARTIALLY OBSCURED BY VERTEX SUPPRESSION DURING ANALYSIS INTERNAL (REQUIRING CORRECTION)

Subtracting $V_{t_{a_1}}$ from $V_{t_{a_2}}$ yields:

$$V_{t_{a_2}} - V_{t_{a_1}} = C_a \left(t_2^{1/2} - t_1^{1/2}\right) = V_D \qquad \text{(III 3)}$$

and subtracting $V_{t_{a_0}}$ from $V_{t_{a_2}}$ yields:

$$V_{t_{a_2}} - V_{t_{a_0}} = C_a \, t_2^{1/2} = V_D + V_A \qquad \text{(III 4)}$$

Dividing (3) by (4) yields the ratios of parabolic segments:

$$\frac{V_{t_{a_2}} - V_{t_{a_1}}}{V_{t_{a_2}} - V_{t_{a_0}}} = \frac{t_2^{1/2} - t_1^{1/2}}{t_2^{1/2}} = \frac{V_D + V_C}{V_D + V_A} \quad , \qquad \text{(III 5a)}$$

or

$$\frac{V_D + V_C}{V_D + V_A} = 1 - \left(\frac{t_1}{t_2}\right)^{1/2} \quad . \qquad \text{(III 5b)}$$

Since all quantities in (III) are measurable except V_C, Equation (III), solved for V_C, yields:

$$V_C = (V_A + V_D)\left[1 - \left(\frac{t_1}{t_2}\right)^{1/2}\right] - V_D \quad . \qquad \text{(III 6)}$$

V_C is then to be added to the observed voltage deflection, V_D, to give the true value of the deflection term that is to be compared with other deflections that are not suppressed.

To illustrate the use of (III), let V_D = 1 division deflection observed on the recorder chart between 1 and 4.5 seconds after pulse initiation. The ambient temperature is 26 deg. C and the radiometer reference source temperature is 31 deg. C, so that a temperature difference of 5 deg. C exists. This 5 deg. C difference is determined to correspond to a recorder deflection of 10 divisions (see Figure 8).

Substituting these values into (6) gives:

$$V_C = (10+1)\left[\,1 - \left(\frac{1}{4.5}\right)^{1/2}\,\right] - 1$$

$$= 11 \times 0.53 - 1$$

$$= 4.83 \text{ divisions.}$$

V_C (4.83 divs.) is then to be added to V_D (1 divs.) to give a true value for the deflection (5.83 divs.). A graphical relationship between V_C and V_D, for a few values of V_A, is shown in Figure 24.

APPENDIX IV

Derivation of Emissivity Correction to the Self-Emitted Recorder Deflection History

In accordance with Equations (9) and (10), the recorder deflection (signal voltage difference) of an ideal history within a time interval, t_1 to t_2, can be expressed as:

$$\Delta V \equiv V_{t_2} - V_{t_1} = \left[A \frac{\left(t_2^{1/2} - t_1^{1/2} \right)}{(k\rho C_p)^{1/2}} \right] \epsilon_\lambda^2 , \qquad \text{(IV 1)}$$

where $A = 3KF \sigma T_c^{\prime 3} / \pi^{3/2}$ constant. From reflectance measurements for known opaque surface emissivities, it was determined that a reflected recorder deflection of 20 divisions on the 10 mv/div. sensitivity scale corresponded to a reflectivity equal to 0.0367. Thus, since the coating material is regarded as opaque in this application, it has an emissivity equal to 1-0.0367 = 0.9633. The emissivity change per division of reflection is then 0.0367/20 = 0.00183 per div.

A relationship for ΔV for a reflected recorder deflection different from 20 divisions, say y divisions, is:

$$\frac{\Delta V_{20\ DIVS.}}{\Delta V_{y\ DIVS.}} = \frac{\epsilon_\lambda^2}{\left[\epsilon_\lambda - (y-20)(0.00183) \right]^2} . \qquad \text{(IV 2)}$$

For $\epsilon_\lambda = 0.9633$, Equation (IV 2) can be written as:

$$\Delta V_{20\ DIVS.} = \left[\frac{1}{1 - 0.0019\,(y - 20)} \right]^2 \Delta V_{y\ DIVS.} \qquad \text{(IV 3a)}$$

$$= K_{R_y} \Delta V_y , \qquad \text{(IV 3b)}$$

which states that a self-emitted recorder deflection, ΔV_y, having a reflected recorder deflection component of y divisions, is to be multiplied by the corresponding correction factor, K_{R_y}, to give a self-emitted deflection that is corrected, or normalized to 20 divisions. For example, if y = 24 divisions, then $K_{R_{24}} = 1.015$, so that the corrected $\Delta V_{20} = 1.015\ \Delta V_{24}$. A graph of K_{R_y} as a function of reflection amplitude is shown in Figure 7.

Page 152 is intentionally blank

APPENDIX V

Effect of Density on the Thermal Conductivity of Graphite

The thermal parameter $(k\rho\ C_p)^{1/2}$ is inversely proportional to recorder deflection for semi-infinite materials (since recorder deflection is proportional to surface temperature rise within an observation interval in which the correction for vertex suppression is unnecessary). Thus,

$$(k\rho\ C_p)^{1/2} = \frac{K}{D} \qquad \text{(V1)}$$

where K is a proportionality constant and D is recorder deflection. Solving for k gives:

$$k = \frac{K'}{D^2\rho}\ , \qquad \text{(V2)}$$

where $K' = K^2/C_p$ = constant for graphite, since C_p = constant. Differentiation of (V) yields the following expression:

$$\frac{\Delta k}{k} = -\left[\frac{2\Delta D}{D} + \frac{\Delta\rho}{\rho}\right], \qquad \text{(V3)}$$

which is interpreted to state that the relative change in thermal conductivity, $\Delta k/k$, equals the negative of the sum of twice the relative change in recorder deflection and of the relative change in density. Multiplying (V) by $k/\Delta\rho$ gives:

$$\frac{\Delta k}{\Delta\rho} = -k\left[\frac{2}{D}\cdot\frac{\Delta D}{\Delta\rho} + \frac{1}{\rho}\right]\ . \qquad \text{(V4)}$$

Since $-\Delta D/\Delta\rho$ = 1 division/0.06 gm/cm^3 obtained graphically from the plot of deflection vs. density for the cubic-shaped graphite specimens (see Figure 27), then (V) takes the form:

$$\frac{\Delta k}{\Delta\rho} = -k\left[-\frac{33.3}{D} + \frac{1}{\rho}\right]\ . \qquad \text{(V5)}$$

For graphite in the direction with the grain orientation, D = 14.8 divs. for a ρ = 1.73 gm/cm^3; in a direction against the grain orientation, D = 10.3 for ρ = 1.73 gm/cm^3. Substituting these values into (V5) gives:

$$\left(\frac{\Delta k}{\Delta \rho}\right)_{Ag} = 1.44\, k_{Ag} \qquad \text{(V6a)}$$

$$\left(\frac{\Delta k}{\Delta \rho}\right)_{W} = 1.67\, k_{W} \qquad \text{(V6b)}$$

Restating (V6) in terms of relative change yields:

$$\left(\frac{\Delta k}{k}\right)_{Ag} = 2.5\ \frac{\Delta \rho}{\rho} \qquad \text{(V7a)}$$

$$\left(\frac{\Delta k}{k}\right)_{W} = 2.9\ \frac{\Delta \rho}{\rho} \qquad \text{(V7b)}$$

Thus, it can be said, for example, that a 1 percent increase in density at a density of 1.73 gm/cm^3 will give rise to increases in thermal conductivity of 2.5 percent and 2.9 percent for ATJ graphite in directions against and with the grain orientation, respectively.

Although these numerical results were derived using finite deflection data, they are very nearly as valid as if semi-infinite data had been used, because of the uniform sizes of the specimens tested. These results are compatible with plots of equivalent thermal conductivity as a function of density shown in Figure 28; the equivalent thermal conductivity being inversely proportional to the product of density and the square of recorder deflection.

Unclassified
Security Classification

DOCUMENT CONTROL DATA - R&D
(Security classification of title, body of abstract and indexing annotation must be entered when the overall report is classified)

1. ORIGINATING ACTIVITY (Corporate author)
Avco Missiles, Space and Electronics Group
Space Systems Division
201 Lowell Street
Wilmington, Massachusetts 01887

2a. REPORT SECURITY CLASSIFICATION
Unclassified

2b. GROUP

3. REPORT TITLE
Investigation of Nondestructive Methods for the Evaluation of Graphite Materials

4. DESCRIPTIVE NOTES (Type of report and inclusive dates)

5. AUTHOR(S) (Last name, first name, initial)
Lockyer, G. E., Shultz, A. W., Serabian, S., Carter, S. W.

6. REPORT DATE	7a. TOTAL NO. OF PAGES	7b. NO. OF REFS
June 1967		19

8a. CONTRACT OR GRANT NO.	9a. ORIGINATOR'S REPORT NUMBER(S)
AF 33(615)-3942	AFML-TR-67-128
b. PROJECT NO.	
c.	9b. OTHER REPORT NO(S) (Any other numbers that may be assigned this report)
d.	AVSSD-228-67-CR

10. AVAILABILITY/LIMITATION NOTICES
This document may be further distributed by any holder only with specific prior approval of the processing and NDT branch, metals and ceramics division (MAM), Air Force materials laboratory, Wright-Patterson AFB, Ohio 45433.

11. SUPPLEMENTARY NOTES	12. SPONSORING MILITARY ACTIVITY
	Air Force Materials Laboratory Directorate of Laboratories Air Force Systems Command Wright-Patterson Air Force Base, Ohio

13. ABSTRACT
A program of investigation was begun in April 1964, to determine nondestructive methods and techniques for evaluating and characterizing graphite materials. The properties and behavior characteristics of graphite which are important to ablative applications were identified and correlated with the applicable NDT methods and techniques during the first year. During the second year, development of a novel infrared technique to measure thermal properties was initiated. Additionally, studies were performed to evaluate complex thermal and mechanical loading characteristics for graphite. In this regard, combined use of the various NDT techniques in relation to thermomechanical stresses and related thermal shock phenomena was also studied. During the past year, emphasis was directed in verification of the applicability of the various NDT techniques and correlation to characterize graphite in relation to service performance has been an item of major concern. Statistical analysis of these correlations has established the significance of the correlations for predicting the related material properties. An extensive analysis of the application of NDT flaw testing and properties evaluation in regard to quality and reliability is presented. A detailed discussion of infrared technique development activities for measuring thermal properties is also presented. The influence of attenuation and the related effects of frequency distortion on velocity measurements is evaluated and described.

DD FORM 1 JAN 64 1473

Unclassified
Security Classification

14 KEY WORDS	LINK A		LINK B		LINK C	
	ROLE	WT	ROLE	WT	ROLE	WT

INSTRUCTIONS

1. ORIGINATING ACTIVITY: Enter the name and address of the contractor, subcontractor, grantee, Department of Defense activity or other organization *(corporate author)* issuing the report.

2a. REPORT SECURITY CLASSIFICATION: Enter the overall security classification of the report. Indicate whether "Restricted Data" is included. Marking is to be in accordance with appropriate security regulations.

2b. GROUP: Automatic downgrading is specified in DoD Directive 5200.10 and Armed Forces Industrial Manual. Enter the group number. Also, when applicable, show that optional markings have been used for Group 3 and Group 4 as authorized.

3. REPORT TITLE: Enter the complete report title in all capital letters. Titles in all cases should be unclassified. If a meaningful title cannot be selected without classification, show title classification in all capitals in parenthesis immediately following the title.

4. DESCRIPTIVE NOTES: If appropriate, enter the type of report, e.g., interim, progress, summary, annual, or final. Give the inclusive dates when a specific reporting period is covered.

5. AUTHOR(S): Enter the name(s) of author(s) as shown on or in the report. Enter last name, first name, middle initial. If military, show rank and branch of service. The name of the principal author is an absolute minimum requirement.

6. REPORT DATE: Enter the date of the report as day, month, year, or month, year. If more than one date appears on the report, use date of publication.

7a. TOTAL NUMBER OF PAGES: The total page count should follow normal pagination procedures, i.e., enter the number of pages containing information.

7b. NUMBER OF REFERENCES: Enter the total number of references cited in the report.

8a. CONTRACT OR GRANT NUMBER: If appropriate, enter the applicable number of the contract or grant under which the report was written.

8b, 8c, & 8d. PROJECT NUMBER: Enter the appropriate military department identification, such as project number, subproject number, system numbers, task number, etc.

9a. ORIGINATOR'S REPORT NUMBER(S): Enter the official report number by which the document will be identified and controlled by the originating activity. This number must be unique to this report.

9b. OTHER REPORT NUMBER(S): If the report has been assigned any other report numbers *(either by the originator or by the sponsor)*, also enter this number(s).

10. AVAILABILITY/LIMITATION NOTICES: Enter any limitations on further dissemination of the report, other than those imposed by security classification, using standard statements such as:

(1) "Qualified requesters may obtain copies of this report from DDC."

(2) "Foreign announcement and dissemination of this report by DDC is not authorized."

(3) "U. S. Government agencies may obtain copies of this report directly from DDC. Other qualified DDC users shall request through _____."

(4) "U. S. military agencies may obtain copies of this report directly from DDC. Other qualified users shall request through _____."

(5) "All distribution of this report is controlled. Qualified DDC users shall request through _____."

If the report has been furnished to the Office of Technical Services, Department of Commerce, for sale to the public, indicate this fact and enter the price, if known.

11. SUPPLEMENTARY NOTES: Use for additional explanatory notes.

12. SPONSORING MILITARY ACTIVITY: Enter the name of the departmental project office or laboratory sponsoring *(paying for)* the research and development. Include address.

13. ABSTRACT: Enter an abstract giving a brief and factual summary of the document indicative of the report, even though it may also appear elsewhere in the body of the technical report. If additional space is required, a continuation sheet shall be attached.

It is highly desirable that the abstract of classified reports be unclassified. Each paragraph of the abstract shall end with an indication of the military security classification of the information in the paragraph, represented as *(TS)*, *(S)*, *(C)*, or *(U)*.

There is no limitation on the length of the abstract. However, the suggested length is from 150 to 225 words.

14. KEY WORDS: Key words are technically meaningful terms or short phrases that characterize a report and may be used as index entries for cataloging the report. Key words must be selected so that no security classification is required. Identifiers, such as equipment model designation, trade name, military project code name, geographic location, may be used as key words but will be followed by an indication of technical context. The assignment of links, rules, and weights is optional.